Universidade de Aveiro
2021

Ricardo Rodrigues Oliveira

Algoritmos de inteligência artificial para geradores eletromagnéticos auto-adaptativos

Artificial intelligence algorithms for self-adaptive electromagnetic generators

Universidade de Aveiro
2021

Ricardo Rodrigues Oliveira

Algoritmos de inteligência artificial para geradores eletromagnéticos auto-adaptativos

Artificial intelligence algorithms for self-adaptive electromagnetic generators

Dissertação apresentada à Universidade de Aveiro para cumprimento dos requisitos necessários à obtenção do grau de mestre em engenharia de automação industrial, realizada sob orientação científica de Marco Paulo Soares dos Santos, Professor Auxiliar em Regime Laboral do Departamento de Engenharia Mecânica da Universidade de Aveiro.

Este trabalho teve o apoio financeiro dos projetos UIDB/00481/2020 e UIDP/00481/2020-FCT-Fundação para Ciência e Tecnologia; e CENTRO-01-0145-FEDER-022083-Programa Operacional Regional do Centro (Centro2020), no âmbito do Acordo de Parceria Portugal 2020. através do Fundo Europeu de Desenvolvimento Regional. Referência do projeto: POCI-0145-FEDER-031132

O júri / The jury

Presidente / President	**Prof. Doutor Miguel Armando Riem de Oliveira** Professor Auxiliar da Universidade de Aveiro
Vogais / Committee	**Prof. Doutor Marco Paulo Soares dos Santos** Professor Auxiliar em Regime Laboral da Universidade de Aveiro (orientador)
	Prof. Doutor Manuel José Cabral dos Santos Reis Professor Associado com Agregação da Universidade de Trás-os-Montes e Alto Douro

Agradecimentos / Acknowledgements

Gostaria de agradecer a Deus pela oportunidade e motivação de realizar esse curso assim como essa tese, foram dois anos de muitos desafios e aprendizados e sou grato por tudo que pude viver nessa experiência. Agradeço a meus pais, Sergio e Lúcia, por todo o apoio que me deram, e mesmo estando longe souberam me dar o suporte necessário para que eu pudesse correr atrás dos meus objetivos. Obrigado por serem a minha base e exemplo ao longo da vida e por, juntos com minhas irmãs Helena e Beatriz serem a minha melhor rede de apoio. Gostaria de agradecer muito ao meu orientador, professor Marco Santos, por todo o incentivo e suporte que me prestou nesse ano de tese e por todos os momentos de sabedoria em sala de aula. Obrigado por ser um exemplo de orientador que muito me motivou a completar esse trabalho e me inspirou a ser um aluno melhor. Agradeço também à Inês Peres, que aceitou também o encargo de me ajudar ao longo dessa tese, obrigado por toda solicitude e toda a ajuda que foram imprescindíveis para a conclusão do trabalho. Gostaria também de agradecer ao Pedro Carneiro e ao Pedro Rolo pela ajuda com os dados experimentais e todos os outros integrantes do projeto. Agradeço também aos meus colegas de curso, pelos momentos compartilhados, trabalhos em grupo, ajudas em estudos. Obrigado por terem me acolhido ao longo desses dois anos. De forma especial, agradeço ao Tiago Padilha, por toda a ajuda nesse processo de tese, e ao João Ribau e Pedro Gonçalves. Gostaria também de registrar meu agradecimento ao Centro Universitário de Fé e Cultura (CUFC) na pessoa do seu diretor, Sr. Padre Leonel, por ter sido um lugar onde fui muito bem acolhido e pude encontrar o apoio emocional, espiritual e afetivo, como também fazer muitas amizades sinceras e verdadeiras. Gostaria também de agradecer seus membros, por todos os momentos vividos ao longo desses dois anos, sejam orações, passeios, almoços etc., meus mais sinceros agradecimentos. Não citarei nomes por medo de esquecer algum de vocês, mas sintam-se homenageados. Por último, mas não menos importante, deixo aqui meu profundo agradecimento à pessoa do Seu Armando, que por muitos dias, mesmo chuvosos, chegou a estar desde às 5:45 da manhã me prestando suporte, meu muito obrigado!

Palavras-chave Inteligência artificial; geração de energia; gerador eletromagnético; sistemas adaptativos; redes neuronais artificiais

Resumo O desenvolvimento na área da robótica e automação tem gerado uma maior procura por sistemas autónomos. Essa realidade, assim como o desenvolvimento de dispositivos com um consumo energético cada vez menor, tem sido factor de incentivo à pesquisa e desenvolvimento de métodos de geração autónoma de energia renovável que tenham um baixo custo e sejam capazes de alimentar diversos sistemas de pequena escala. Uma possível solução para esse tipo de aplicação são os geradores eletromagnéticos. Esse trabalho tem por foco o uso de algoritmos de inteligência artificial para melhor desenvolvimento do inovador conceito de geradores eletromagnéticos de energia elétrica com arquitetura em levitação magnética. É importante, para que sua aplicação seja efetiva, que o dispositivo seja capaz de adaptar seu desempenho com a alteração dinâmica da excitação mecânica. O principal objetivo do projeto é prever o comportamento desses geradores utilizando uma rede neuronal artificial para esse fim por ser uma solução capaz de prever com alta precisão o comportamento de sistemas não lineares. Para esse projeto, foi desenvolvido um algoritmo no MatLab. Optou-se pela configuração denominada NARX e foram testadas diferentes configurações, além de dois tipos diferentes de algoritmos de treino, com o objetivo de se obter o melhor resultado possível. Para o treino da rede neuronal, foram utilizados dados simulados obtidos previamente a este trabalho, no fim a rede foi testada tentando prever o comportamento do gerador com seus dados experimentais. Os resultados mostram que a rede foi capaz de prever o comportamento do gerador em mais de 80% dos casos de forma satisfatória. Esses resultados indicam a possibilidade do desenvolvimento de uma rede neuronal capaz de realizar a auto-adaptação de um gerador de vibrações mecânicas, tornando-o capaz de gerar energia para uma grande gama de frequências de excitação.

Keywords Artificial intelligence; energy generators; autonomous energy; triboelectric; electromagnetic; optimization; neural ntwork; algorithm; genetic algorithm; NARX

Abstract The development in the area of robotics and automation has generated a greater demand for autonomous systems. This reality, as well as the development of devices with increasingly lower energy consumption, has been a factor that encourages the research and development of methods for autonomous generation of renewable energy that have a low cost and are capable of powering several small-scale systems. One possible solution for this type of application is electromagnetic generators. This work focuses on the use of artificial intelligence algorithms to better develop the innovative concept of electromagnetic power generators with magnetic levitation architecture. It is important, for its effective application, that the device is able to adapt its performance with the dynamic change of the mechanical excitation. The main objective of the project is to predict the behavior of these generators using an artificial neural network for this purpose because it is a solution capable of predicting with high accuracy the behavior of nonlinear systems. For this project, an algorithm was developed in MatLab. The configuration called NARX was chosen, and different configurations were tested, as well as two different types of training algorithms, with the objective of obtaining the best possible result. For training the neural network, simulated data obtained previously to this work was used, in the end the network was tested trying to predict the behavior of the generator with its experimental data. The results show that the network was able to predict the behavior of the generator in more than 80% of the cases satisfactorily. These results indicate the possibility of developing a neural network capable of performing self-adaptation of a mechanical vibration generator, making it capable of generating energy for a wide range of excitation frequencies.

Contents

List of Tables

List of Figures

Acronyms

ANN Artificial Neural Network.

CPSO Co-Evolutionary Particle Swarm Optimizatio.

EMG Electromagnetic Generator.

FEM Finite Elements Method.

FTENG Freestanding Triboelectric-Layer Mode.

GA Genetic Algorithm.

IDE Integrated Development Environment.

LBEH Levitation Based Energy Harvesters.

LSTENG Lateral Sliding Mode.

ML Machine learning.

MPE Mean percentage error.

MSE Mean square error.

NARX Nonlinear Autoregressive Network with Exogenous Inputs.

PDMS Polydimethylsiloxane.

PSO Two-Particle Swarm Optimization.

PTFE Polytetrafluoroethylene.

SETENG Single-Electrode mode.

SOMA Self-Organizing Migration Algorithm.

SVM Support Vector Machine.

t-SNE T-distributed stochastic neighbor embedding.

TENG Triboelectric electromagnetic generator.

VCTENG Vertical Contact-Separation Mode.

Chapter 1

Introduction

1.1 Motivation

Energy generation has long been a major concern for society. As more and more equipments that depend on energy are being developed, this concern increases. With the growing demand for energy, the employed energy sources also become more important, with new techniques for generating energy from renewable sources being increasingly desired. Renewable energy sources are virtually inexhaustible once it is naturally replenished, therefore being more environmentally sustainable. Several countries already foresee a shift from non-renewable to renewable energy sources in the next few years.

One of the major challenges of the most common renewable sources for large-scale energy production, such as thermal and wind power, is production management, since they are intermittent and dependent on natural factors, which increases production costs. In contrast, other sources, which are non-intermittent, such as ocean tidal power, require very complex systems which leads to a high maintenance cost, in addition to the difficult adaptation of these systems for different energy sources.

Thus, there is a demand for the development of solutions for renewable energy generation, in an efficient and reliable way, with a low production and maintenance cost. In addition, system adaptation for variations in the energy source without performance decrease is also desirable. In this way, technological advances in energy harvesting have been very relevant for several social sectors. Energy harvesting, also known as energy scavenging, is the process of producing electrical energy using certain sources in the environment, such as wind, sunlight and mechanical vibrations [11] [5]. With the growth in the utilization of small low-power electronic devices, along with the increase of wireless communications utilization, the research for small-scale power generation systems has also increased, aiming for the energetic autonomy of these systems. They are used in cases such as remote and autonomous sensors, portable devices and biomedical implants, for example. In these cases, the energy source should be enough to power the entire system, besides being dedicated to it, which would reduce the need for external interventions, battery shortage problems, electronic noise, difficulty to connect to a power grid and other problems related to the utilization of common energy sources [13] [11] [5]. Currently, among the challenges for the development of generators for these applications are the generated electrical current intensity (which must be sufficient to supply the system) self-adaptability, and the maintenance cost [13] [1]. The importance of developing systems which do not depend on external batteries is especially significant in

biomechanical implants, since the necessary surgical interventions to replace the batteries cause a great deal of discomfort for the patient [1]. Additionally, external power sources bring a risk of serious system failures, endangering the patient's well-being and life [1]. The utilization of power generators based on mechanical vibrations has the potential to meet this demand and enable the development of new implants that can perform more complex functions and have a long enough lifespan that surgical interventions are no longer needed [1]. Besides the abundance of mechanical vibrations around the human body makes this energy generation system even more suitable for biomedical implants. The most commonly used mechanical vibration generators are: electromagnetic (EMG) [12], triboelectric (TENG) [2] and piezoelectric [4].

This dissertation is on the scope of the project ref. POCI-01-0145-FEDER-031132 with the title "The next-generation of biomechanical self-powering systems for multi-functional implantable medical devices", which aims to investigate new approaches to implement hybrid generators based on peptide systems, triboelectric generators and electromagnetic generators using magnetic levitation architecture. The technology developed in this work only takes into account electromagnetic generation, but since the main goal of the project in which it is inserted is to develop a hybrid triboelectric-electromagnetic generator, the triboelectric generator is also framed in the state of the art section.

1.2 Objectives

The objective of this work is to develop an artificial intelligence algorithm to predict the behavior of a self-adaptive electromagnetic generator with magnetic levitation architecture, a very innovative and promising technology. Several characteristics make its development very attractive, such as its non-complex design, long duration capacity in autonomous operation, and low requirements for its maintenance, since its levitation system replaces the need of mechanical transmission systems, reducing mechanical wear, as well as reducing the loss by mechanical dissipation.

In general, the excitation frequency of generators is usually a limiting factor, since they only generate a significant amount of power when the mechanical excitation frequency is close to the generator's natural frequency. Therefore, through an Artificial Neural Network (ANN), it is desired to make such generator capable of adaptation to different excitation frequencies, which increases the range of usable frequencies. With the ANN ability to predict the generator behavior for each input frequency, it would be possible to control the generator features, like the input impedance, and change the natural frequency to one close to the input frequency.

Therefore, the specific objectives of this work boil down to:

- Development of a neural network to predict the generator's output;
- Training of the neural network;
- Validation of the ANN using simulated and experimental data.

Chapter 2

State of the art review

2.1 Mechanical Vibration Generators

Some examples of energy sources used in the energy harvesting field are presented by Çelik *et al.* [11], such as air flow, environment temperature and vibrations, which is the focus of this work. This type of energy conversion is important for the development of autonomous electronic devices. Some examples of energy harvesting that help elucidate well this concept are presented by Chaari *et al.* [14], where energy can be generated from the electromagnetic radiation of a compact phosphorescent lamp.

As pointed out by Blasco *et al.* [13], this kind of technology can extend the service life of some communication networks that use remote elements. The great advance brought about by this concept is that batteries, which have a limited lifespan, used in embedded systems, for example, can be replaced by power generators, which, in theory, have an unlimited lifespan.

Mechanical vibration generators have received special attention due to the fact that they have an abundant and generally easily accessible power source. The excitation frequency of the generators comes from mechanical vibrations from the environment around the generator or from mechanical impacts. As noted earlier, they are generally generators with low generated power capacity usually in the mW range.

Borca-Tasciuc *et al.* [15] conducted a review of the state of the art regarding mechanical vibration micro generators of the following types: electromagnetic, piezoelectric and electrostatic, with a greater emphasis on the latter. A comparison between these generators was also made by Nabavi and Zhang [16], but in this case the major emphasis is on the piezoelectric ones.

In this work two of these generators will be highlighted: the electromagnetic and the triboelectric. A comparison between them is made by Zhao *et al.* [3] for low amplitude frequencies applications, highlighting the output difference between the two types of generators. The former presents a higher output current and a lower voltage in comparison with the latter, as exemplified in Figure 2.1. One way to overcome this constraint is to develop a hybrid electromagnetic-triboelectric generator, as presented by Zang *et al.* [17], where such generator, applying biomechanical energy for self-sustaining devices to be used during a walk, is demonstrated. The idea is to integrate the generator into a commercial shoe to generate energy to power sensors and LEDs used by the shoe. Therefore, an important specification is the capability to generate power from an intermittent, low frequency$<$10 Hz) excitation frequency. In this work, a generator with dimensions

of $5 \times 5 \times 2.5$ cm^3 and a weight of 6 g has been developed, bringing the two types of generator together, with the triboelectric being able to generate a peak power of 4.9 mW with a load of 6 MΩ and the electromagnetic generating a peak power of 3.5 mW over a load of 2 kΩ.

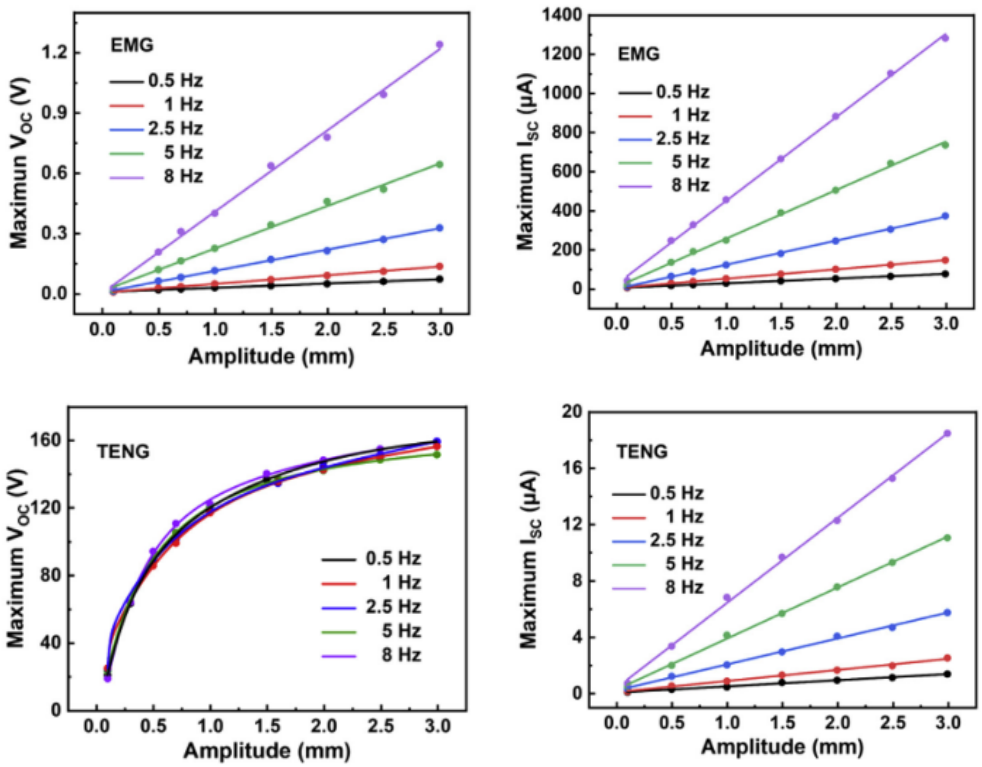

Figure 2.1: Voltage and current outputs of the electromagnetic and triboelectric generator developed by Zhao *et al.* [3].

2.1.1 Electromagnetic GeneratorsEMG)

Electromagnetic generators were the first kinetic energy converters proposed [15]. This type of generator works from the principle of electromagnetic induction obtained by the movement of a magnet near to a coil. The applied excitation frequency generates oscillation to the permanent magnet. This generates voltage in the coil, according to Faraday's Law, which states that the variation of the magnetic field flow through conducting materials induces the appearance of an electric current. A generic schematic is shown in Figure 2.2 and the operating steps in Figure 2.3.

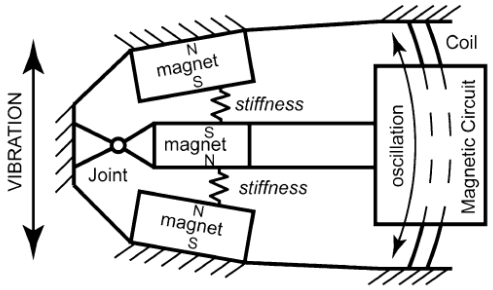

Figure 2.2: Example of electromagnetic generator model [4].

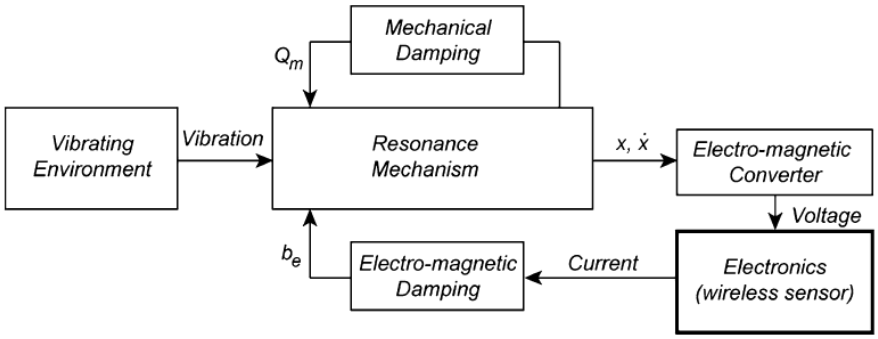

Figure 2.3: Working model of an electromagnetic generator [4].

Hadas *et al.* [4] aim to present an optimized solution for this generator, with the smallest volume and maximum possible power for aeronautical applications. According to the authors, the maximum output energy occurs when the mechanical damping is equal to the electrical damping. Two different sets of design parameters were chosen through the use of two neural networks that each used a different algorithm and the models were tested through simulation using an analytical model in Matlab/SimuLink (MathWorks). The artificial intelligence algorithms used were the Self-Organizing Migration Algorithm (SOMA) and the Genetic Algorithm (GA). As presented in Figure 2.4, the algorithms are quite similar, with a difference in the feature selection process that will advance to the next iteration. As stated by the authors, the advantage of using SOMA is that the algorithm is very robust for fast conversions to global extremes. The performance index is the function that measures the performance of the neural network, with a smaller score indicating a better performance of the network. According to Hadas *et al.* [4], the index used was derived from Equation 2.1, which has as a major drawback the necessity and difficulty to find the c_i coefficients. Hence, the application of Equation 2.2, which uses weighted magnitudes.

$$f = c_1 \frac{1}{V_{out}} + c_2 \frac{1}{P_{out}} + c_3 Volume \tag{2.1}$$

$$f_{pu} = c_1 g_1 + c_2 g_2 + c_3 g_3 \tag{2.2}$$

where,

$$g_1 = 1 - \frac{V_{out}}{V_{desejado}}$$
$$g_2 = 1 - \frac{P_{out}}{P_{desejado}}$$
$$g_3 = \frac{Volume_{out}}{Volume_{desejado}}$$

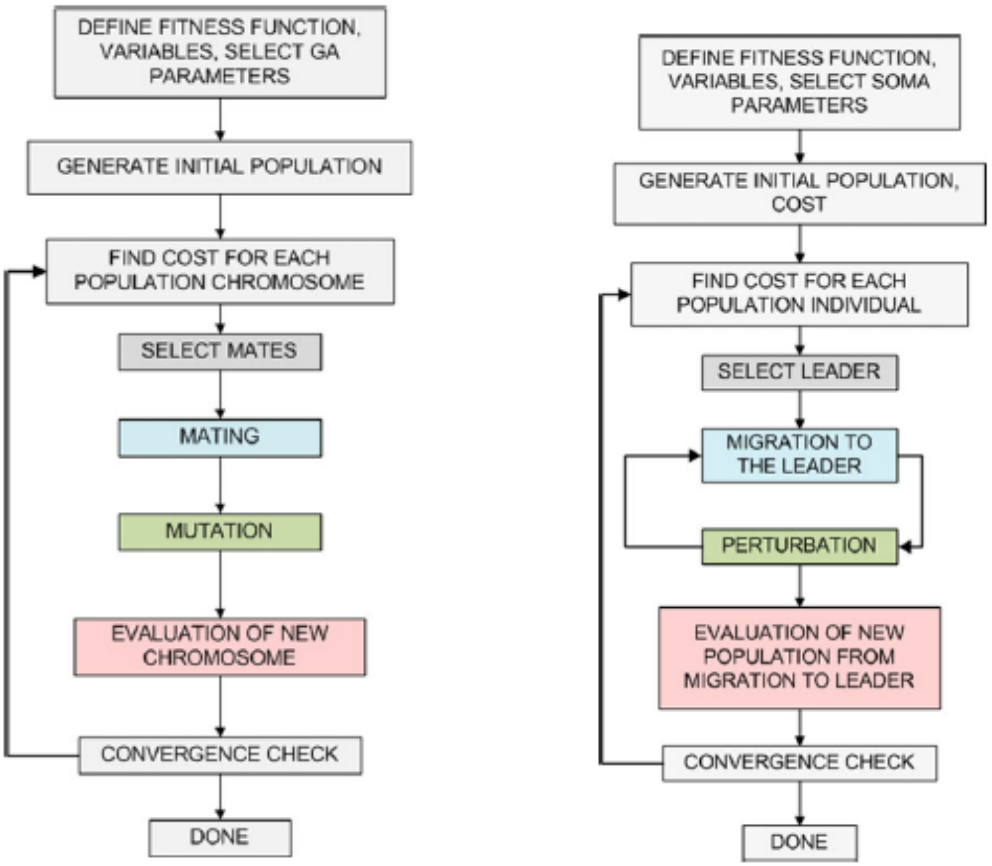

(a) Algoritmo Genético (b) SOMA

Figure 2.4: SOMA and GA structure [4].

The output powers found by Hadas *et al.* [4], according to the applied resistive load for different amplitudes of the excitation waves, are illustrated in Figure 2.5. In all cases, the input frequency was $17Hz$.

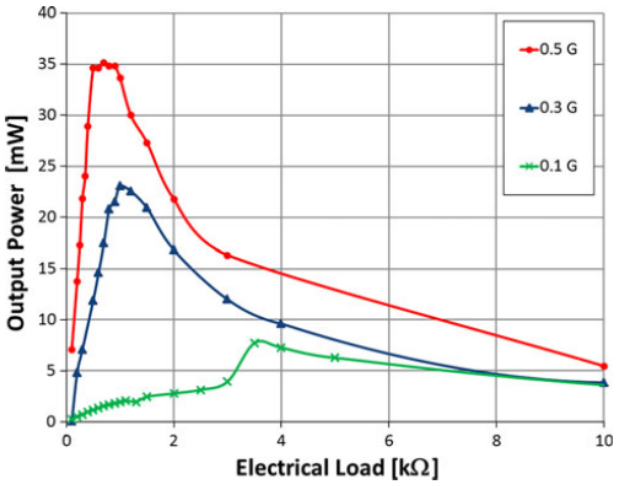

Figure 2.5: Power output[4].

Magnetic levitation energy harvesting (LBEH)

The specific generator to be used in this work will be based on a magnetic levitation architecture. In this architecture, the moving magnet is sustained by the electromagnetic force generated by two other permanent magnets, each one fixed at the end of the generator's container, so there are no mechanical structures in permanent contact with the oscillating mass. The operating principle of the technology is simple, efficient, and the absence of mechanical contact reduces the need for maintenance, by reducing mechanical wear on the parts of the generator, and also reduces the energy dissipation of mechanical energy associated with springs and other elements. The association of magnetic levitation and electromagnetic induction is increasingly proving to be a robust and versatile solution for power generation applications; moreover, it is a low cost solution that can act autonomously for a long period of time.

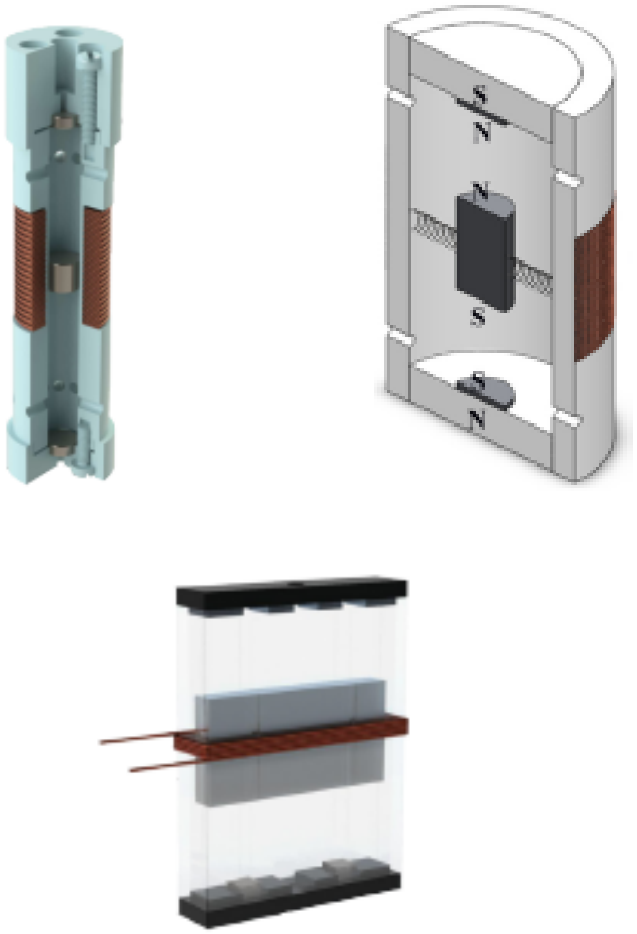

Figure 2.6: Examples of magnetic levitation generators[5].

In Carneiro *et al.* [1] a review of the state of the art of LBEH is given. In it, the division into four different categories is found. Category 1 has only a floating magnet and a coil, 3 possible configurations are presented. In Category 2, with one coil and multiple floating magnets, 8 different configurations are presented. Category 3, with one magnet and multiple coils, has 5 configurations. And Category 4, with multiple magnets and multiple coils, features 5 configurations.

The paper also classifies the generators by their modeling type. As highlighted in the paper, the importance of modeling is due to the fact that it is very complex to obtain an efficient performance from these generators. Despite the abundance of mechanical energy in the environment, the paper points out some setbacks in the performance optimization, these being: (1) the highly non-linear behavior of this type of generator makes prior geometric optimization difficult; (2) the need for a self-adaptive architecture to be able to effectively generate energy from excitation frequencies that are unknown and time variant; and (3) the physical constraints of the dimensions that must be considered for practical uses. The models already developed were: empirical, analytical, semi-analytical, and finite element method (FEM) as shown in Table 2.2. As noted, most authors use

Categories	No. of Coils	No. of Magnets	Configurations
Category 1	1	1	3
Category 2	1	>1	8
Category 3	>1	1	5
Category 4	>1	>1	5

Table 2.1: Categories of LBEH classification in Carneiro *et al.* [1].

hybrid models. The table also show the other features of each model, thus being the optimization methodology, the excitation type, the electrical current and voltage.

Reference	Model	Architecture	Optimization Methodology	Excitation	I (mA)	U (V)
Hadas *et al.* [4]	Analytic (Matlab)	Pendular	SOMA	f=17Hz; A=0.1G	1,48	5,17
			GA	f=17Hz; A=0.1G	1.44	5.05
Categoria 1						
Constantinou *et al.* [18]	Semi-Analytic Analytic	LBEH	Distance between fixed magnets.	4.3gsin($2\pi 46t$)	140 (RMS)	13(RMS)
Constantinou *et al.* [19]	Semi-Analytic Analytic Empirical	LBEH	Material of the shaft and bearing contact surface.	2gsin($2\pi 37t$)	150 (AVR)	0,6(AVR)
Bernal and García [20]	Analytic FEM	LBEH	Not Optimized	ND	ND	ND
Foisal*et al.* [21]	Analytic	LBEH	Number of windings, width, position of the coil, and distance between fixed magnets	$0.5gsin(24\pi ft)7 < f <$ 10	ND	ND
					ND	ND
Foisal *et al.* [22]	Analytic FEM	LBEH	Permanent magnet dimensions, position, and coil width.	$0.16gsin(2\pi 9t)$	3.5 (MAX)	0,3(MAX)
Foisal and Chung[23]	Analytic FEM	LBEH	Inertial mass, fixed magnet size, width and position of the bonine.	$0.13gsin(2\pi 8.1t)$	23.4 (MAX)	2,3(MAX)
Berdy *et al.* [24]	Analytic Semi-Analytic Empirical	LBEH	Frame section (rectangular), permanent magnet dimensions, number of windings, and coil position.	$0.1gsin(2\pi 6.7t)$	0.6 (MAX)	0,6(MAX)
Berdy *et al.* [25]	Analytic Semi-Analytic Empirical	LBEH	Section of the structure (with or without guide shaft) and its material.	0.075gsin($2\pi 6.7t$)	ND	ND
				$cust.4.8 - 9.7km/h$	0.3-0.6 (RMS)	0.3-0.6 (RMS)
Liu *et al.* [26]	Analytic Empirical	LBEH	Distance between fixed magnets and coil width.	$Asin(2\pi ft)0.45g < A < 0.6g4.4 < f < 4.8$	1.2-5.3 (RMS)	0.012-0.053 (RMS)
				$cust.f = 4.5; A = 0.01m$	$\approx 1 - 5.6(RMS)$	$\approx 0.035 - 0.094(RMS)$

Reference	Model	Architecture	Optimization Methodology	Excitation	I (mA)	U (V)
				$cust.f = 6.7; A = 0.01/0.02m$	7. 5/8. 1 (RMS)	$\approx 0.075/0.081(RMS)$
Santos *et al.* [27]	Analytic Semi-Analytic	LBEH	Not Optimized	$Asin(2\pi ft)0.84g < A < 1.96g3.5 < f < 9$	$\approx 0.51.7(MAX)$	$\approx 1.7 - 6(MAX)$
				$Asin(2\pi ft)0.84g < A < 1.8g3.5 < f < 8$	$\approx 0.039 - 0.1(MAX)$	$\approx 3.5 - 10(MAX)$
Kecik *et al.* [28]	Analytic Empirical	LBEH	Not Optimized	$Asin(2\pi ft)A < 10.2gf < 15.9$	$\approx 0 - 38(MAX)$	ND
Kecik[29]	Analytic Empirical	LBEH	Magnetic repulsive force, inductance of the coil, and the influence of the coupling effect.	$\text{Asin}(2\pi ft)0.05g < A < 14.3g1.6 < f < 15.9$	$\approx 0 - 56(MAX)$	ND
Category 2						
Saha *et al.* [30]	Analytic FEM Empirical	LBEH	Not Optimized	$0.039gsin(2\pi 7.6t)$ cust.	0.045 (MAX) 1-1.8 (AVR)	0,3 (MAX) 0.9-1.4 (AVR)
				2<f<2.75;0.5g<A<1g		
Pillago *et al.* [31]	Analytic FEM Empirical	LBEH	Not Optimized	$1gsin(2)f = 9/10.4$	$\approx 0.2 - 25$	$\approx 0.25 - 3.2$
Munaz *et al.* [32]	Semi-Analytic Analytic FEM	LBEH	Length of fixed magnets and number of floating magnets.	0.5gcos(2 6t)	2.2 (RMS)	2.2 (RMS)
Masoumi and Wang[33]	Analytic FEM Empirical	LBEH	Magnet assembly mounting configuration, magnet spacing, and magnet material.	$3.4gsin(2\pi ft)6 < f < 12$	13.8-42.9 (MAX)	13.8-42.9 (MAX)
				$\text{Asin}(2\pi 9t)1.22g < A < 3.41g$	1.9-43.4 (MAX)	1.9-43.4 (MAX)
Wang *et al.* [34]	Analytic FEM Empirical	LBEH	Magnet assembly mounting configuration, number of moving magnets, and spacing between fixed magnets.	$\text{Asin}(2\pi ft)0.35g < A < 0.85g4 < f < 10$	0-0.09 (MAX)	0-0.9 (MAX)
				cust. 5-9 km/h	8.9-34.6 (AVR)	0.2-0.7 (MAX)
Pancharoen *et al.* [35]	Analytic FEM Empirical	LBEH	Coil Resistance	$0.5\text{gsin}(2\pi 14t)$	0.2	0.04
Struwig *et al.* [36]	Analytic FEM Empirical	LBEH	Number of coils, height and spacing of coils, number of magnets, distance between floating magnets, and overall device size.	cust. A = 2.2g	6.5-6.8 (AVR)	0.26-0.27 (AVR)
Category 3						
Mann and Sims[37]	Analytic Empirical	LBEH	Not Optimized	$\text{Asin}(2\pi ft)0.21g < A < 0.95g6 < f < 13$	$\approx 410^4 - 1.210^2(MAX)$	$\approx 0.4 - 11.6(MAX)$
Bonisoli *et al.* [38]	Analytic	LBEH	Not Optimized	cust. 40-100 km/h	ND	2-8 (MAX)

Reference	Model	Architecture	Optimization Methodology	Excitation	I (mA)	U (V)
Morais *et al.* [39]	Analytic Empirical	LBEH	Coil length and height, length and weight of the inertial mass.	$A\sin(2\pi ft)0.09g < A < 0.55g0.75 < f < 1.85$	$\approx 0.21.1(RMS)$	$\approx 1.2 - 5.6(RMS)$
Morgado *et al.* [40]	Semi-Analytic Analytic Empirical	LBEH	Not Optimized	Free fall from a height of 15 mm.	-	-
Yang *et al.* [41]	Semi-Analytic Analytic FEM	LBEH	Not Optimized	$8g\sin(2\pi 20t)$	10.59 (MAX)	2.67 (MAX)
Aldawood *et al.* [42]	Semi-Analytic Analytic FEM	LBEH	Not Optimized	$0.04g\sin(2\pi 11t)$	$\approx 21,5$	≈ 3.2
Categoria 4						
Saravia *et al.* [43]	Analytic Empirical FEM	LBEH	Number of floating magnets, influence of the separated and the spacing between the fixed magnets.	$1g\sin(2\pi ft)4 < f < 10$	$\approx 7.1 - 29.2(MAX)$	$\approx 0.8 - 2.9(MAX)$
Geisler *et al.* [44]	Semi-Analytic Analytic FEM	LBEH	Permanent magnet dimensions, total inertial mass, magnetic period, number of windings in the coil, resistance and outer diameter of the coil, average magnetic flux and electric damping.	$1g\sin(2\pi 9.5t)$	$\approx 1.5(MAX)$	$\approx 1.5(MAX)$
				cust. 6.4/8 km/h	2-2.3 (AVR)	1.9-2.2 (AVR)
				cust. f = 6;A = 2g	2.6 (AVR)	2.5 (AVR)
Apo e Priya[45]	Analytic Empirical FEM	LBEH	Dimensions and number of floating magnets and height of the coil.	$A\sin(2\pi ft)0.25g < A < 1g13 < f < 16$	1.2-1.8 (RMS)	4.7-7 (RMS)
Zhang *et al.* [46]	Semi-Analytic Analytic FEM	LBEH	Not Optimized	$A\sin(2\pi 4t)0.03g < A < 0.11g$	0.6-3.5(RMS)	0.1-0.7 (RMS)
				cust. 1.6-12.9 km/h	$\approx 0 - 18.3$	$\approx 0 - 1.8$

Table 2.2: Comparison of electromagnetic generators by different authors based on Carneiro *et al.* [1].

Terminology: ND - not defined; cust. - customized; AVR - average; MAX - maximum; RMS - root mean square.

Carneiro *et al.* [1] separate the models used by the authors according to the different quantities modeled: Magnetic field, damping coefficient or force, repulsive magnetic force, coupling coefficient, electric current and induced voltage. The graph in Figure 2.7 presents the quantity for each type of model used for each modeled magnitude by number of papers. It can be seen that the most chosen model in most cases is the analytical model, which is superior in all magnitudes, except the magnetic field, where the most used is the FEM. Another factor that should be noted is that the electric current is the

one with the most papers where it is not modeled.

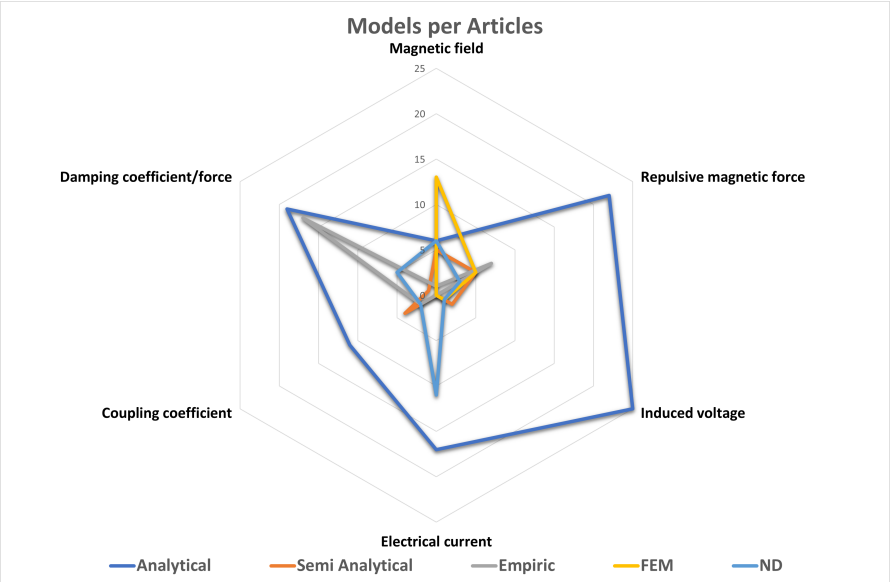

Figure 2.7: Comparison of model types by elements in number of papers according to Carneiro *et al.* [1].

In Carneiro *et al.* [12] is presented a study about the generator that will be used for this project. In this, a model of the generator was developed, tested and validated. The model will be further explorer in this work, once it will be used.

2.1.2 EMG and artificial inteligence

A preliminary study of the use of artificial intelligence in EMG were made in Rocha [5]. The author model a generator dynamics using an ANN to developed structural design for the generator. It uses different network architectures, based on the Nonlinear Autoregressive with eXogenous Input (NARX), and training algorithms in order to optimize the model features.

The author points out that the main limitations of the harvester behavior prediction made in his work when compared with other works. His approach is constrained to the intrinsic features of the generator used for data collection, while others make it possible to vary parameters that are unique to each device, like damping or friction coefficients. Beside this, the work didn't focused in use a artificial neural network to predict the harvester behavior for a broad range of excitation frequencies and for different configuration for the generator, as input load resistance for example.

2.1.3 Triboelectric Generators (TENG)

Triboelectric nanogenerators are a new power generation technology that converts small-scale mechanical energy into electrical energy. The working principle of a triboelectric generator is based on the effect that bears the same name, triboelectric effect, and electroinduction. The triboelectric effect consists in the act of transferring a small charge of static electricity generated by contact between two different surfaces. This

contact makes the surfaces electrically charged with opposite charges from each other, as presented in Khorsand *et al.* [7]. This effect can be obtained by friction or by contact and separation between two tribomaterials. This two materials need to have different electrical charge properties, one with the property of gaining charge and the other of loosing charge. This two operating principles of such generators are: contact and sliding, as is pointed out in Niu *et al.* [47]. In Wang *et al.* [6] the triboelectric effect and its basic equations for the contact mode are described. As described, the potential difference created by the separation (x) of the post electrification surfaces ($V_{OC}(x)$), the amount of charge exchanged ($Q_{SC}(x)$) and the capacitance ($C(x)$) of the generator (they tend to have a capacitive behavior) affect the voltage of the charged generator according to Equation 2.3.

$$V = -\frac{1}{C(x)}Q_{SC}(x) + V_{OC}(x) \tag{2.3}$$

Under short circuit conditions the charge will be carried between the two electrodes, this condition can be expressed by Equation 2.4.

$$0 = -\frac{1}{C(x)}Q_{SC}(x) + V_{OC}(x) \tag{2.4}$$

The current generated can be expressed by Equation 2.5

$$I = C\frac{\delta V}{\delta t} + \frac{\delta C}{\delta t} \tag{2.5}$$

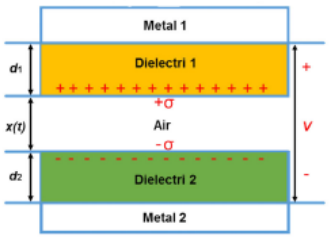

Figure 2.8: Theoretical model of a triboelectric generator for the Equations 2.3 e 2.4 [6].

Rodrigues *et al.* [2] describe the four basic operation modes of a TENG: (i) The Vertical Contact-Separation Mode (VCTENG), which operates with the excitation coming from the discontinuous impact on the generator, and can be dielectric-dielectric or conductor-dielectric. This mode of operation is characterized by simple design, high power density. (ii) Lateral Sliding Mode (LSTENG), with a structural design identical to VCTENG, the difference being that there is a fixed part at the bottom while the top part moves longitudinally and parallel to the former in order to generate contact and separation with it. In this mode, the excitation is printed laterally, with the potential difference arising from the constant change of surface in contact. Some applications example include wind energy transformation, hydraulic energy and gas flow. (iii) Single-Electrode mode (SETENG), which can be used in association with the two aforementioned modes. The principle of operation is shown in Figure 2.9a. The primary

electrode can be triboelectric or be attached to a triboelectric material. The other electrode serves as a reference to generate the potential difference. According to the author, this is the most practical and feasible mode because it is the only one that allows one of the plates with triboelectric material to move freely. (iv) Freestanding Triboelectric-Layer Mode (FTENG), a newer mode of TENG, with the two typical configurations, contact and sliding. As presented in Figure 2.9b, in this mode the triboelectric material approaches the two fixed electrodes. The author highlights a higher energy conversion efficiency compared to the other modes, in addition to the use of a smaller surface area and more long-term stability. Faced with LSTENG, this mode is able to generate energy without physical contact between surfaces, uses less material, and generates less heat. The author then presents the equations that describe each of these modes. That equations are presented in Table 2.3.

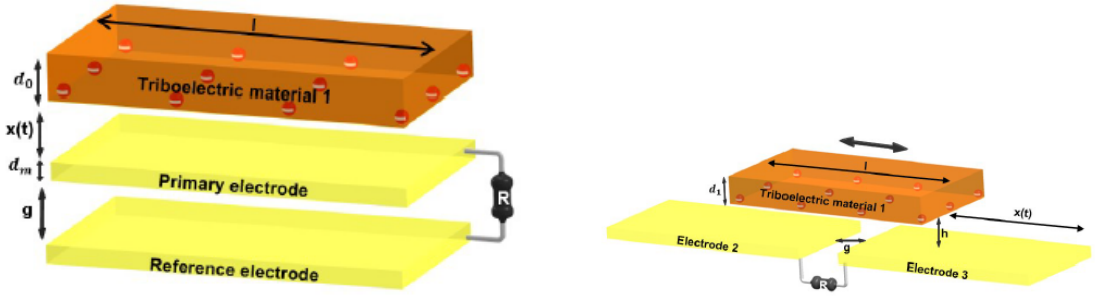

(a) SETENG operation diagram. [2] (b) FTENG operation diagram.[2]

Figure 2.9: Examples of different modes of TENG

Mode	Q_{SC}	V_{OC}	V-Q-x
VCTENG	$\frac{S\sigma x(t)}{d_0+x(t)}$	$\frac{\sigma x(t)}{\epsilon_0}$	$V=-\frac{Q}{S\epsilon_0}[d_0+x(t)]+\frac{\sigma x(t)}{\epsilon_0}$
LSTENG	σxw	$\frac{\sigma x d_0}{\epsilon_0(1-x)}$	$V=\frac{d_0}{\epsilon_0 w(1-x)}Q+\frac{\sigma d_0 x}{\epsilon_0(1-x)}$
SETENG	$\frac{\sigma xl}{1+\frac{C_1(x)}{C_2(x)}}$	$\frac{\sigma xlC_2}{C_1C_2+C_2C_3+C_1C_3}$	-
FTENG	$\frac{2\sigma Sx}{d_0+g}$	$\frac{2\sigma x}{\epsilon_0}$	$V=\frac{d_0+g}{\epsilon_0 S}Q+\frac{2\sigma x}{\epsilon_0}$

Table 2.3: TENG modes equations [2].

Compared to other energy harvesting methods, the triboelectric has the advantage the high output power, high efficiency for various types of mechanical energy sources, wide variety of materials, good cost-effectiveness and easy manufacturing, able to power equipment and sensors for various applications, as pointed out by Niu *et al.* [47], Chen *et al.* [48], Rodrigues *et al.* [2] and Wang *et al.* [6]. It is a technology with great potential for energy production from environmental sources.

In Wang *et al.* [6] the use of a TENG as a flexible generator for use in flexible technologies is discussed. The aim of the paper is to present the state of the art regarding such generators. This approach includes fundamental design structures, operating mechanisms and performance, as well as solutions for performance improvement. The

paper covers two modes of operation of this type of generator: contact and separation. This mode of operation has two types of configurations, dielectric-dielectric, example illustrated in Figure 2.8, and conductor-dielectric for the different materials. For the conductor-dielectric generators, the difference is that one of the plates is replaced by a conductor that can be used as a triboelectric layer in addition to its layer electrode. According to the author, the latter is more practical, since it is easier to move the triboelectric layer around. Also cited in the paper are solutions for hybrid generators and also some examples of practical applications, these being: LED driving, wireless sensors and biomechanical monitoring.

A more specific approach is taken in Rodrigues *et al.* [2] and in Xi *et al* [49], for the use of TENGS associated with sea waves. In the first, a review of the state of the art of the use of TENG to generate energy from this type of source is made. According to the author, triboelectric generators are a good solution to power equipment and sensors for offshore use because of their high power. Therefore, the author emphasizes their use in conjunction with more traditional power generation technologies for this purpose. The author also discusses the advantages of using this system over traditional alternatives, as well as possible applications that will benefit from the high efficiency with low amplitude excitations of these generators. In the second paper, a system of intelligent buoys self-powered by TENG using tidal power is proposed.

The performance of TENG strongly depends on the choice of triboelectric materials to be used, since they directly impact the amount of charge that can be exchanged by the surfaces, so Rodrigues *et al.* [2] highlight the types of triboelectric materials and presents them like it is represented in Figure 2.10, according to their respective polarities in addition to the charge exchange capacity of each material. The polarity of a material relates to its ability to gain or lose electrons, positive polarity materials tend to lose and negative polarity materials tend to gain. In the figure, the farther one material is from the other, the greater the capacity for charge exchange between them. The paper also points out different ways to improve performance through some changes in the materials, such as chemical changes.

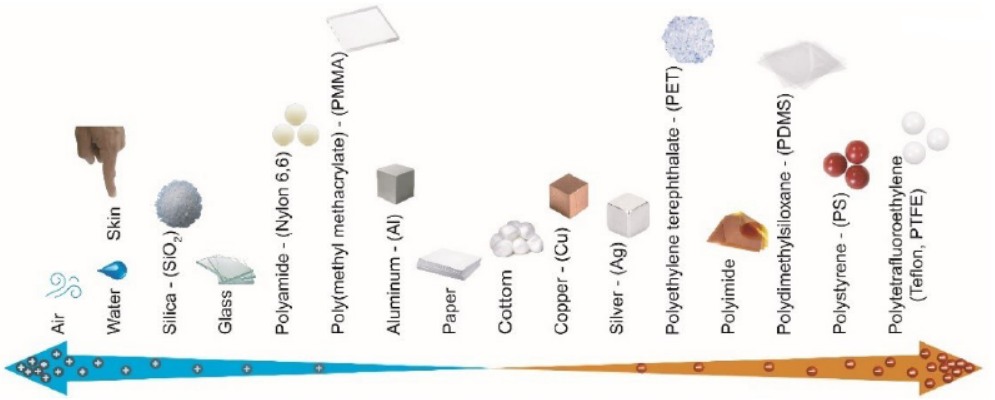

Figure 2.10: Most promising triboelectric materials [2]

The equations related to LSTENG are also presented in Niu *et al.* [47]. Due to the difficulty in finding the precise analytical V-Q-x relationship for these generators, the

FEM was used to calculate the electric potential and based on this, analytical and semi-analytical models were constructed by interpolation. This theoretical analysis is done for the two types of LSTENG, the conductor-dielectric and the dielectric-dielectric. The approach in the paper is only theoretical.

Hybrid generators based on triboelectric generators are the subject of study presented by Chen *et al.* [48]. In the paper, the possibilities of creating generators that use, along with triboelectric technology, electromagnetic and piezoelectric generator technology are demonstrated, and comparisons are made between these generators and the triboelectric one. Another paper that deals with hybrid generators is presented by Vidal *et al.* [50], where review of hybrid triboelectric-electromagnetic nanogenerators is provided focusing on recent advances in the area of electromagnetic-triboelectric vibrational energy harvesting.

Other applications of TENG are discribed in Wu *et al.* [51], in that paper the generators are applied to recognize the way a user types pattern on their keyboard, with a focus on cyber-security. In He *et al.* [52] a triboelectric sensor is used to realize a human-machine interface. In Gua *et al.* [53] a 3D printed triboelectric generator is used for voice print recognition. All of these papers address how triboelectric generators work in different ways, giving a better idea of how it can be applied and how it works.

2.1.4 TENG and artificial inteligence

Different approaches for the use of artificial intelligence associated with TENG were proposed, ranging from its use for modeling a generator dynamics and find the best features possible to deter patterns in the generator output to make predictions about the input applied. Three studies were found were artificial intelligence is used along side the TENG. In Table 2.4 these generators are compered by presenting the outputs, architectures, optimization methods and type of external excitation, if suitable, of each one of them.

In Khorsand *et al.* [7] the goal is to simulate models of lightweight sliding mode generators (LSTENG) with a high output voltage (close to 6 V), that has its diagram displayed at Figure 2.11. In the work it is intended to find the best choice of characteristics for such a generator, so that it can be as light as possible. The pair of triboelectric materials chosen was polytetrafluoroethylene (PTFE) and polyamide (Nylon 66), both, initially, with the same dimensions (L=10 cm, W=10 cm and t=250 μm), each connected to a chromium metal electrode (t= 50 nm) and with a gold coating (t=500 nm) on the contact surface. The paper analyzes the effects of changing the main characteristics of the generator, contact surface, dielectric plate thickness and external charge, on its outputs, current and voltage, and on its total weight. Two parallel artificial intelligence methods, the Two-Particle Swarm Optimization (PSO) method and the Co-Evolutionary Particle Swarm Optimization(CPSO) method, are used to identify the best choice of parameters of dynamics. The algorithm, demonstrated by the schematic in Figure 2.12, has two loops. The inner one that searches for the optimization at the predetermined values within the search space, and the outer one, which applies the penalty constraints. According to the authors the algorithm showed a greater performance when compared with other artificial intelligence methods capability. The algorithm was coded using MATLAB.

A similar approach is chosen in Khorsand *et al.* [8], where the optimal modeling of a disk-shaped rotating generator is studied, as shown in the diagram in Figure 2.13a.

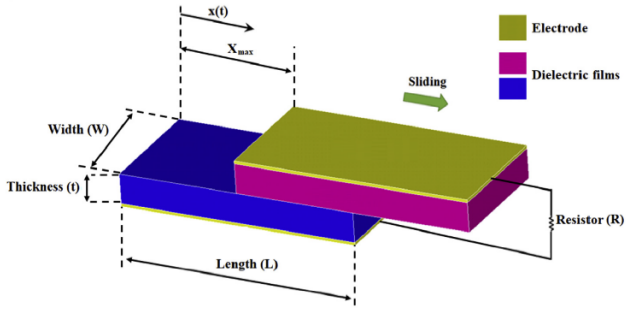

Figure 2.11: Diagram of triboelectric lateral sliding gerator [7].

According to the paper, the choice of this design format is due to the fact that it enables efficient generation of energy from random sources, particularly in cases of *blue energy*. The paper introduces the characteristics of this type of generator, to study the effects of kinematics and the chosen geometry on the generator outputs. Both a theoretical and experimental approach is taken to validate the results. The output values of the generator are also predicted under various conditions. The triboelectric pair chosen is PTFE (stationary disk) and nylon 66 (rotational disk). The disks have inner radii of 5 mm and outer radii of 50 mm, and a thickness of 250 μm. This generator shows a 5% loss in its power after performing 10,000 cycles, as presented by Figure 2.13b, due to wear of the gold layer covering the triboelectric film. Another factor that is highlighted in the paper is the edge effect, which for rotating TENG is quite considerable, which ends up generating interaction between two adjacent rods in the disks, that entails a decrease in sensitivity to the potential variation that occurs due to the rotation of the disk, thus affecting the output power of the generator. The proposed solution is to choose a large value of the ratio of the disk's arc to its thickness (L/d), thus decreasing the negative consequences of the edge effect.

The optimization method chosen by Khorsand *et al.* [8] was an artificial intelligence algorithm, shown in Figure 2.14, that encompasses and is based on a method known as grey wolf, which basically has three main steps: searching for a prey in the search space, enclosing the prey, and attacking the prey. This algorithm goes through several iterations, in which the local and global results are considered in the search for the optimal result. In parallel to this algorithm two mathematical computation algorithms calculate all the derivatives and integrals for each iteration. The goal is to find the values of the design variables considered for the optimal performance of the generator. The advantages of the chosen method include the fact that it is generalist and therefore can be used for the analysis of several TENG structures, besides the chosen artificial intelligence being able to perform any prediction and optimization study, with a good cost-benefit relation in what concerns processing power and time demanded and not being stuck in local maxima.

In Ji *et al.* [54] solutions are presented using TENG for acquisition of writing and voice signals. The idea stems from the high sensitivity of TENG to micro vibrations, and advantages, such as their manufacturing cost-effective and a flexible structure that favors a wide variety of usage possibilities also reinforce their choice. For this, a contact TENG with copper mesh (with a thickness of $\approx$98 μm) and Sodium chloride (NaCl) molded Polydimethylsiloxane (PDMS) were used as triboelectric plates, with the copper mesh in

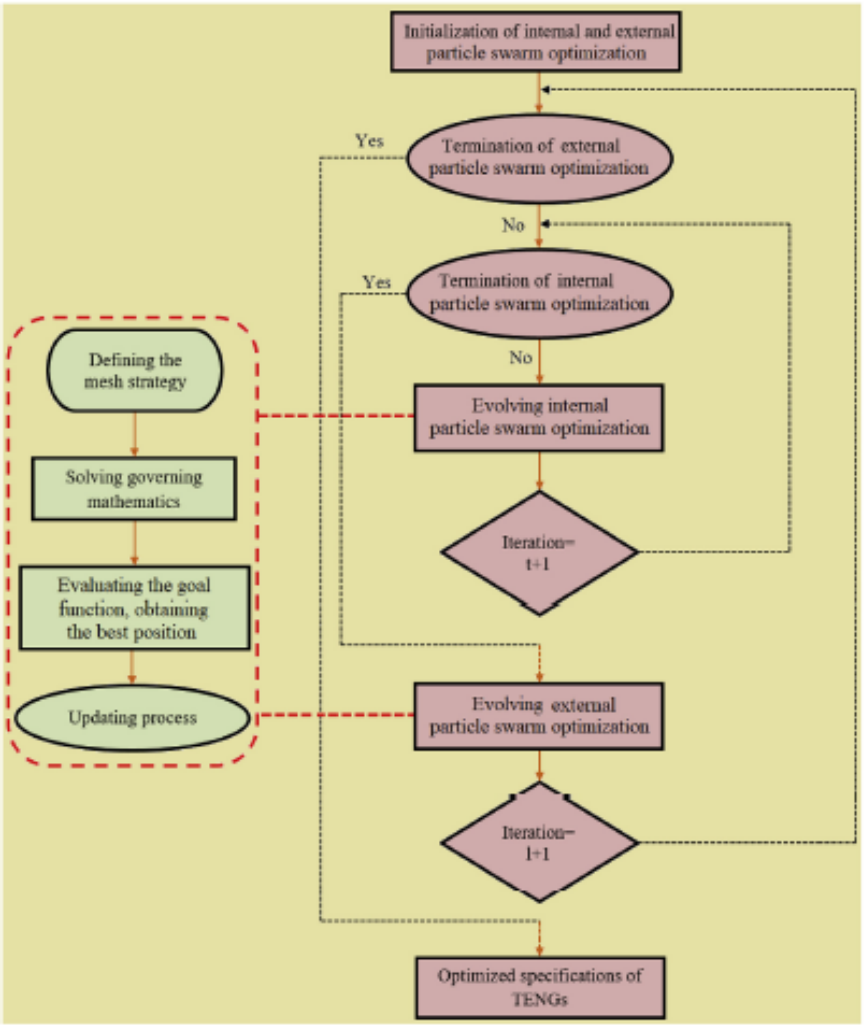

Figure 2.12: TENG optimization algorithm [7].

the top layer of the generator.

The machine learning (ML) method used by Ji *et al.* [54] is the Support Vector Machine (SVM), which is a supervised method for linear and nonlinear classification. This algorithm defines lines or hyperplanes based on edge functions to perform the classification of the data into classes. To reduce the processing required, another method, t-distributed stochastic neighbor embedding (t-SNE), was used, which can identify only the most important set of variables, thus reducing the size of the data vector.

2.2 Artificial Neural Networks

Artificial neural networks are computational systems that are inspired by the central nervous system (brain) of some animals. Its great attractiveness is the capacity of solving non-linear problems through their learning capabilities using several computational processing elements, the neurons, which act in layers interconnected to each other, as

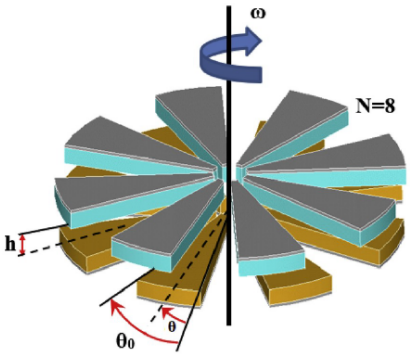

(a) Disk triboelectric generator [8].

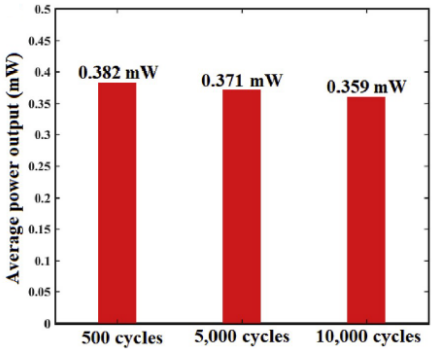

(b) Average power for cycle of the disk TENG [8].

Figure 2.13: Disk TENG diagram and its respective average power per cycle graph [8].

Reference	Tribo-materials	Architecture	Optimization Methodology	Excitation	I (μA)	U (V)
khorsand *et al.* [7]	Nylon 66 PTFE	SLTENG	PSO CPSO	-	$\approx$ 3.75 (Max)	$\approx 0.1 - 1.4 \times 10^4$
khorsand *et al.* [8]	Nylon 66 PTFE	Disk TENG	Grey wolf	$4.58Hz$ (SC) $15.0Hz$(OC)	$\approx$ 2.12 RMS (SC)	$\approx$ 500 pico (OC)
Ji *et al.* [54]	NaCl PDMS	VCTENG	-	1 N-10 N pressure	NA	0.2 V (Max)

Table 2.4: Comparison of triboelectric generators.
Terminology: NA - not applicable; MAX - maximum; RMS - root mean square; OC - open circuit; SC - shot circuit.

illustrated by Çelik *et al.* [11]. These layers can be input, output, or hidden layers, which are the intermediate layers of the network. With this, without prior knowledge of the data of a given system, it is possible to predict the system behavior for different inputs. They are able to solve problems with complex, non-linear, or even unknown characteristic equations.

A general and introductory approach to neural networks is presented in Hagan *et al.* [9] as well as several examples of algorithms. For a neural network, each neuron can have multiple inputs (p), but is only able to generate one output (a). A neuron output is obtained by a multiplying the input by this neuron weight (W), that indicates the impact that each variation on the input that neuron will have in the system as a whole, and summed with a value named bias. The value obtained with this two operations is inputted in the neuron transfer function (f), which can be the most diverse and its choice is related to the problem to be solved, for example a linear function, sigmoid and hyperbolic tangent. The output for a neuron can be described by the matrix expression $a = f(Wp + p)$, as illustrated in Figure 2.15.

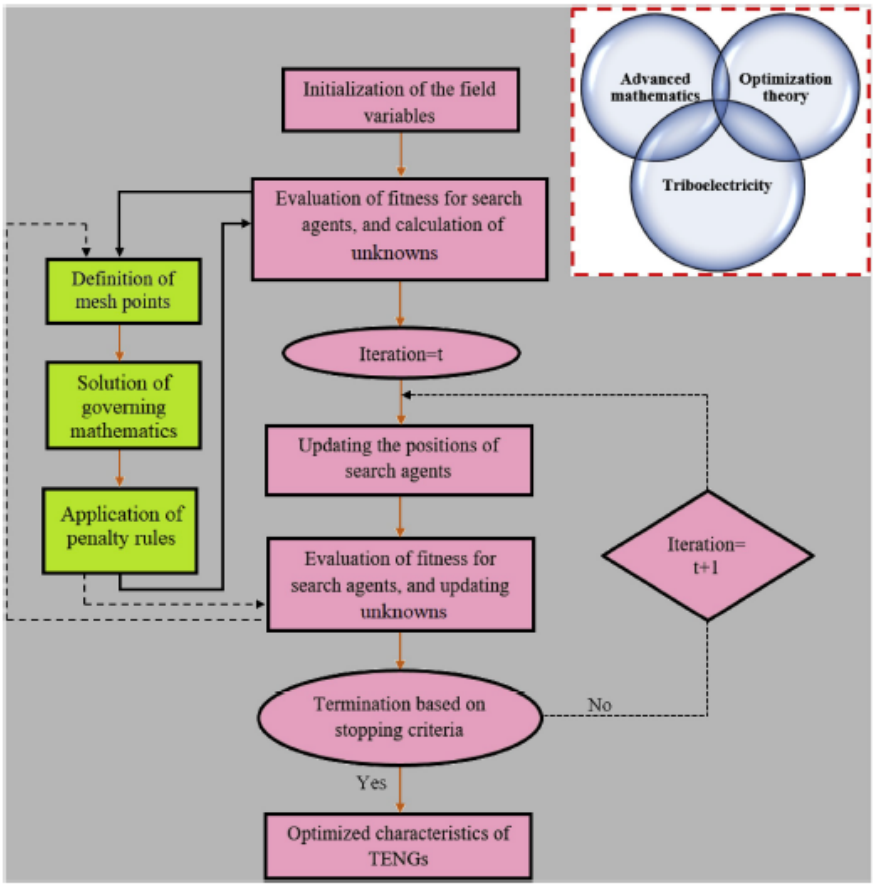

Figure 2.14: Grey wolf based algorithm for design optimization [8].

The neurons are separated in layers. The output of each neuron serves as input for the next layer neurons, repeating the same process, in the next neurons, until the last layer where the neurons output represent the network output, as shown in Figure 2.16. The weights of neurons of each layers are organized in a matrix W, while its bias are in matrix b, with the layer number being superscript. For the matrix W the row indices indicate the neuron and the collumn represents the input. So the element W_{ij} is the input j at the neuron i.

A thing that is very useful in artificial neural networks is the building blocks. The only one that will be used in this work would be the delay block, illustrated in Figure 2.17. According to Hagan *et al.* [9], the delay output $a(t)$ is computed by $a(t) = u(t-1)$, with the $u(t)$ being the block input.

The error of each neuron is calculated by calculating the difference between the intended value for the output (target value) and the network actual output. The performance index, that indicates how close to the target values the output is, is calculated using this error. Normally the performance index is the mean square errorMSE), which is the squared sum of the error, indicated by Equation 2.6, where $d(n)$ is the desired output and $y(n)$ is the predicted value. The weights and biases of all layers were adjusted so as to minimize the index during the process called training, making it possible for a ANN to adapt to different types of problem. The equation to calculate the new set of weights

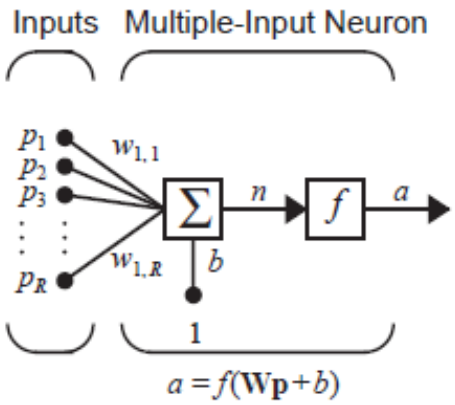

Figure 2.15: Multiple-input neuron [9].

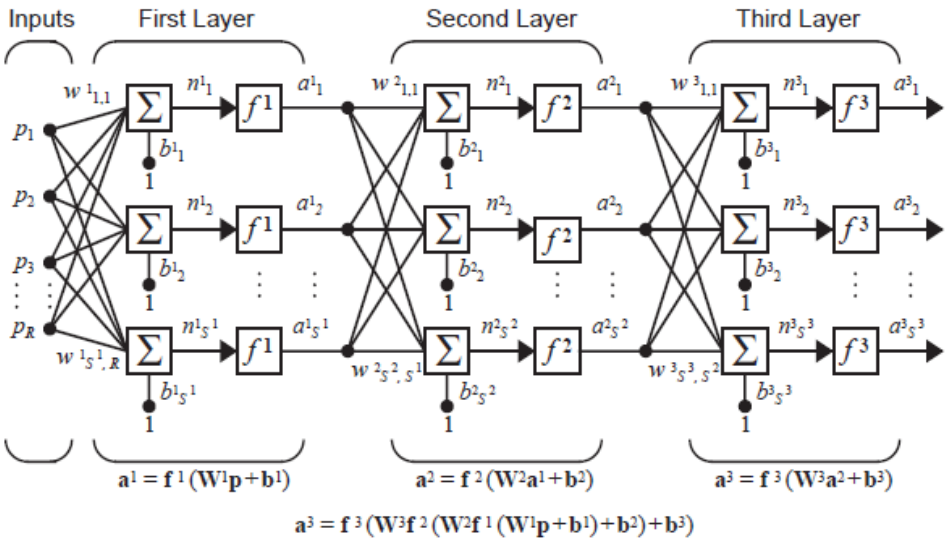

Figure 2.16: Three-Layer network [9].

and bias depends on the training algorithm.

$$E(n) = [d(n) - y(n)]^2 = e^2(n) \tag{2.6}$$

One of the training algorithms is called back-propagation. Algorithms based on it present a very steep and descending approximation graph, which uses the chain rule to calculate the derivatives of the quadratic errors, its name comes from the fact that the derivatives are calculated starting from the last layer of the network and propagating to the first, using the aforementioned chain rule to calculate the derivatives in the intermediate layers. Weights and biases are calculated from Equation 2.7 and 2.8, with α being the learning coefficient.

$$w_{i,j}^m(k+1) = w_{i,j}^m(k+1) - \alpha \frac{\delta E}{\delta w_{i,j}^m} \tag{2.7}$$

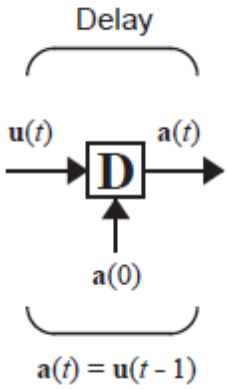

Figure 2.17: Delay block [9].

$$b_i^m(k+1) = b_i^m(k+1) - \alpha \frac{\delta E}{\delta b_i^m} \tag{2.8}$$

2.3 ANN in energy harvesting

The use of artificial intelligence in renewable energy production is already a reality that aims not only to optimize energy conversion, but also to improve the management and distribution of that energy, as presented by Jha *et al.* [55]. In the paper one finds several applications and techniques of artificial intelligence in this area. Although it does not directly address the same type of generator to be used in this work, different techniques applied to energy production were analyzed.

Since mechanical vibration micro-generators have a very short operating bandwidth, as already mentioned, for some applications it is necessary to use some techniques to adjust this frequency to the frequency of the environment. In Singh *et al.* [10], the goal is to accomplish this adjust in a piezoelectric generator that will be used to power a smart tire sensors system from the mechanical vibrations coming from the tire itself and generated by its rotation. In the paper, it is observed that the impedance load to which the generator is connected influences its vibration frequency and, consequently, the output voltage, With this, the optimal load is calculated as a function of frequency and the electromechanical coupling coefficient. A buck-boost topology circuit is used to perform the AC-DC conversion in addition to introducing impedance to the generator. With this, to maximize its power, the input impedance can be controlled by changing the duty-cycleD) of the circuit, according to Equation 2.9.

$$R_{in} = \frac{2Lf_s}{D^2} \tag{2.9}$$

To control the duty-cycle an adaptive system was created from an ANN based on a closed loop system. The objective of the work was to create a network capable of estimating the optimal impedance for each frequency to which the tires could be submitted. The inputs to the ANN are: acceleration signal, tire pressure, speed, and load on the tiresonly for offline training). The network goes through an offline training, and then

operates in the online system. During the offline training, test data was generated, which was used for recognition during the online procedure, disregarding bad inputs using the normalGaussian) distribution method.

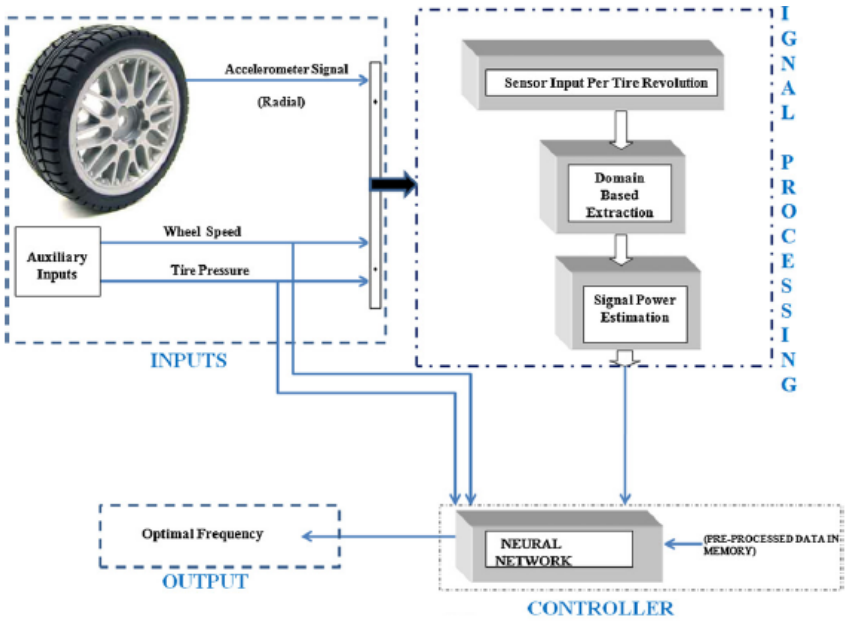

Figure 2.18: Smart tires system architecture [10].

The chosen architecture was a two-layer feedfoward ANN and the use of back-propagation for its training. The activation functions of all layers were defined as tangent sigmoid or hyperbolic tangent.

The Levenberg-Marquardt algorithm, which is a type of back-propagation, was used in order to train the network. The effects of the number of neurons in the hidden layer on the performance of the network were tested, finally a hidden layer of 8 neurons was chosen. The base scheme for this architecture is shown in Figure 2.19.

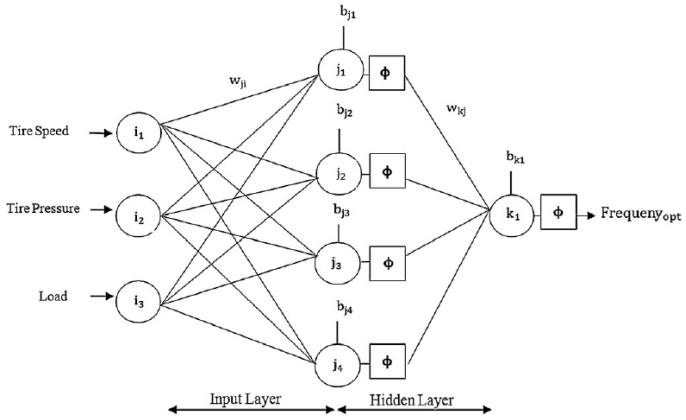

Figure 2.19: Architecture diagram for the ANN [10].

The results obtained by Singh *et al.* [10] are displayed in the graphs in Figure 2.20.

As noted, the tests were performed for both the tires in dry and also wet conditions. It can be seen that the largest estimated frequency error is no greater than 6%.

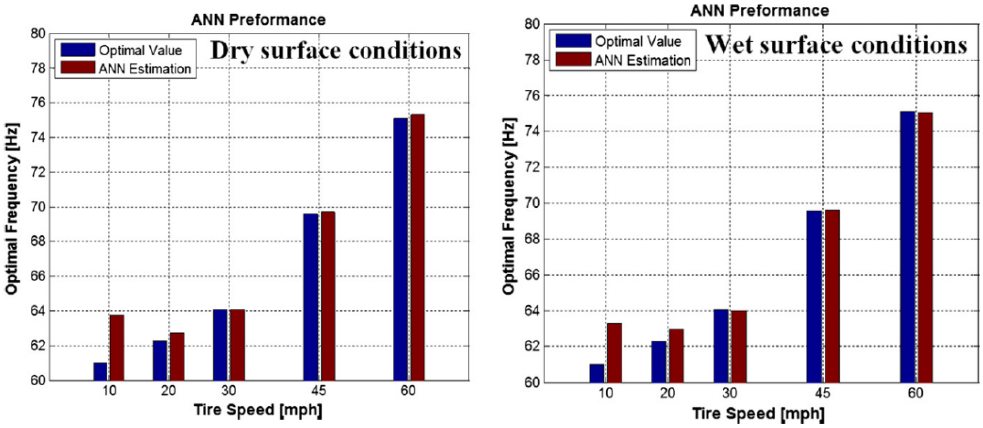

(a) Dry tires tests results

(b) Wet tires tests results

Figure 2.20: Comparison between experimental results and ANN prediction values [10].

Whereas in Çelik *et al.* [11], the frequency tuning of a physical piezoelectric pendulum generator, which in that case will be magnetically excited, is performed. The architecture of the neural network shown in Figure 2.21 has as inputs the resistive load of the generatorR_L) and the excitation frequency$f$) and relates them to their respective generated powerP_{out}), which is the output of the ANN. The network is multi-layer with feedfoward, with one input layer, two hidden layers, the first with 15 neurons with the hyperbolic tangent as transfer function, and 10 neurons in the second with a linear function, and one output. In this particular network, the chosen biases as well as their activation functions were determined by trial and error. The inputs and outputs were normalized according to Equation 2.10 before starting the training process, where x_r is the real value, x_n the normalized value, and x_{max} and x_{min} the maximum and minimum values, respectively. According to the author, normalizing the system's inputs and outputs improves its performance and decreases the processing time considerably.

$$x_n = \frac{x_r - x_{min}}{x_{max} - x_{min}} \tag{2.10}$$

For training some data was benchmarked to be used. Some values of R_L, with values of $10.0M\Omega$, $5.6M\Omega$, $3.2M\Omega$ and $1.0M\Omega$, and the excitation frequency, within the range of 4.25 to 6.53 Hz, were used to determine their respective output powers. For each resistive value, the outputs for 28 different frequency values were measured.

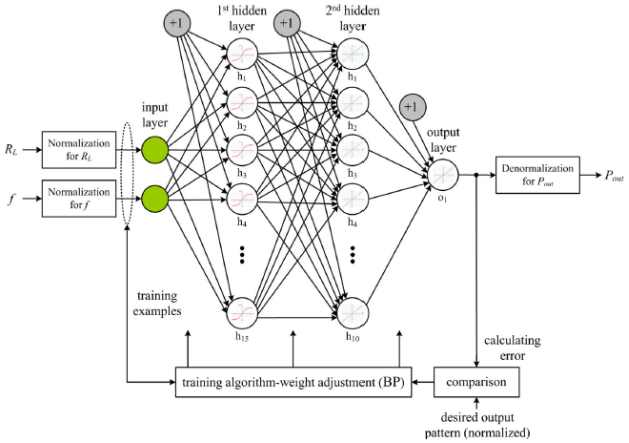

Figure 2.21: ANN presented by Celik *et al.* [11].

The network was trained using the back-propagation method, which at each iteration adjusted the values of the weights, that started with random values between -1 and 1. The training was done in an offline simulation system in ANSI C. At the end of the training, the values of the weights assigned to each neuron began to characterize the ANN, and thus it could be tested with new values not yet processed by it. Low values for the learning coefficient and momentum were chosen by the author in order to minimize the error curve gradually, once the network was been inefficient at the beginning of the training process. After 800,000 training cycles, the error became 6.65×10^{-3}. At the end, the prediction capability of the net proved to be efficient for new untrained values.

Chapter 3

Materials and Methods

This chapter will discuss the following topics: Experimental setup, development setup training data, ANN development, experimental data and data analysis.

3.1 Experimental Setup

The data used in this work, both simulated and experimental, is based on the generator shown in Figure 3.1, described by Carneiro *et al.* [12], not published but submitted, under a sinusoidal external excitation $A\cos(2\pi ft)$. According to the author,an EMG prototype was developed which is composed by a hollow cylindrical structure, three cylindrical annuli hard-magnetic elements and two multi-layer coils connected in series, with a central stacked free-magnet experiencing levitation by opposite poles facing each other. To create an adaptive performance, instrumentation was introduced to the EMG. This consisted in control the distance between fixed magnets, acting as an external mechanical energy source, which excites the harvester by a time-varying function. This instrumented harvester incorporates a microcontroller, an accelerometer and a step motor to axially move one of the non-levitating magnets to an optimal position by a open-loop control system as demonstrated in Figure 3.1a-e.The harvester aperture parameter describes the distance between the two fixed magnets, between 0 and 40 mm, which correlates to distances between 60 and 100 mm, as shown in Figure 3.1d. Furthermore, an ultrasonic sensor is used to monitor the levitating stack dynamics.

The simulated data is originated from the model to the electromagnetic generator and described in Carneiro *et al.* [12]. Thereby, the Equations 3.1, 3.2, 3.3, 3.4 [12] were used to describe the behavior of the generator and also used in the ANN training, as will be further discussed in this work. At the model used, the relations between the current position coordinates in each referential system is described by the Equation 3.1, with R_{iI} being unitary rotation matrix and T_I a translation vector. The Equation 3.2 describes the voltage, where ${}^{EM}\alpha$ is the electromagnetic coupling coefficient, which is described in Equation 3.3, the inner equivalent resistance of the coil is R_1 and L_1 is its equivalent inductance, described in Equation 3.4, being N_I the number of loops of the coil. As such, ${}^{EM}\alpha$ is dependable on the relative position between the free-magnet and the coils, as well as increases according to the number of loops present in the coil, as reported by Carneiro *et al.* [12]. This model was previously validated and tested using the experimental data.

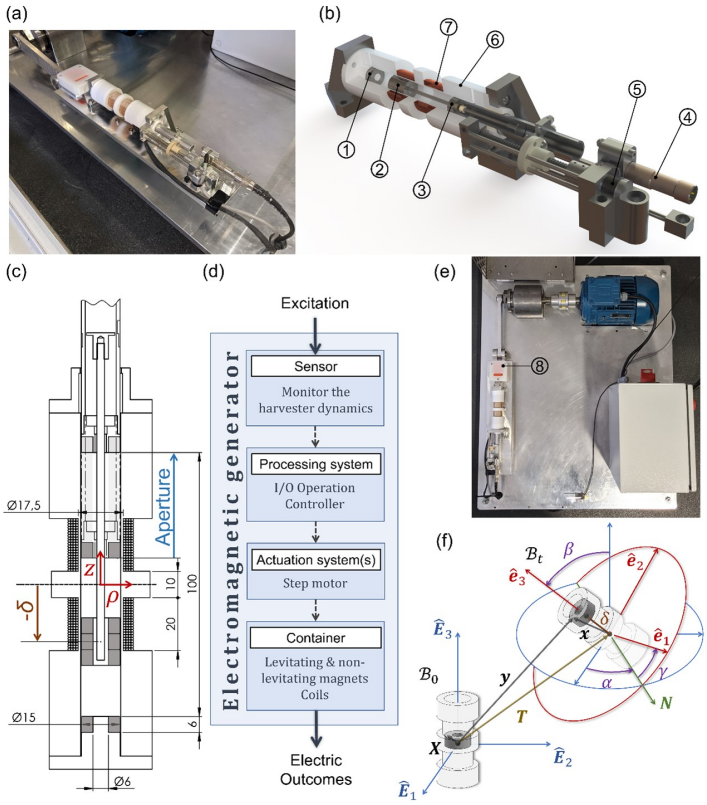

Figure 3.1: (a)Instrumented harvester photo; (b) Photo-realistic view (1 – non-levitating magnet; 2 – levitating magnet; 3 – adaptive non-levitating magnet; 4 – ultrasonic sensor; 5 – stepper motor; 6 – container; 7 – coil); (c) Cross-sectional view; (d) Diagram representing the open-loop control approach using data from the mechanical excitation dynamics; (e) Custom experimental platform and adaptive electromagnetic energy harvester (8 – accelerometer); (f) Translations and rotations of the cylindrical container and free-magnet, in relation to a time-independent reference configuration, in inertial and non-inertial frames [12].

$$y_I = R_{iI} x_i + T_I \tag{3.1}$$

$$V = -R_I I - L_I \dot{I} - {}^{EM}\alpha \dot{\sigma} \tag{3.2}$$

$${}^{EM}\alpha = \sum (\pm 1)_i^{EM} \alpha_i \tag{3.3}$$

$$L_I = \sum_{i=1}^{N_I} \sum_{j=1}^{N_I} (\pm 1)_i L_{ij} (\pm 1)_j \tag{3.4}$$

As described by Carneiro *et al.* [12], the experimental data were obtain in some tests made with the harvester. A motor, presented in the experimental setup, shown in Figure 3.1, imposes an axial motion on the generator with a sinusoidal time-changing

inertial force. In each experiment the authors vary a range of different external excitation frequencies, load resistance, harvester length variation and excitation amplitude. The outputs measured were the inertial mass dynamics and the signal from the two central coils connected in series, were measured.

3.2 Development setup

3.2.1 Hardware specifications

A university workstation was choose to run all developed algorithms due to the processing power required. The workstation's specifications are presented in the Table 3.1.

Processor	Intel(R) Xeon(R) CPU E5-2690 v4 @ 2.60 GHz 2.60 GHz (2 processors)
Memory (RAM)	256 GB
System type	64 bits

Table 3.1: Workstation specifications.

3.2.2 Neural Net Time Series

The MATLAB application that was used, the Neural Net Time Series, have its own Integrated Development Environment (IDE). Utilizing this, the user is able to choose some configurations both from the architecture and the training. All the development of the Network was coded, but the application is the base of it, thus being the configurations of it will be presented. Like it was previously referred, the chosen base architecture was the NARX, the first screen presented in the Figure 3.2, since it was needed to predict the output value using the input and past values of the series. In this configuration the default number of layers is two. Even not being possible to change the number of layers by using the application, it is possible to do it by code, however, since this number of layers were capable of solving the problem it was not needed to increase it.

Other configuration that was used for all the tests and developed networks was the data percentage of usage, as shown in the Figure 3.3. The training data is used in the network during the training process, with its weights and the bias being adjusted according to its error, that in this case is the performance index. The validation data is used to measure the network generalization, and to halt training when this generalization stops improving, as indicated by an increase in the mean square error of the validation samples. The testing data is used only to calculate the network's performance index. Dispite this, part of the data was previously separated for further development, as it will be presented forward. For this, the configuration chosen was the default one, 75% for training, 15% for validation and testing. It is important to highlight that each one of these dataset will have its performance calculated separately by the application. The way that this data is divided according to this percentage is also changeable. For all the ANN developed in this work, the data were randomly divided in blocks, what means that the input blocks (the set of data that includes all the inputs) were separated as a whole, so all the signal is selected together instead of being divided in peaces, that is the default of MATLAB.

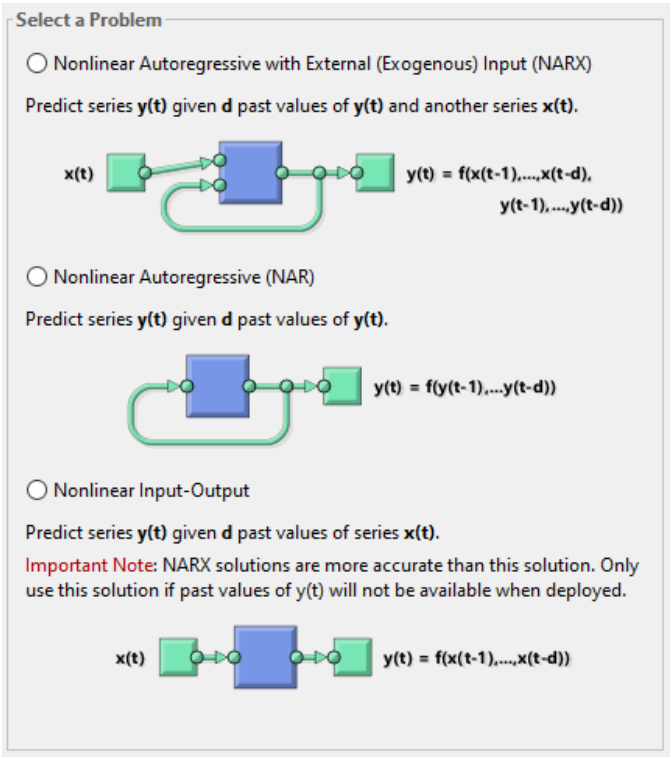

Figure 3.2: First application screen to choose the desire architecture.

The next parameter to be set is the number of delays and neurons utilized. The default value for neurons is 10 and for delays is 2. For the developed networks this numbers will vary for each case, as it will be later discussed. In some cases, that include the final network, a for loop was utilized to decide the better architecture. The example of this screen is shown in Figure 3.4.

The final selection is the training method. Although the deep learning library presents a variety of possibilities for feedforward network structure the application only presents three:

- Levenberg-Marquardt;
- Bayesian Regularization;
- Scaled Conjugate Gradient.

Two of these were the ones chosen to be tested in this project to be fitted for the problem presented, that being the Bayesian regularization and the Levenberg-Marquardt algorithms. This choice is justified because the problem presented on this work, a prediction problem, is close to function approximation problems. The Bayesian regularization algorithm is appropriate to solve this kind of problem [5]. The Levenberg–Marquardt, that is the default of the application, also uses the Bayesian regularization within it during its training process. According to the own application, the last algorithm typically requires more memory but less time and the second algorithm typically requires more time, but can result in good generalization for difficult, small or noisy datasets. Training stops according to adaptive weight minimization in this case.

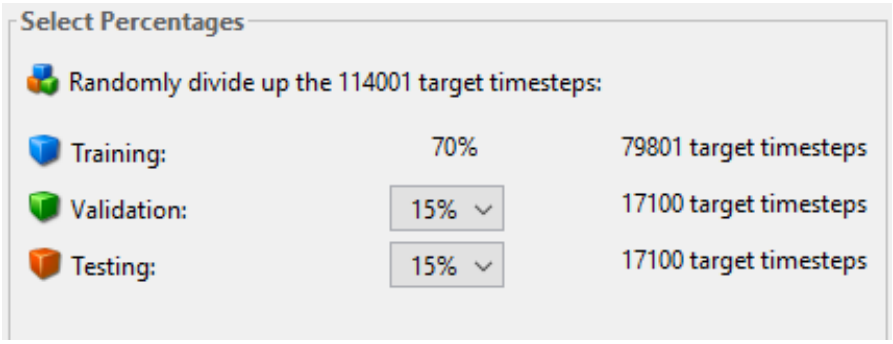

Figure 3.3: Screen to choose the percentage of data used in the training, validation and testing.

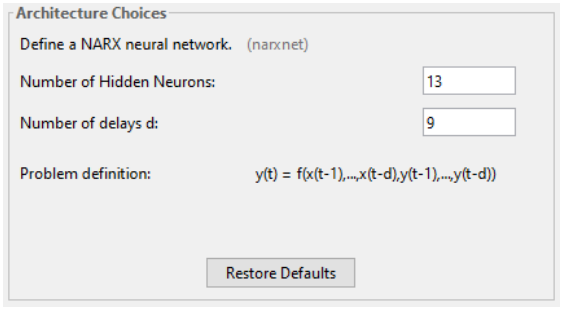

Figure 3.4: Screen to select the number of neurons and delays.

3.3 Training data

The ANN training was made only with the simulated data. The output considered for this work was the generator output voltage. For the training data, the time-variant signal for the generator's voltage was related with the excitation frequency (f), the excitation amplitude (A), the load resistance (R) and the harvester length variation (d). For each variable and related value a table with 2001 samples was built with the output. The database also contains the sampling time.

Firstly, the training data considered only the simulation data obtained with the upward frequencies trajectory output. This is important to expose once this kind of harvester dynamics presents a hysteretic behavior, as it will be discussed forward. For the final construction of the network all simulated data were used, upward and downward.

3.3.1 Hysteretic behavior

The EMG is a system that has, for some cases, a hysteretic behavior. Regarding the maximum value of the voltage signal for each frequency, amplitude, resistance and harvester length variation, depending on the approach, upward or downward frequency values, the system can exhibit two solutions for the same initial condition (frequency), as shown in the example in Figure 3.5. The theoretical behavior is presented, which due to the non-linearity was observed for upward and downward frequency sweeps, are identified by the black and red solid lines (stable periodic solutions), while the blue dashed line illustrates unstable periodic solutions.

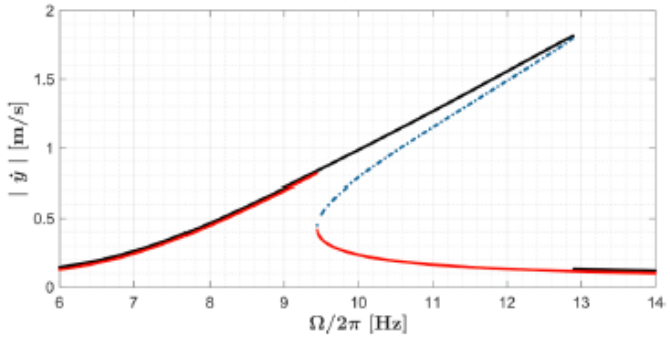

Figure 3.5: Relative velocity response with excitation amplitudes of 4 m/s^2 [1].

Thus, the hysteretic behavior factor can be a problem for the network to predict the system output and have to be considered in training for a fully functioning network. Hence, the base study was divided in two major parts, at first the data was obtained considering only upward frequencies; then, with that data, a network was modeled and tested. After this, the downward frequencies were introduced, and a final network was trained. In this work it will be considered that the classification of the input in upward or downward frequencies was already done.

3.3.2 Data quantity

One of the challenges of the work was to manage the algorithm run time mostly due to the data size to be processed. The number of files to be read is 66975 for the descending frequency trajectory and the same number for the ascending one. Each one of these files has around 51.5 KB, which in total is around 6.9 GB of data to be processed.

Such amount of data demands more processing power from the hardware in order to run the algorithm, which ends up to making it run exceptionally slow. To solve the problem, the program was divided in smaller subroutines. At the end of each one, all the variable were saved in data sets according to the subroutine that each variable should use next, and all the variables are cleared. Therefore, at the beginning of a new subroutine the needed data is loaded. With this method, using the memory with less data, the algorithm could have a smaller run time.

3.3.3 Data configuration

For the external excitation simulated signal, the data were aggregated for different frequencies with the same amplitudes, load resistance and harvester length variation, thus constituting a time-varying sinusoidal wave with the frequency gradually increasing with every 2000 samples, as observed in the example at the Figure 3.6. For the purpose of training, the same process was made for each value of the variables. All the possible values for each element are presented in the Table 3.2. The only exception is the load resistance, but all the other variables have values with fixed intervals in between (interval column in the Table 3.2). Thus being, for the load resistance, the intervals between the values used in the simulations is 1000 Ω, from 2000 to 10000 Ω, and 5000 Ω after this value.

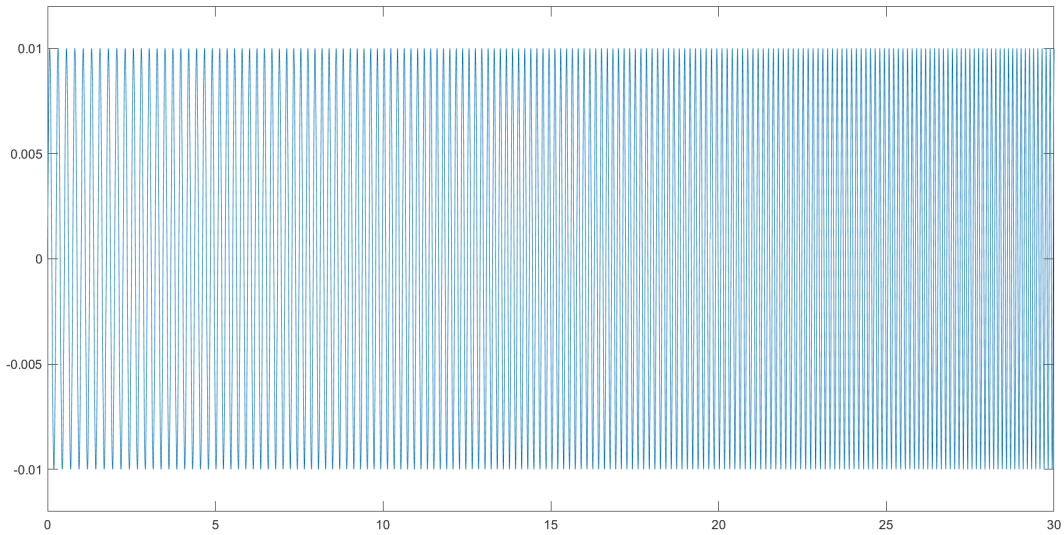

Figure 3.6: Example of one excitation wave for the network input.

Element	Unit	Minimum value	Maximum value	Interval	Number of elements
Resistance	Ω	2000	200000	1000 and 5000	47
Length variation	mm	0	40	10	5
Amplitude	m	0.002	0.01	0.002	5
Frequency	Hz	4	18	0.25	57

Table 3.2: Range of possible values for each variable at the simulated data.

The same idea is applied for the target signal, that is the desire of network's output. The values were gathered together one after another for the same corresponding input block. In the case of this training the chosen output signal was the generator voltage. An example of output signal is showed in Figure 3.7, it is possible to notice that the amplitude of the output should increase as the input frequency increase.

All data, inputs and targets, are divided in two variables, one for each. This variables are from the cell array type, so it is a set of arrays. Inside each array, each line would represent a different input or target variable, and each column a set of data. A random example of a cell array utilized is shown in the Table 3.3. Each array inside the cell will contain all the inputs of each block in that index of the signal. So, to exemplified, the first array will have all the first elements of all inputs of all the sets of data. The organization of the data inputted into the ANN will be discussed in more detail in Subsection 3.4.1.

	Set of data 1	Set of data 2	Set of data 3
Input 1	2000	20000	20
Input 2	0	40	25
Input 3	0.002	0.01	29
Input 4	4	18	46

Table 3.3: Example of the use of the cell array in this work with ramdon values.

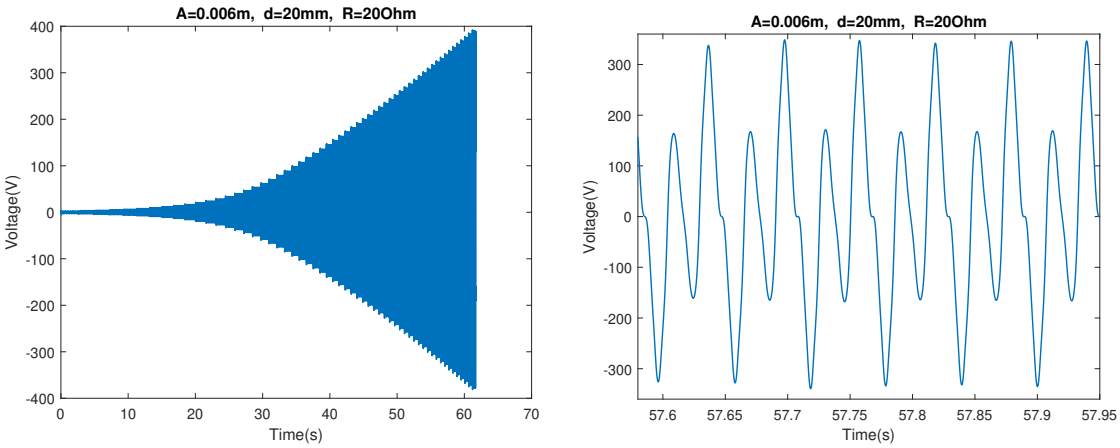

(a) Complete output signal

(b) Output signal at a closer view

Figure 3.7: Example of an output voltage signal block generated for the training and test of the ANN.

3.4 ANN development

3.4.1 Development steps for upward frequency values

Since there are four varying values for the dataset, namely frequency, amplitude, load resistance and harvester length variation, it was opted for a progressive approach, in order to validate the chosen architecture and learning algorithm, for the upward excitation frequencies. For initial considerations, the proposed network had two inputs and one output. Regarding the inputs, one was the sinusoidal external excitation signal and the other was a sing with a constant value equal to the value of the harvester length variation value. The output signal was the simulated voltage output of the generator.

Varying frequency

A representation of the input signal is shown in Figure 3.8. As it is demonstrated, the values of resistance, amplitude and harvester length variation were fixed. It was evaluated according to the Table 3.4. For this network all the input data were joined at the same block, with the sinusoidal signal being only one.

Element	Unit	Value	Symbol
Resistance	Ω	2000	R_0
harvester length variation	mm	0	d_0
Amplitude	m	0.01	A_0
Frequency	Hz	4-18	F_0, F_1,..., F_n

Table 3.4: Values introduced in the first ANN.

For this test, the number of neurons were varied from 10 to 20 and the number of delays from 2 to 10. The best performance was obtained with 13 neurons and 9 delays. For the training method was used the default Levenberg-Marquardt. The Bayesian

Regularization was not tested. All the available data were used according to the data division previously referred.

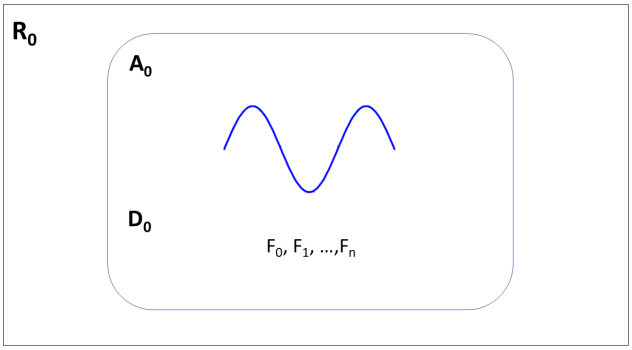

Figure 3.8: Scheme for input signal with only the frequency varying.

Varying frequency and amplitude

For the second ANN developed the amplitude value was also varied, as shown in the Figure 3.9 each square represents one data block. The inputs were the same as the previous network with the addition of a third input, that is also a constant signal that has load resistance value, and the number of neurons and delays was also the same as the training method. In the Table 3.5 shows the possible values for each element, with the now variant amplitude.

Element	Unit	Value	Symbol
Resistance	Ω	2000	R_0
harvester length variation	mm	0	d_0
Amplitude	m	0.002-0.01	A_0, A_1,..., A_n
Frequency	Hz	4-18	F_0, F_1,..., F_n

Table 3.5: Values introduced in the ANN with variation of the frequency, amplitude and resistance.

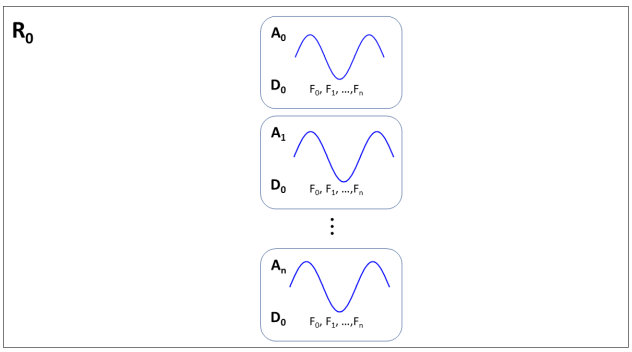

Figure 3.9: Scheme for input signal with varying frequency and amplitude.

Varying frequency, amplitude and harvester length variation

The next step was to use the harvester length variation values. The inputs and outputs remained the same, for the first time the variation of one of the constant signals was used in the network. So now, between the data blocks, like is shown in Figure 3.10, the excitation signal is not the only difference. The possible values are exposed in Table 3.6. For this study the method to find the best architecture were used, for this were tested values ranging from 10 to 20 for the number of neurons and from 2 to 10 for the number of delays, moreover, the both learning algorithm were test. The best architecture found was 13 neurons and 6 delays. Due to the amount of data to be processed, this test kind of test would not be done again, thus, this architecture would be the one used through the next phases of this work as the training algorithm, that was selected the Levenberg–Marquardt algorithm that was the best at this stage.

For this particular test, 1/3 of the whole data were separated randomly for statistical tests. In order to do that, it was chosen between the unique values of amplitude and harvester length variation 1/3 of the possible values, and these values were put in a different variable and not used in the development of the network. After that, it was calculated the statistical models for the network using the inputs and their respective targets.

Element	Unit	Value	Symbol
Resistance	Ω	2000	R_0
harvester length variation	mm	0-40	d_0, d_1,..., d_n
Amplitude	m	0.002-0.01	A_0, A_1,..., A_n
Frequency	Hz	4-18	F_0, F_1,..., F_n

Table 3.6: All possible values to be introduced in the ANN.

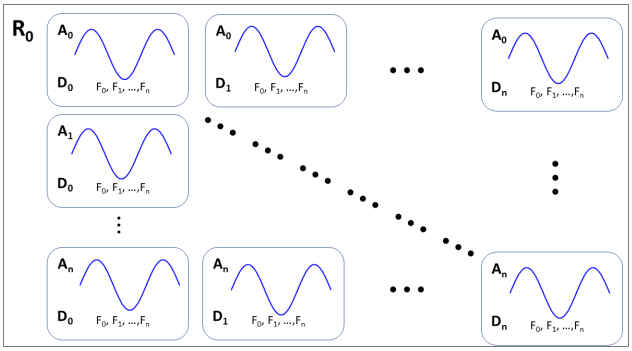

Figure 3.10: Scheme for input signal with varying frequency, amplitude and harvester length.

Using the complete upward dataset

In the last test, all upward data were used as illustrated by Figure 3.11. At this stage, the processing time starts to be a complex issue. The network training process lasted around 2 days. Similar to the previous case, the data set was previously divided

for future tests, in 1/3 for this purpose. All the possible values were used at this stage as expressed by Table 3.2.

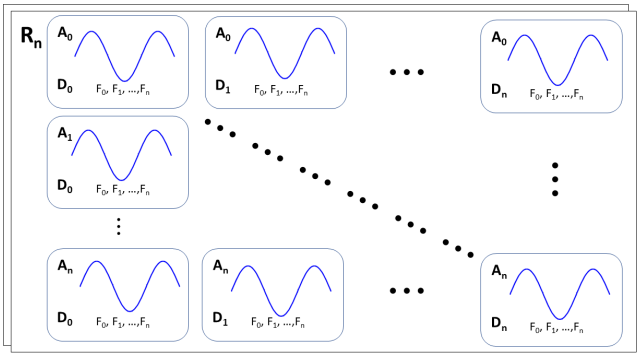

Figure 3.11: Scheme for input signal with all the elements varying.

3.4.2 Final network development

For the development of the final ANN, all the simulation data was used upward and downward. Thus, being a new input introduced in the neural network, since it is needed to differentiate the two cases, as expressed before. This input will be a constant signal with a value of $+1$ for upward frequencies and -1 for downward ones. Similar to the previous tests, 1/3 of the each kind of data was randomly selected to be separated to be only used in the statistical evaluation.

The final algorithm was composed of six different parts, four of these were about the simulation data, the first two aims to gather the data, separate it into training data and testing data and setting this data to be used in the network, being one part for the upward frequencies and the other to the downward ones. The third part is to actually train the neural network, putting together the upward and downward data to be used as input and target of the ANN. The forth part has the objective of produce the statistical evaluation from the simulation data comparing the target values with the output ones. The other 2 parts aim to extract and test the experimental data, doing the same statistical survey.

The final architecture was composed by 13 neurons and 6 delays with 2 layers. The selected training function was Levenberg–Marquardt. All the algorithm scripts are presented at the Appendix B.

3.5 Experimental Data

The experimental data were used only for testing the performance of the generator with results extracted from the real generator, indicated in Section 3.1. The data were divided according to each test specification, namely: load resistance, excitation amplitude and the harvester length variation. For each test it is used the same frequencies range as the simulated data. All the possible values are expressed in Table 3.7. From each one of these tests is possible to obtain the sample time, external excitation frequency and the signal from the 2 central coils connected in series, thus being the generator voltage.

Element	Unit	Minimum value	Maximum value	Interval	Number of elements
Resistance	Ω	1.008 k	10.54 M	-	19
Harvester length variation	mm	0	40	10	5
Amplitude	mm	3	10	2/3	4
Frequency	Hz	4	18	0.5	30

Table 3.7: Range of possible values for each variable at the experimental data.

In each test the frequency was raised each 4 seconds, with a variation time of 0.5 seconds, as displayed in Figure 3.12. At the end of the the test, the engine was turned down, that is why the trajectory has a severe drop at the end, since this is also an element measured by the test.

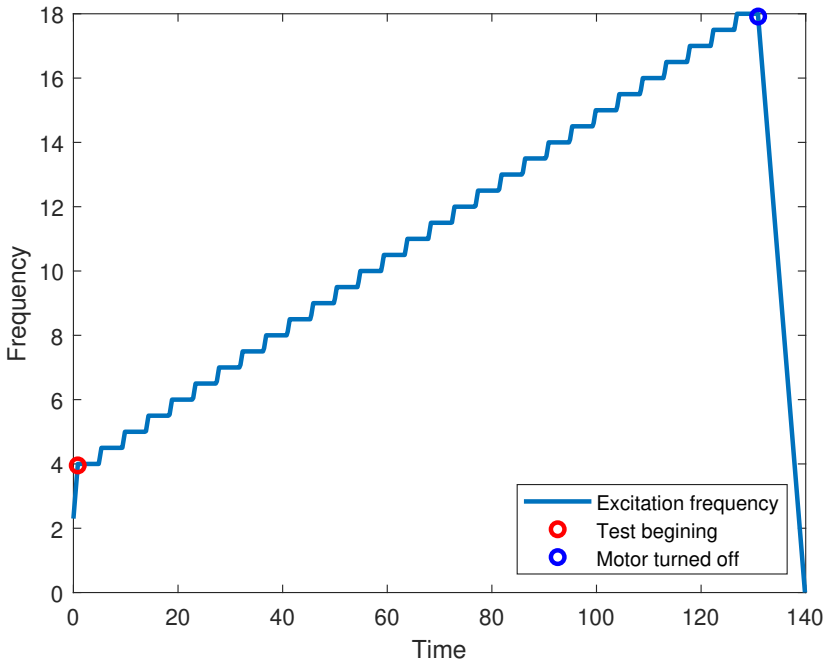

Figure 3.12: Plot showing the operating cycle of the excitation frequency for all tests.

Since the simulation data used to train the network didn't have a variation period, every change in the input frequency happened instantly, this event on the experimental data caused the ANN to wrongly predict the generator output, increasing the mean square error (MSE) and the other measurements. Therefore, the input excitation frequency was considered to be changed instantly, with the value being fixating in the last fixed valued until the next step value to be reached, as presented in the Figure 3.13.

It was used the same input format, using the values obtained by these data. So the resistances and harvester length variations with the external input excitation signal of $A\sin(2\pi ft)$, being A the amplitude, f the frequency and t the time were used to compose the network input. Since these data corresponds only to upward frequencies, a constant signal of value 1 was also used in the ANN input.

For the network target the harvester voltage was employed. The problem with the

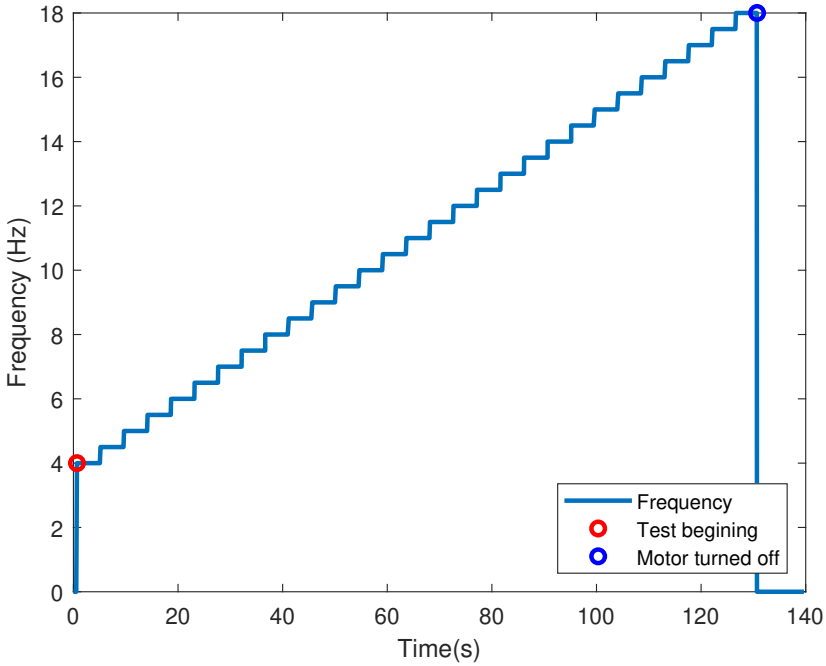

Figure 3.13: Plot showing the operating cycle of the frequency without the variation time that was inputted in the network.

experimental data, is that it has a lot of noise in the output signal, which make the ANN incapable of predicting the generator output with a good performance index (a low MSE value). To solve this, a filter was used to smooth the output curve, thus being more approximated with the developed model. The filter was made using the discrete Fourier transform (DFT), computed by the $fft(x)$ command of MATLAB that utilizes the fast Fourier transform algorithm. The custom function used in the filtering process is presented in Appendix B.8. For some cases it was not possible to filter the noise out of the signal, since the excessive noise do not allow the filter to differentiate the noise from the actual data. A graphical example of the filter action on the signal is exposed in Figure 3.14, where an output signal and its filtered signal are illustrated.

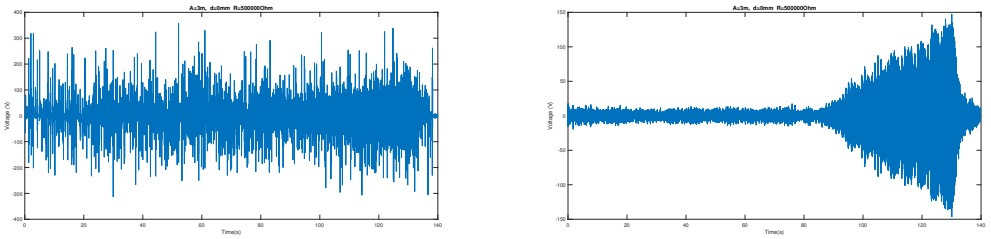

(a) (b)

Figure 3.14: (a) Example of experimental output signal without filtering; (b) Signal filtered after processing.

3.6 Data analysis

The followup criteria were used in both tests (for simulated and experimental data), the statistical measurements were the same. Three performance criteria were chosen to operate as performance index: mean square error, cross correlation and mean percentage error (MPE). The MSE was used to evaluate how close a prediction is to the actual value, as the MPE was used just to observe how distant from the intended value the error is. The objective to do the cross correlation is to track the similarity between trajectory of the target and the network output and how the match up to each other.

For the results of the simulation data, it will be considered the results of the data set that was previously separated randomly for that purpose. That data were divided in data blocks, as was done with the training data. For each one of this blocks, the three measurements were calculated, as it will be presented forward. The number of experiments was 783. Due to the large number of tests, all the results will be presented and discussed in graphics presentations, and only some selected output and target comparison will be chosen to be expose, with the preference given to the natural frequency or values around it due to the fact that the generator is only functional close to it, which justify this choice. The maximum output voltage will also be presented as a function of the frequencies. The selection made was to present the hysteretic behavior in comparison with other non hysteretic outputs. The graphic presented will display the trajectories considering different values load resistance plotted together according to the combination of external excitation amplitude and harvester length variation, comparing the model output (target) and the ANN output.

For the experimental data, analogously to the simulated data results, it will be presentedfurther with the same performance criteria together with some output and target comparison.

Chapter 4

Results

In this chapter the results for the simulated and experimental data will be presented. In the next chapter (Chapter 5) this results will be discussed.

4.1 Simulated data results

Firstly, the ANN performance were calculated considering the previously mention performance criteria for the data separated for testing. Figure 4.1 shows the statistical results of this 783 tests, being the first 392 for the upward frequencies and the last 391 for the downward ones. As these plots shows, the network's output and the target trajectories are very similar, with almost the same values, as indicated by the maximum value for the MSE in this dataset, 0.04, and the MSE mean value, of 0.004. Together with this, the cross correlation, that is very close to 100%, have minimum value (worst result) of 99,99991% and a mean value is 99,999986%, which indicates this close relation of both curves. In the case of the mean percentage error the maximum value is 0.25% with a mean value of 0.028%. For the three measures the vast majority of the data is below the mean value, which also indicates that for the majority of the tests the results were even better than the average. The table with all the tests results is presented at the Appendix A.1.

A representation of the generator behavior according to the input frequency is shown in Figure 4.2. As shown in it, the generator produces a higher voltage around the natural frequency. In the graphics shown in the Figures 4.2a, 4.2b, 4.2c and 4.2e, as for the remaining two graphics the resonance frequencies are beyond the range used in this work.

A closer look of the data represented in Figures 4.2b, 4.2c and 4.2e is presented in Figure 4.3 where the network output signal is shown during a time period for a input signal with the system's natural frequency for each respective setup. The target value and the ANN's output are very close, not being possible to observe the difference between the two, thus being, a more close view from the graphic in Figure 4.3c is presented in Figure 4.4. It is possible to observe that althought not being a exact match the two lines are very close, with a difference of around 0.01V in this case, which highlights the previously commented statistical results.

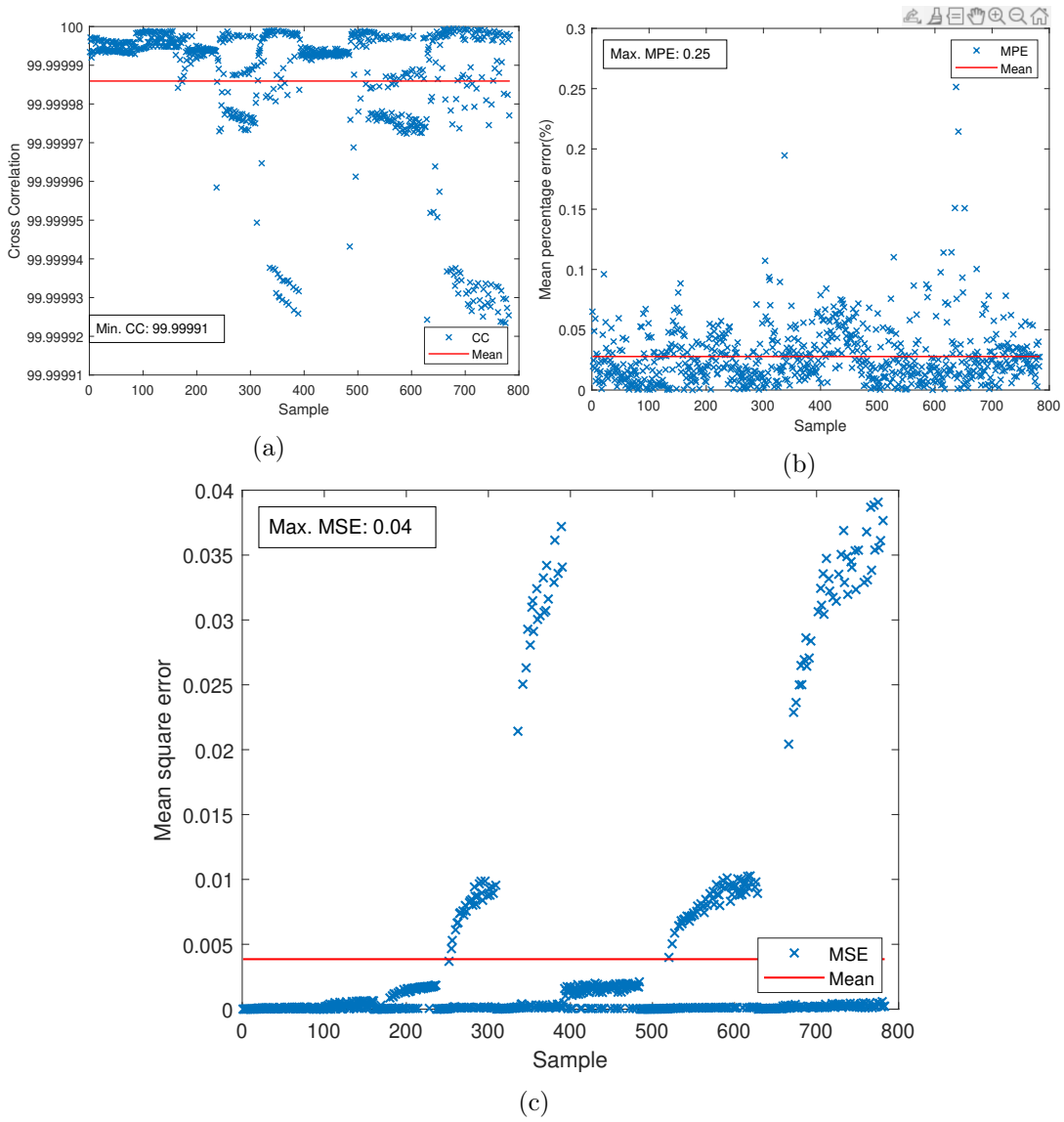

Figure 4.1: Statistical survey of tests with simulated data.

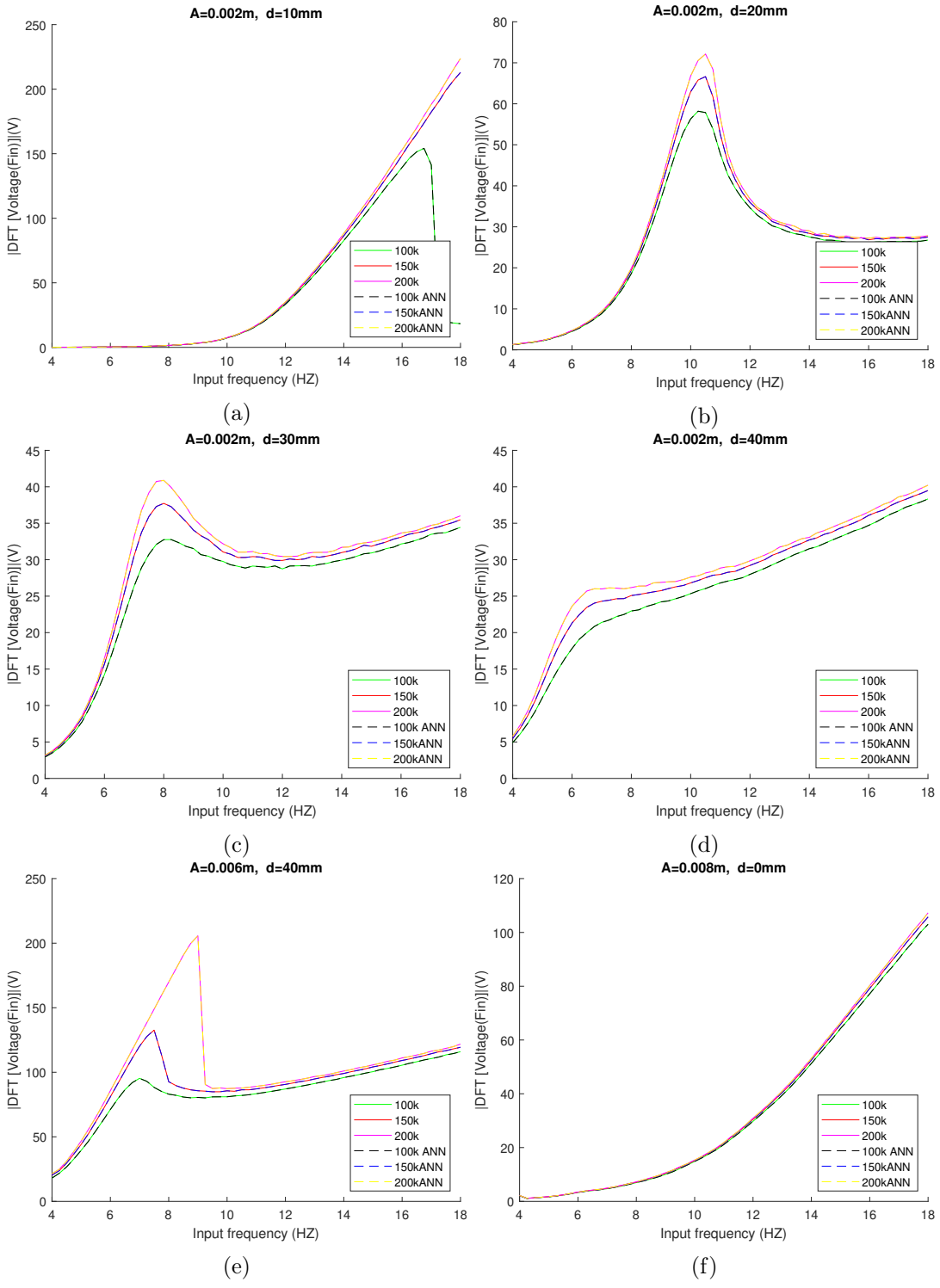

Figure 4.2: Maximum generator's voltage according to the input frequency for various set ups for simulated data.

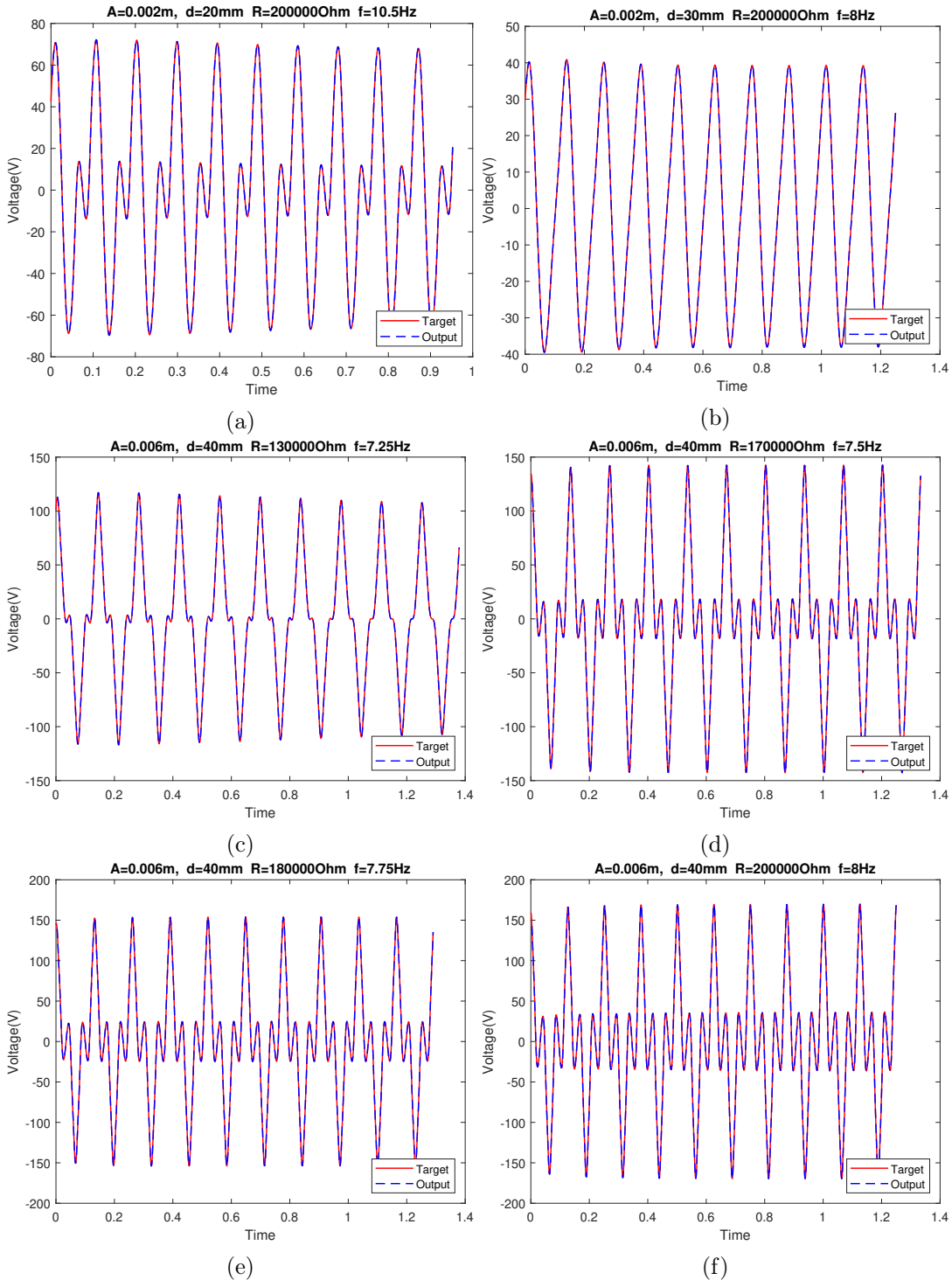

Figure 4.3: Network's target and output comparison for sumulated data.

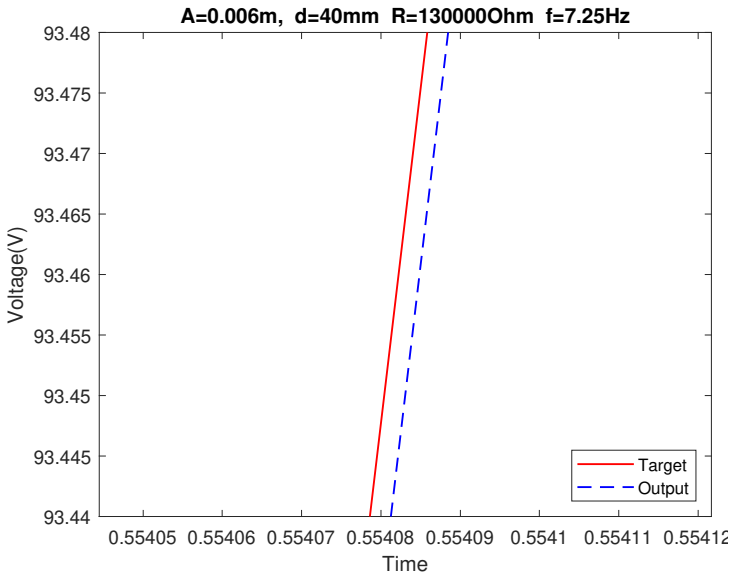

Figure 4.4: Close comparison between simulated target and output.

4.2 Experimental data results

The prediction capability of the network for real data was tested with the experimental data. A total of 177 tests were made and the statistical survey of the results are exposed in Figure 4.5. For the MSE criteria, the mean value was 69.26, for the cross correlation it was 94% and for the MPE it was 59%. 87% of the analyzed data has a MSE lower than 150, 94% has a cross correlation bigger than 70% and 87% has a MPE lower than 30%. This numbers are expressed in the Table 4.1.

	Mean	Max	Min	Best than mean	% Best	Valid	%Valid
MSE	69,26	269,80	3,80	116	66%	154	87%
CC	94%	100%	9%	143	81%	167	94%
MPE	59%	6963%	0,02%	164	93%	154	87%

Table 4.1: Statistical analysis of the experimental data.

One example of a good prediction made by the network is show in Figure 4.6 where the two signals, the filtered output signal and the ANN output are shown and a closer look of this signal is presented in Figure 4.6b-c.

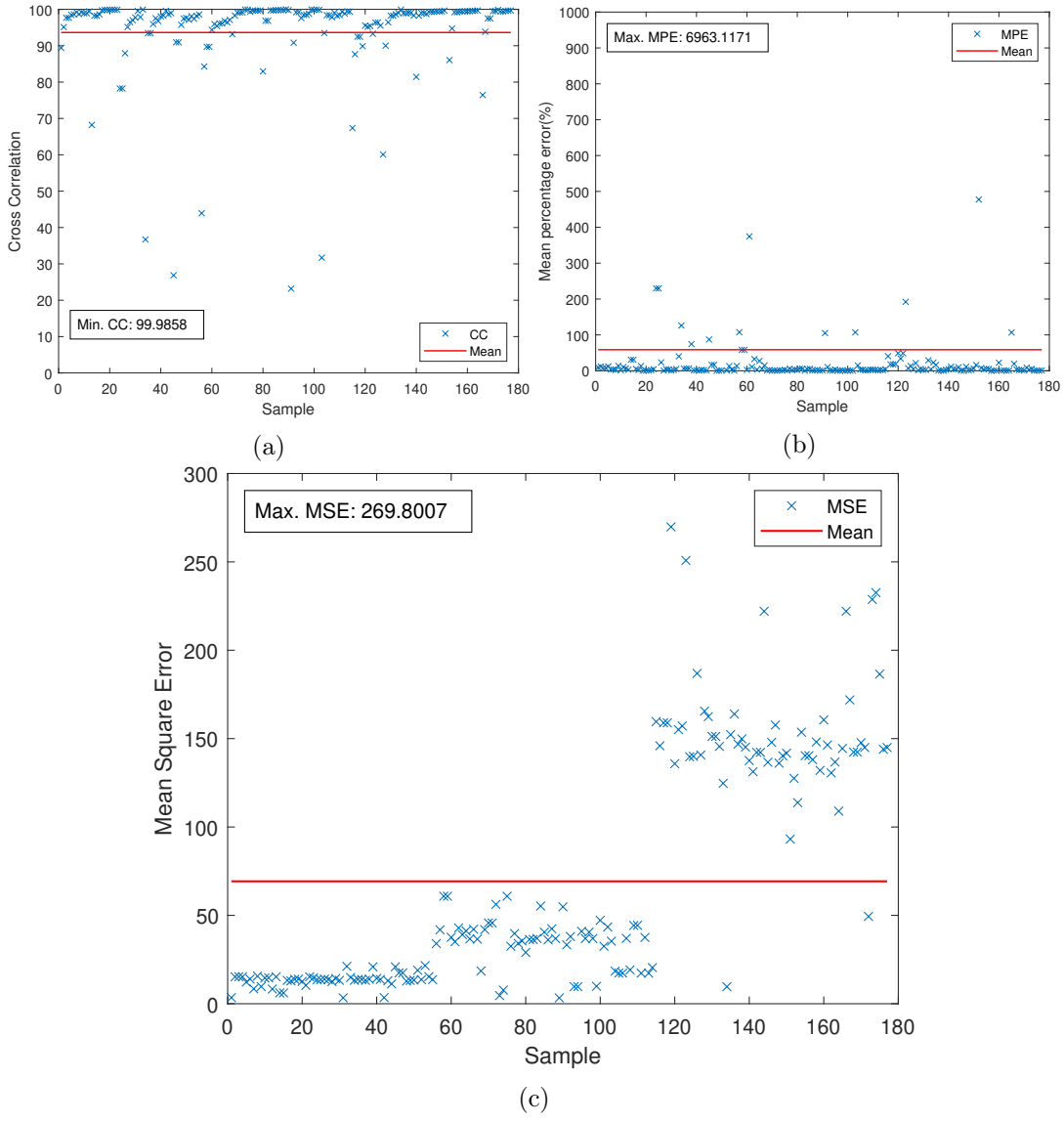

Figure 4.5: Statistical survey of tests with experimental data.

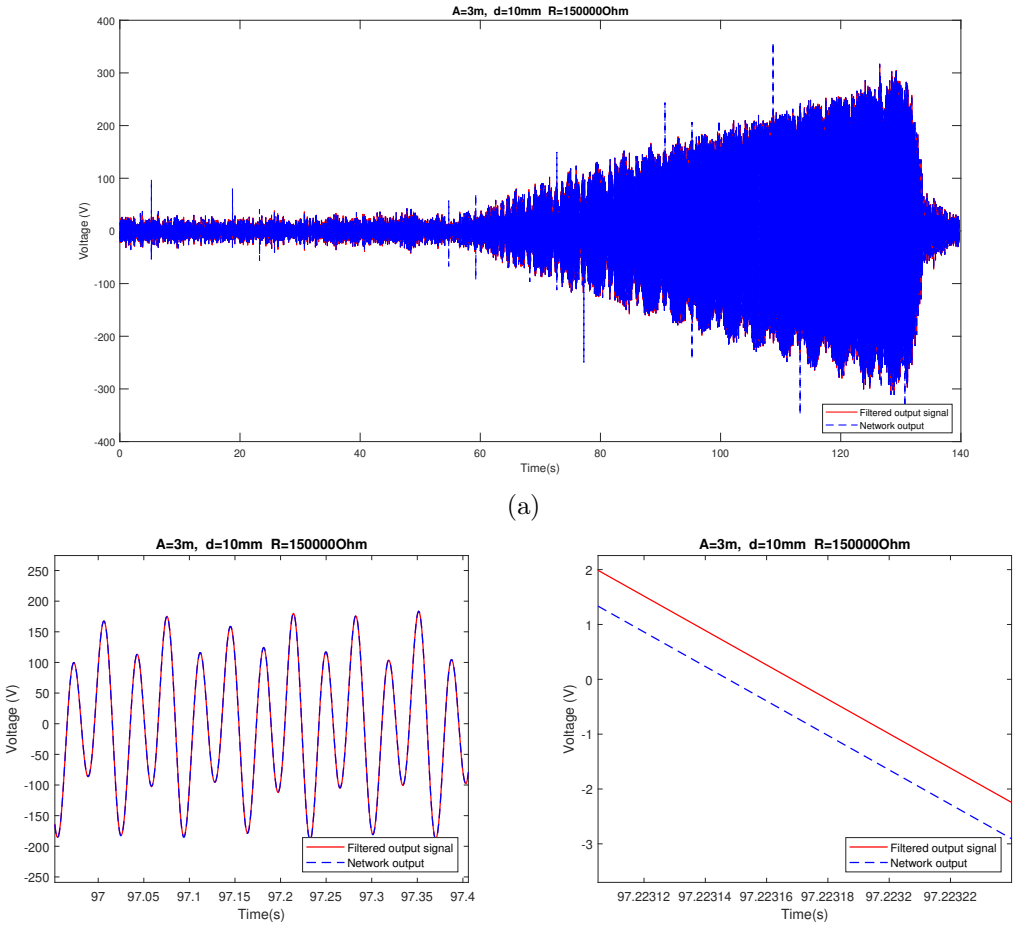

Figure 4.6: (a) Comparison between the filtered generator output signal and the network output; (b) and (c) Closer view of the two signals.

Chapter 5

Discussion and conclusions

The last chapter has the objective to conclude the developed project, analyzing and discussing the obtained results, as what could be done in future works. This chapter will also refer the importance and advances made by this work.

5.1 Discussion

There is a lack of papers about the use of neural networks to predict the electric dynamics of mechanical vibration generators, specially the EMGs. In addition to that, the use of this kind of generators in bio-medicine is also a new and promising idea. Hence, this becomes a opportunity to investigate this field with a major possibility of new findings. That is why this work and its results are significantly relevant and it proved to be a valuable step in the project that it is inserted.

The network performance in what regards the simulation data was excellent, since it was able to predict very closely the system behavior. Since in this case the data was obtained from a simulation, it was expected that the ANN's performance could be very good. The high cross correlation value and low error (MSE and MPE) show exactly how good the network performance was. It is possible to observe the same thing when looking the plotted comparison between the target and output in the natural frequency.

The results opened the possibility to test this network in experimental data that showed that this use of a neural network to predict the electric dynamics of this kind of generator, that is something new, is possible, thus being this work opens new possibilities to implement new solutions to this field of study. This results stretches the forms of using neural networks in the field energy harvesting. The experimental results were satisfactory, with some limitations, though. In some tests the network were unable to predict the behavior of the generator, resulting in a major error bye it, but in the majority of the cases, this was not what happened, with the network having a good and some times great performance.

This being, it is safe to say that the algorithm developed can make a good approximation of the generator output. Some improvements can be done in order to better the performance of the network with the experimental data. For the project that this work is inserted in, it demonstrated the capability of further development of a ANN using with EMGs and gives a idea of how it would perform in a real time application. This permits the continuity the project objective to develop a self-adaptive generator

for biomedical proposes. For further develop the project, new approaches are needed to develop a network that works in real-time with the fisical generator.

5.2 Conclusions and future work

The results presented in this work indicate that the proposed objectives were achieved. The performance of the final developed ANN can be considered suitable both for the simulated data and experimental data according with the statistical survey presented. The neural network structure used through the course of this work, the NARX, together with the MATLAB application used, proved capable to realize the propose of the work as it did perform according to expectation.

The performance using the experimental data validates the neural network developed in this work, being a interesting result, once the network was trained using only simulated data. The network was able to predict the behavior of the generator practically, which proves a possibility of using this approach for this kind of application. The NARX predicting capability with a relative precision, in what regards the generator behavior, indicates the possibility to convert a NARX neural network to actually actuate in it and the potential of this network structure to solve similar problems. This would enable the EMG to work properly in a wider range of frequencies. Nonetheless, it is possible to notice the need to improve the network performance for future applications.

Regarding the prediction to the hysteretic behavior the only tests made were with the simulated data, in which the results were excellent, which demonstrates the possibility of using the ANN approach for this kind of system. For this to be done completely, a differentiation method must be developed in future works, in order to predict the hysteresis output. In this case, another ANN could be use to identify the frequency trajectory (if it is upward or downward) using the Preisach Model. This would allow the differentiation to be done in real-time with the excitation input in the generator. Test the network with descending experimental data would also be required for a complete validation.

To further approach the real-time self-adaptation a dynamical network should be develop to work with the EMG. This network would be capable of training while functioning with a continuous learning and receiving new data while the generator works. This kind of ANN could be implemented within the generator and in this case it would be created a smart electromagnetic generator, capable of predict how to adapt to the different external excitation being more precise with time. After this, that smart generator could be integrated in others hybrid generators.

Bibliography

[1] P. Carneiro, M. P. Soares dos Santos, A. Rodrigues, J. A. Ferreira, J. A. Simões, A. T. Marques, and A. L. Kholkin, "Electromagnetic energy harvesting using magnetic levitation architectures: A review," *Applied Energy*, vol. 260, no. July 2019, p. 114191, 2020.

[2] C. Rodrigues, D. Nunes, D. Clemente, N. Mathias, J. M. Correia, P. Rosa-Santos, F. Taveira-Pinto, T. Morais, A. Pereira, and J. Ventura, "Emerging triboelectric nanogenerators for ocean wave energy harvesting: State of the art and future perspectives," *Energy and Environmental Science*, vol. 13, no. 9, pp. 2657–2683, 2020.

[3] J. Zhao, G. Zhen, G. Liu, T. Bu, W. Liu, X. Fu, P. Zhang, C. Zhang, and Z. L. Wang, "Remarkable merits of triboelectric nanogenerator than electromagnetic generator for harvesting small-amplitude mechanical energy," *Nano Energy*, vol. 61, no. March, pp. 111–118, 2019.

[4] Z. Hadas, J. Kurfurst, C. Ondrusek, and V. Singule, "Artificial intelligence based optimization for vibration energy harvesting applications," *Microsystem Technologies*, vol. 18, no. 7-8, pp. 1003–1014, 2012.

[5] R. Rocha, "Modelação de gerador eletromagnético com redes neuronais artificiais," Master's thesis, Universidade de Aveiro, 2017.

[6] Y. Wang, Y. Yang, and Z. L. Wang, "Triboelectric nanogenerators as flexible power sources," *npj Flexible Electronics*, vol. 1, no. 1, pp. 1–9, 2017.

[7] M. Khorsand, J. Tavakoli, K. Kamanya, and Y. Tang, "Simulation of high-output and lightweight sliding-mode triboelectric nanogenerators," *Nano Energy*, vol. 66, no. August, p. 104115, 2019.

[8] M. Khorsand, J. Tavakoli, H. Guan, and Y. Tang, "Artificial intelligence enhanced mathematical modeling on rotary triboelectric nanogenerators under various kinematic and geometric conditions," *Nano Energy*, vol. 75, no. March, p. 104993, 2020.

[9] M. T. Hagan, H. B. Demuth, and M. H. Beale, *Neural Network Design*. 1995.

[10] K. B. Singh, V. Bedekar, S. Taheri, and S. Priya, "Piezoelectric vibration energy harvesting system with an adaptive frequency tuning mechanism for intelligent tires," *Mechatronics*, vol. 22, no. 7, pp. 970–988, 2012.

[11] E. Çelik, Y. Uzun, E. Kurt, N. Öztürk, and N. Topaloğlu, "A Neural Network Design for the Estimation of Nonlinear Behavior of a Magnetically-Excited Piezoelectric Harvester," *Journal of Electronic Materials*, vol. 47, no. 8, pp. 4412–4420, 2018.

[12] P. M. R. Carneiro, J. V. Vidal, P. Rolo, I. Peres, J. A. Ferreira, A. L. Kholkin, and M. dos Santos, "Self-adaptive instrumented electromagnetic generator."

[13] P. Blasco, D. Gunduz, and M. Dohler, "A learning theoretic approach to energy harvesting communication system optimization," *IEEE Transactions on Wireless Communications*, vol. 12, no. 4, pp. 1872–1882, 2013.

[14] M. Chaari, H. Ghariani, and M. Lahiani, "Energy Harvesting from Eletromagnetic Radiation Emissions by Compact Fluoresent Lamp," *ICACI*, pp. 7–10, 2017.

[15] D. A. Borca-Tasciuc, A. Kempitiya, and M. Hella, "Micro-Power Generators for Ambient Intelligence Applications," *SOFA*, pp. 19–24, 2010.

[16] S. Nabavi and L. Zhang, "MEMS piezoelectric energy harvester design and optimization based on Genetic Algorithm," *IEEE International Ultrasonics Symposium, IUS*, vol. 2016-Novem, pp. 0–3, 2016.

[17] K. Zhang, X. Wang, Y. Yang, and Z. L. Wang, "Hybridized Electromagnetic-Triboelectric Nanogenerator for Scavenging Biomechanical Energy for Sustainably Powering Wearable Electronics," *ACS Nano*, vol. 9, no. 4, pp. 3521–3529, 2015.

[18] P. Constantinou, P. H. Mellor, and P. D. Wilcox, "A Magnetically Sprung Generator for Energy Harvesting Applications," *IEEE/ASME Transactions on Mechatronics*, vol. 17, no. 3, pp. 415–424, 2012.

[19] P. Constantinou, P. H. Mellor, and P. Wilcox, "A Model of a Magnetically Sprung Vibration Generator for Power Harvesting Applications," in *2007 IEEE International Electric Machines Drives Conference*, vol. 1, pp. 725–730, 2007.

[20] A. G. Avila Bernal and L. E. Linares García, "The modelling of an electromagnetic energy harvesting architecture," *Applied Mathematical Modelling*, vol. 36, no. 10, pp. 4728–4741, 2012.

[21] A. R. M. Foisal, C. Hong, and G.-S. Chung, "Multi-frequency electromagnetic energy harvester using a magnetic spring cantilever," *Sensors and Actuators A: Physical*, vol. 182, pp. 106–113, 2012.

[22] A. R. M. Foisal, B. Lee, and G. Chung, "Fabrication and performance optimization of an AA size electromagnetic energy harvester using magnetic spring," in *SENSORS, 2011 IEEE*, pp. 1125–1128, 2011.

[23] A. R. M. Foisal and G. S. Chung, "Design and analysis of a vibration-driven AA size electromagnetic energy harvester using magnetic spring," *Transactions on Electrical and Electronic Materials*, vol. 13, no. 3, pp. 125–128, 2012.

[24] D. F. Berdy, D. J. Valentino, and D. Peroulis, "Design and optimization of a magnetically sprung block magnet vibration energy harvester," *Sensors and Actuators A: Physical*, vol. 218, pp. 69–79, 2014.

[25] D. F. Berdy, D. J. Valentino, and D. Peroulis, "Kinetic energy harvesting from human walking and running using a magnetic levitation energy harvester," *Sensors and Actuators A: Physical*, vol. 222, pp. 262–271, 2015.

[26] H. Liu, S. Gudla, F. A. Hassani, C. H. Heng, Y. Lian, and C. Lee, "Investigation of the Nonlinear Electromagnetic Energy Harvesters From Hand Shaking," *IEEE Sensors Journal*, vol. 15, no. 4, pp. 2356–2364, 2015.

[27] M. P. Soares Dos Santos, J. A. Ferreira, J. A. Simões, R. Pascoal, J. Torrão, X. Xue, and E. P. Furlani, "Magnetic levitation-based electromagnetic energy harvesting: A semi-Analytical non-linear model for energy transduction," *Scientific Reports*, vol. 6, no. August 2015, pp. 1–9, 2016.

[28] K. Kecik, A. Mitura, S. Lenci, and J. Warminski, "Energy harvesting from a magnetic levitation system," *International Journal of Non-Linear Mechanics*, vol. 94, pp. 200–206, 2017.

[29] K. Kçcik, "Energy recovery from a non-linear electromagnetic system," *Acta Mechanica et Automatica*, vol. 12, no. 1, pp. 11–18, 2018.

[30] C. R. Saha, T. O'Donnell, N. Wang, and P. McCloskey, "Electromagnetic generator for harvesting energy from human motion," *Sensors and Actuators A: Physical*, vol. 147, no. 1, pp. 248–253, 2008.

[31] E. Dallago, M. Marchesi, and G. Venchi, "Analytical Model of a Vibrating Electromagnetic Harvester Considering Nonlinear Effects," *IEEE Transactions on Power Electronics*, vol. 25, no. 8, pp. 1989–1997, 2010.

[32] A. Munaz, B.-C. Lee, and G.-S. Chung, "A study of an electromagnetic energy harvester using multi-pole magnet," *Sensors and Actuators A: Physical*, vol. 201, pp. 134–140, 2013.

[33] M. Masoumi and Y. Wang, "Repulsive magnetic levitation-based ocean wave energy harvester with variable resonance: Modeling, simulation and experiment," *Journal of Sound and Vibration*, vol. 381, pp. 192–205, 2016.

[34] W. Wang, J. Cao, N. Zhang, J. Lin, and W.-H. Liao, "Magnetic-spring based energy harvesting from human motions: Design, modeling and experiments," *Energy Conversion and Management*, vol. 132, pp. 189–197, 2017.

[35] K. Pancharoen, D. Zhu, and S. P. Beeby, "Temperature dependence of a magnetically levitated electromagnetic vibration energy harvester," *Sensors and Actuators A: Physical*, vol. 256, pp. 1–11, 2017.

[36] M. N. Struwig, R. Wolhuter, and T. Niesler, "Nonlinear model and optimization method for a single-axis linear-motion energy harvester for footstep excitation," *Smart Materials and Structures*, vol. 27, p. 125007, nov 2018.

[37] B. P. Mann and N. D. Sims, "Energy harvesting from the nonlinear oscillations of magnetic levitation," *Journal of Sound and Vibration*, vol. 319, no. 1, pp. 515–530, 2009.

[38] E. Bonisoli, A. Canova, F. Freschi, S. Moos, M. Repetto, and S. Tornincasa, "Dynamic Simulation of an Electromechanical Energy Scavenging Device," *IEEE Transactions on Magnetics*, vol. 46, no. 8, pp. 2856–2859, 2010.

[39] R. Morais, N. M. Silva, P. M. Santos, C. M. Frias, J. A. F. Ferreira, A. M. Ramos, J. A. O. Simões, J. M. R. Baptista, and M. C. Reis, "Double permanent magnet vibration power generator for smart hip prosthesis," *Sensors and Actuators A: Physical*, vol. 172, no. 1, pp. 259–268, 2011.

[40] M. L. Morgado, L. F. Morgado, N. Silva, and R. Morais, "Mathematical modelling of cylindrical electromagnetic vibration energy harvesters," *International Journal of Computer Mathematics*, vol. 92, no. 1, pp. 101–109, 2015.

[41] X. Yang, B. Zhang, J. Li, and Y. Wang, "Model and Experimental Research on an Electromagnetic Vibration-Powered Generator With Annular Permanent Magnet Spring," *IEEE Transactions on Applied Superconductivity*, vol. 22, no. 3, p. 5201504, 2012.

[42] G. Aldawood, H. T. Nguyen, and H. Bardaweel, "High power density spring-assisted nonlinear electromagnetic vibration energy harvester for low base-accelerations," *Applied Energy*, vol. 253, p. 113546, 2019.

[43] C. M. Saravia, J. M. Ramírez, and C. D. Gatti, "A hybrid numerical-analytical approach for modeling levitation based vibration energy harvesters," *Sensors and Actuators A: Physical*, vol. 257, pp. 20–29, 2017.

[44] M. Geisler, S. Boisseau, M. Perez, P. Gasnier, J. Willemin, I. Ait-Ali, and S. Perraud, "Human-motion energy harvester for autonomous body area sensors," *Smart Materials and Structures*, vol. 26, no. 3, p. 35028, 2017.

[45] D. Apo and S. Priya, "High power density levitation-induced vibration energy harvester.," no. Energy Harvesting Syst, 2014.

[46] Q. Zhang, Y. Wang, and E. S. Kim, "Power generation from human body motion through magnet and coil arrays with magnetic spring," *Journal of Applied Physics*, vol. 115, no. 6, 2014.

[47] S. Niu, Y. Liu, S. Wang, L. Lin, Y. S. Zhou, Y. Hu, and Z. L. Wang, "Theory of sliding-mode triboelectric nanogenerators," *Advanced Materials*, vol. 25, no. 43, pp. 6184–6193, 2013.

[48] X. Chen, Z. Ren, M. Han, J. Wan, and H. Zhang, "Hybrid energy cells based on triboelectric nanogenerator: From principle to system," *Nano Energy*, vol. 75, no. April, p. 104980, 2020.

[49] F. Xi, Y. Pang, G. Liu, S. Wang, W. Li, C. Zhang, and Z. L. Wang, "Self-powered intelligent buoy system by water wave energy for sustainable and autonomous wireless sensing and data transmission," *Nano Energy*, vol. 61, no. March, pp. 1–9, 2019.

[50] J. V. Vidal, V. Slabov, A. L. Kholkin, and M. P. dos Santos, *Hybrid Triboelectric-Electromagnetic Nanogenerators for Mechanical Energy Harvesting: A Review*, vol. 13. Springer Singapore, 2021.

[51] C. Wu, W. Ding, R. Liu, J. Wang, A. C. Wang, J. Wang, S. Li, Y. Zi, and Z. L. Wang, "Keystroke dynamics enabled authentication and identification using triboelectric nanogenerator array," *Materials Today*, vol. 21, no. 3, pp. 216–222, 2018.

[52] Q. He, Y. Wu, Z. Feng, C. Sun, W. Fan, Z. Zhou, K. Meng, E. Fan, and J. Yang, "Triboelectric vibration sensor for a human-machine interface built on ubiquitous surfaces," *Nano Energy*, vol. 59, no. March, pp. 689–696, 2019.

[53] R. Guo, H. Zhang, Z. Pei, S. Yang, C. Ge, S. Sang, and R. Hao, "A Voiceprint Recognition Sensor Based on a Fully 3D-Printed Triboelectric Nanogenerator via a One-Step Molding Route," *Advanced Engineering Materials*, vol. 22, no. 5, 2020.

[54] X. Ji, T. Zhao, X. Zhao, X. Lu, and T. Li, "Triboelectric Nanogenerator Based Smart Electronics via Machine Learning," *Advanced Materials Technologies*, vol. 5, no. 2, pp. 1–11, 2020.

[55] S. K. Jha, J. Bilalovic, A. Jha, N. Patel, and H. Zhang, "Renewable energy: Present research and future scope of Artificial Intelligence," *Renewable and Sustainable Energy Reviews*, vol. 77, no. April, pp. 297–317, 2017.

Part I

Appendices

Appendix A

Simulation data results

A.1 Results Table

	Displacement (mm)	Resitence (Ohm)	Amplitude (m)	MSE	Cross Correlation	Mean Percentage Error
1	0	2000	0,008	4,72E-06	99,99999341	0,064988894
2	0	3000	0,004	1,85E-06	99,99999717	0,019673699
3	0	3000	0,006	3,78E-06	99,99999628	0,024526445
4	0	3000	0,01	1,34E-05	99,99999199	0,048868515
5	0	5000	0,002	4,20E-06	99,99999297	0,018000604
6	0	5000	0,01	2,23E-05	99,99999346	0,059168421
7	0	6000	0,002	4,80E-06	99,99999367	0,007340516
8	0	6000	0,01	2,69E-05	99,99999369	0,030108176
9	0	7000	0,006	1,04E-05	99,99999664	0,016807971
10	0	8000	0,004	6,84E-06	99,99999707	0,028314876
11	0	8000	0,006	1,17E-05	99,99999671	0,008974863
12	0	8000	0,008	2,13E-05	99,99999551	0,022308925
13	0	9000	0,006	1,26E-05	99,99999687	0,005859948
14	0	10000	0,004	8,56E-06	99,99999707	0,013150087
15	0	15000	0,002	1,28E-05	99,99999339	0,015535351
16	0	20000	0,002	1,52E-05	99,99999362	0,023686194
17	0	20000	0,006	2,78E-05	99,9999963	0,000936845
18	0	25000	0,002	1,70E-05	99,99999377	0,007172288
19	0	25000	0,01	8,26E-05	99,99999405	0,045850427
20	0	30000	0,002	1,87E-05	99,99999373	0,005739952
21	0	30000	0,01	8,88E-05	99,99999413	0,096041432
22	0	35000	0,004	2,25E-05	99,9999966	0,02362821
23	0	35000	0,006	3,67E-05	99,9999963	0,025225912
24	0	35000	0,01	9,46E-05	99,99999414	0,056219356
25	0	40000	0,008	6,54E-05	99,99999524	0,034786038
26	0	40000	0,01	1,01E-04	99,99999403	0,011383156
27	0	45000	0,004	2,54E-05	99,9999965	0,013965236
28	0	45000	0,008	6,79E-05	99,99999525	0,009615429
29	0	45000	0,01	1,07E-04	99,99999394	0,031088479
30	0	50000	0,002	2,47E-05	99,99999327	0,013826435
31	0	55000	0,01	1,14E-04	99,99999392	0,015326624
32	0	60000	0,006	4,43E-05	99,99999624	0,024736296
33	0	60000	0,01	1,15E-04	99,999994	0,02155662
34	0	65000	0,002	2,50E-05	99,99999366	0,051392159
35	0	65000	0,004	3,05E-05	99,99999621	0,012454307
36	0	70000	0,002	2,64E-05	99,99999343	0,030585929
37	0	70000	0,01	1,21E-04	99,99999388	0,019926621
38	0	75000	0,002	2,54E-05	99,99999379	0,040176249
39	0	75000	0,008	8,01E-05	99,99999509	0,014285463
40	0	80000	0,002	2,64E-05	99,99999362	0,008112623
41	0	80000	0,004	3,32E-05	99,99999606	0,015658392
42	0	85000	0,002	2,67E-05	99,99999364	0,019581095
43	0	85000	0,004	3,41E-05	99,99999599	0,018462219

	Displacement (mm)	Resitence (Ohm)	Amplitude (m)	MSE	Cross Correlation	Mean Percentage Error
44	0	85000	0,006	4,86E-05	99,99999617	0,002782456
45	0	85000	0,01	1,32E-04	99,99999357	0,014389957
46	0	90000	0,008	8,31E-05	99,99999507	0,016931968
47	0	90000	0,01	1,34E-04	99,99999357	0,059536777
48	0	95000	0,002	2,70E-05	99,99999369	0,006611857
49	0	95000	0,004	3,48E-05	99,999996	0,03342742
50	0	95000	0,006	4,95E-05	99,99999617	0,008481703
51	0	95000	0,008	8,51E-05	99,999995	0,010575655
52	0	95000	0,01	1,35E-04	99,99999358	0,012691233
53	0	105000	0,002	2,84E-05	99,99999349	0,032537251
54	0	105000	0,008	8,66E-05	99,99999499	0,04320672
55	0	105000	0,01	1,38E-04	99,99999353	0,021362535
56	0	115000	0,004	3,77E-05	99,99999578	0,008784105
57	0	115000	0,01	1,42E-04	99,99999342	0,013770751
58	0	120000	0,002	2,81E-05	99,99999368	0,008426991
59	0	130000	0,006	5,39E-05	99,99999601	0,003770776
60	0	130000	0,008	9,05E-05	99,99999491	0,041932646
61	0	130000	0,01	1,46E-04	99,99999332	0,00922706
62	0	135000	0,004	3,83E-05	99,9999958	0,015805438
63	0	135000	0,008	9,18E-05	99,99999486	0,001904285
64	0	135000	0,01	1,48E-04	99,99999327	0,009757893
65	0	140000	0,002	2,91E-05	99,99999358	0,00045205
66	0	145000	0,004	3,83E-05	99,99999584	0,004976968
67	0	145000	0,01	1,52E-04	99,99999315	0,012762863
68	0	150000	0,004	3,89E-05	99,99999579	0,020096514
69	0	150000	0,01	1,53E-04	99,99999313	0,013859816
70	0	155000	0,002	2,96E-05	99,99999356	0,003870027
71	0	155000	0,006	5,55E-05	99,99999597	0,004977176
72	0	160000	0,002	3,05E-05	99,99999339	0,002046251
73	0	160000	0,006	5,49E-05	99,99999602	0,016470728
74	0	160000	0,008	9,63E-05	99,99999471	0,007125617
75	0	160000	0,01	1,52E-04	99,99999324	0,016162023
76	0	165000	0,006	5,55E-05	99,99999599	0,014718686
77	0	170000	0,01	1,56E-04	99,99999306	0,022076199
78	0	175000	0,002	2,94E-05	99,9999937	0,012245195
79	0	175000	0,01	1,58E-04	99,99999304	0,003311639
80	0	180000	0,008	9,75E-05	99,99999469	0,000330272
81	0	185000	0,004	3,87E-05	99,99999589	0,007341467
82	0	185000	0,006	5,72E-05	99,99999591	0,00072878
83	0	190000	0,006	5,81E-05	99,99999585	0,023309001
84	0	190000	0,008	9,70E-05	99,99999474	0,002678977
85	0	195000	0,01	1,63E-04	99,99999286	0,052710431
86	0	200000	0,008	9,77E-05	99,99999473	0,006313389
87	10	3000	0,004	3,33E-06	99,99999828	0,052213667
88	10	3000	0,01	5,11E-05	99,99999397	0,004920278
89	10	4000	0,01	7,66E-05	99,99999407	0,015836682
90	10	5000	0,002	9,62E-07	99,99999841	0,06324301
91	10	5000	0,004	7,64E-06	99,99999838	0,030253132
92	10	5000	0,008	4,95E-05	99,99999681	0,008763289
93	10	5000	0,01	1,03E-04	99,99999414	0,026441669
94	10	6000	0,002	1,19E-06	99,99999851	0,067156723
95	10	6000	0,008	6,51E-05	99,99999667	0,002067541
96	10	6000	0,01	1,28E-04	99,9999942	0,018886811
97	10	7000	0,01	1,52E-04	99,99999427	0,000553387
98	10	8000	0,004	1,73E-05	99,9999984	0,045139885
99	10	9000	0,002	1,95E-06	99,99999862	0,055392054
100	10	9000	0,004	2,17E-05	99,99999839	0,043467021
101	10	9000	0,01	1,96E-04	99,99999436	0,00025449
102	10	10000	0,006	5,20E-05	99,99999823	0,006335009
103	10	10000	0,01	2,16E-04	99,99999441	0,004614918
104	10	15000	0,002	3,57E-06	99,99999868	0,043832078
105	10	15000	0,01	2,96E-04	99,99999456	0,009239105
106	10	20000	0,004	4,47E-05	99,99999888	0,016422686
107	10	25000	0,01	3,95E-04	99,99999471	0,000809669
108	10	30000	0,002	7,67E-06	99,99999871	0,031537138
109	10	30000	0,008	2,91E-04	99,99999599	0,023167275

	Displacement (mm)	Resitence (Ohm)	Amplitude (m)	MSE	Cross Correlation	Mean Percentage Error
110	10	45000	0,008	3,41E-04	99,99999597	0,031001133
111	10	50000	0,004	8,24E-05	99,99999867	0,00261547
112	10	50000	0,008	3,53E-04	99,99999596	0,004818413
113	10	50000	0,01	5,06E-04	99,99999483	0,012454428
114	10	55000	0,002	1,55E-05	99,99999873	0,027821167
115	10	55000	0,006	2,21E-04	99,99999716	0,004460888
116	10	60000	0,004	9,62E-05	99,99999853	0,004333007
117	10	60000	0,006	2,28E-04	99,99999714	0,006737207
118	10	60000	0,008	3,72E-04	99,99999595	0,014676135
119	10	60000	0,01	5,30E-04	99,99999484	0,005886474
120	10	65000	0,002	1,94E-05	99,99999873	0,027175203
121	10	65000	0,004	9,75E-05	99,99999854	0,003895202
122	10	70000	0,002	2,12E-05	99,99999873	0,030963056
123	10	70000	0,008	3,86E-04	99,99999595	0,003543107
124	10	75000	0,004	1,05E-04	99,99999847	0,008287825
125	10	80000	0,008	3,99E-04	99,99999592	0,029155994
126	10	85000	0,006	2,54E-04	99,99999704	0,003331059
127	10	85000	0,01	5,68E-04	99,99999487	0,028662613
128	10	90000	0,006	2,58E-04	99,99999704	0,00406478
129	10	90000	0,008	4,07E-04	99,99999593	0,016909093
130	10	95000	0,002	3,29E-05	99,99999874	0,028278464
131	10	100000	0,002	3,57E-05	99,99999874	0,031827411
132	10	100000	0,004	1,20E-04	99,99999836	0,000460273
133	10	100000	0,006	2,64E-04	99,99999702	0,001709935
134	10	110000	0,01	5,91E-04	99,99999488	0,04799017
135	10	120000	0,006	2,75E-04	99,99999699	0,000231637
136	10	125000	0,002	5,63E-05	99,99999868	0,035209192
137	10	125000	0,006	2,77E-04	99,99999698	0,001732374
138	10	130000	0,008	4,33E-04	99,99999591	0,032595941
139	10	130000	0,01	6,09E-04	99,99999484	0,038093119
140	10	135000	0,002	7,05E-05	99,99999861	0,047305378
141	10	135000	0,004	1,33E-04	99,99999827	0,016924318
142	10	140000	0,01	6,16E-04	99,99999483	0,05728844
143	10	145000	0,004	1,36E-04	99,99999825	0,030073846
144	10	150000	0,01	6,22E-04	99,99999482	0,066239849
145	10	165000	0,004	1,41E-04	99,9999982	0,04807743
146	10	165000	0,008	4,49E-04	99,99999587	0,036622986
147	10	165000	0,01	6,33E-04	99,99999478	0,053542588
148	10	170000	0,006	2,92E-04	99,99999692	0,000896302
149	10	170000	0,01	6,34E-04	99,99999479	0,068134303
150	10	175000	0,008	4,54E-04	99,99999585	0,049485801
151	10	180000	0,002	6,53E-05	99,99999883	0,080853912
152	10	180000	0,006	2,95E-04	99,99999691	0,020688142
153	10	185000	0,004	1,45E-04	99,99999817	0,064372859
154	10	185000	0,008	4,58E-04	99,99999584	0,034051031
155	10	190000	0,002	6,52E-05	99,99999884	0,088457696
156	10	190000	0,006	2,98E-04	99,9999969	0,014970254
157	10	190000	0,008	4,59E-04	99,99999584	0,035560432
158	10	190000	0,01	6,45E-04	99,99999475	0,050509222
159	10	195000	0,008	4,61E-04	99,99999583	0,028537645
160	10	195000	0,01	6,47E-04	99,99999475	0,045937197
161	20	2000	0,004	3,75E-06	99,99999267	0,000295289
162	20	2000	0,006	6,41E-06	99,99999466	0,044817587
163	20	3000	0,004	5,50E-06	99,99999486	0,022017532
164	20	3000	0,006	9,59E-06	99,99999622	0,014295303
165	20	4000	0,002	5,89E-06	99,99998418	0,009896287
166	20	4000	0,008	2,65E-05	99,99999668	0,004123524
167	20	4000	0,01	7,77E-05	99,99999486	0,031171727
168	20	5000	0,008	3,77E-05	99,99999679	0,019220179
169	20	5000	0,01	3,01E-04	99,99999144	0,016532935
170	20	6000	0,002	9,32E-06	99,99998641	0,011865109
171	20	6000	0,004	1,38E-05	99,99999576	0,019636565
172	20	6000	0,006	2,10E-05	99,99999748	0,010534158
173	20	7000	0,002	1,20E-05	99,99998575	0,026271395
174	20	7000	0,004	1,46E-05	99,99999652	0,006699227
175	20	7000	0,008	6,55E-05	99,99999684	0,035756953

	Displacement (mm)	Resitence (Ohm)	Amplitude (m)	MSE	Cross Correlation	Mean Percentage Error
176	20	8000	0,002	1,29E-05	99,99998728	4,772E-06
177	20	8000	0,008	8,32E-05	99,99999681	0,01167118
178	20	9000	0,002	1,29E-05	99,99998912	0,015542067
179	20	9000	0,006	3,54E-05	99,99999768	0,012154924
180	20	20000	0,008	8,66E-04	99,99999341	0,024921599
181	20	25000	0,002	2,94E-05	99,99999128	0,007905381
182	20	25000	0,004	4,84E-05	99,99999742	0,006605399
183	20	30000	0,008	1,03E-03	99,99999378	0,040068517
184	20	35000	0,006	9,54E-04	99,99999451	0,021836397
185	20	35000	0,01	1,19E-03	99,99999354	0,025593827
186	20	40000	0,002	3,39E-05	99,99999286	0,038188984
187	20	40000	0,008	1,16E-03	99,99999392	0,019718053
188	20	45000	0,002	4,15E-05	99,99999173	0,001095403
189	20	50000	0,002	5,04E-05	99,99999038	0,016021443
190	20	50000	0,008	1,25E-03	99,999994	0,017636818
191	20	55000	0,004	1,24E-04	99,99999756	0,014678709
192	20	55000	0,01	1,37E-03	99,99999374	0,015040129
193	20	60000	0,008	1,34E-03	99,99999398	0,03783974
194	20	65000	0,002	4,06E-05	99,99999345	0,015989961
195	20	75000	0,002	4,54E-05	99,99999306	0,011767435
196	20	80000	0,002	4,64E-05	99,99999311	0,01174819
197	20	85000	0,008	1,51E-03	99,9999939	0,017376139
198	20	90000	0,002	5,55E-05	99,999992	0,007442442
199	20	90000	0,004	1,27E-03	99,99999503	0,020111104
200	20	95000	0,002	5,83E-05	99,99999174	0,006623041
201	20	95000	0,008	1,56E-03	99,99999388	0,03560437
202	20	95000	0,01	1,59E-03	99,9999938	0,012267487
203	20	100000	0,004	1,35E-03	99,99999485	0,01964038
204	20	105000	0,002	5,60E-05	99,9999924	0,022042672
205	20	105000	0,004	1,39E-03	99,99999476	0,042456052
206	20	105000	0,006	1,57E-03	99,999994	0,054807362
207	20	105000	0,008	1,60E-03	99,99999387	0,046061968
208	20	110000	0,002	5,77E-05	99,99999229	0,00051681
209	20	110000	0,006	1,59E-03	99,99999398	0,026908231
210	20	115000	0,008	1,64E-03	99,99999385	0,033901035
211	20	120000	0,002	5,72E-05	99,99999258	0,027249528
212	20	120000	0,004	1,48E-03	99,99999454	0,052918384
213	20	120000	0,006	1,63E-03	99,99999394	0,018771845
214	20	125000	0,002	5,78E-05	99,99999259	0,048595216
215	20	125000	0,006	1,66E-03	99,99999389	0,032263706
216	20	130000	0,006	1,67E-03	99,99999389	0,042837535
217	20	130000	0,008	1,70E-03	99,99999379	0,024202093
218	20	135000	0,004	1,56E-03	99,99999435	0,038659643
219	20	135000	0,008	1,71E-03	99,99999378	0,013046217
220	20	135000	0,01	1,70E-03	99,99999381	0,013742043
221	20	140000	0,004	1,59E-03	99,99999429	0,053669839
222	20	140000	0,008	1,72E-03	99,99999378	0,01852663
223	20	145000	0,01	1,72E-03	99,99999381	0,044549911
224	20	155000	0,004	1,65E-03	99,99999415	0,04156237
225	20	155000	0,006	1,75E-03	99,99999377	0,030326896
226	20	160000	0,004	1,67E-03	99,99999411	0,057189527
227	20	160000	0,01	1,75E-03	99,99999379	0,031279247
228	20	170000	0,002	5,93E-05	99,99999306	0,046746309
229	20	170000	0,004	1,70E-03	99,99999405	0,040034997
230	20	170000	0,006	1,79E-03	99,99999372	0,01871706
231	20	175000	0,004	1,71E-03	99,99999401	0,043483058
232	20	175000	0,01	1,78E-03	99,99999376	0,018230068
233	20	185000	0,004	1,74E-03	99,99999395	0,029146963
234	20	185000	0,006	1,82E-03	99,99999368	0,046930995
235	20	195000	0,008	1,84E-03	99,99999364	0,021940791
236	20	200000	0,008	1,84E-03	99,99999364	0,029434814
237	30	2000	0,002	4,36E-06	99,99995844	0,035127846
238	30	2000	0,004	6,23E-06	99,99998573	0,004830826
239	30	2000	0,008	1,43E-05	99,99999182	0,048787913
240	30	2000	0,01	2,42E-05	99,99999116	0,051832347
241	30	3000	0,004	1,02E-05	99,99998909	0,052642778

	Displacement (mm)	Resitence (Ohm)	Amplitude (m)	MSE	Cross Correlation	Mean Percentage Error
242	30	4000	0,002	9,69E-06	99,99997294	0,007792116
243	30	4000	0,008	2,32E-05	99,99999681	0,017067911
244	30	4000	0,01	3,88E-05	99,99999648	0,018747626
245	30	5000	0,002	1,36E-05	99,99997361	0,009489902
246	30	7000	0,002	1,78E-05	99,99997966	0,02624356
247	30	8000	0,002	1,82E-05	99,99998302	0,019320872
248	30	8000	0,008	5,86E-05	99,99999808	0,001194453
249	30	10000	0,004	3,13E-05	99,99999593	0,007849668
250	30	15000	0,002	2,95E-05	99,99998777	0,034658745
251	30	15000	0,004	4,49E-05	99,99999673	0,030670255
252	30	15000	0,01	3,69E-03	99,99997728	0,022497382
253	30	20000	0,004	5,90E-05	99,99999691	0,031056851
254	30	25000	0,004	6,37E-05	99,99999754	0,013549652
255	30	25000	0,008	4,67E-03	99,99997834	0,039399537
256	30	30000	0,01	5,30E-03	99,99997832	0,018011968
257	30	35000	0,006	1,53E-04	99,99999873	0,006420095
258	30	40000	0,002	8,88E-05	99,99998307	0,017124935
259	30	40000	0,006	1,95E-04	99,99999815	0,000675387
260	30	45000	0,01	6,11E-03	99,99997853	0,010929642
261	30	50000	0,004	1,27E-04	99,99999654	0,014176035
262	30	50000	0,008	6,64E-03	99,99997718	0,009266207
263	30	60000	0,01	6,67E-03	99,99997848	0,011279517
264	30	65000	0,004	1,30E-04	99,99999713	0,014549539
265	30	65000	0,006	7,37E-03	99,99997643	0,003954738
266	30	70000	0,008	7,44E-03	99,9999768	0,001072632
267	30	75000	0,002	9,31E-05	99,99998746	0,00210921
268	30	75000	0,004	1,23E-04	99,99999768	0,009410588
269	30	75000	0,008	7,57E-03	99,99997678	0,019602351
270	30	80000	0,01	7,26E-03	99,99997814	0,004294887
271	30	90000	0,002	9,90E-05	99,99998755	0,016769131
272	30	90000	0,008	7,99E-03	99,99997647	0,001322851
273	30	90000	0,01	7,55E-03	99,9999778	0,027576297
274	30	95000	0,002	1,01E-04	99,99998746	0,015943126
275	30	95000	0,004	1,30E-04	99,9999978	0,009100386
276	30	100000	0,004	1,41E-04	99,99999752	0,012133424
277	30	100000	0,008	8,20E-03	99,99997635	0,007027194
278	30	105000	0,008	8,35E-03	99,99997615	0,003410053
279	30	110000	0,004	1,40E-04	99,99999765	0,010625171
280	30	110000	0,008	8,45E-03	99,99997605	0,00601952
281	30	115000	0,01	8,01E-03	99,99997741	0,007265361
282	30	120000	0,002	1,06E-04	99,99998777	0,031190933
283	30	120000	0,006	9,42E-03	99,9999738	0,032058512
284	30	120000	0,008	8,70E-03	99,9999757	0,015632636
285	30	120000	0,01	8,07E-03	99,99997739	0,013060828
286	30	125000	0,004	1,54E-04	99,99999739	0,015710737
287	30	125000	0,008	8,72E-03	99,99997581	0,021964258
288	30	130000	0,002	1,06E-04	99,99998808	0,070977099
289	30	130000	0,006	9,66E-03	99,99997347	0,002699604
290	30	140000	0,002	1,10E-04	99,99998788	0,009371637
291	30	140000	0,006	9,86E-03	99,99997323	0,024013122
292	30	140000	0,008	8,95E-03	99,99997556	0,000362691
293	30	140000	0,01	8,39E-03	99,99997701	0,027626757
294	30	145000	0,002	1,03E-04	99,99998887	0,038202881
295	30	145000	0,004	1,51E-04	99,9999976	0,01399717
296	30	145000	0,006	9,87E-03	99,99997333	0,010028649
297	30	150000	0,002	1,13E-04	99,99998772	0,013299294
298	30	160000	0,002	1,05E-04	99,99998887	0,055372859
299	30	170000	0,01	8,76E-03	99,99997652	0,010161483
300	30	175000	0,004	1,57E-04	99,99999756	0,003958284
301	30	175000	0,008	9,31E-03	99,99997527	0,001785711
302	30	175000	0,01	8,79E-03	99,99997652	0,007783571
303	30	180000	0,002	1,06E-04	99,99998901	0,107242289
304	30	185000	0,002	1,07E-04	99,99998895	0,060938953
305	30	185000	0,008	9,41E-03	99,99997516	0,031713416
306	30	190000	0,01	8,93E-03	99,99997633	0,004536374
307	30	195000	0,002	1,01E-04	99,99998988	0,057456408

	Displacement (mm)	Resitence (Ohm)	Amplitude (m)	MSE	Cross Correlation	Mean Percentage Error
308	30	200000	0,004	1,73E-04	99,99999727	0,014297213
309	30	200000	0,008	9,55E-03	99,99997497	0,008220896
310	40	2000	0,006	1,82E-05	99,99998032	0,093666338
311	40	2000	0,008	2,97E-05	99,99998221	0,091268333
312	40	3000	0,002	9,80E-06	99,99994935	0,070318459
313	40	3000	0,008	3,31E-05	99,99998984	0,054948701
314	40	4000	0,004	1,85E-05	99,9999861	0,019219441
315	40	4000	0,008	4,11E-05	99,99999248	0,041106612
316	40	4000	0,01	5,83E-05	99,99999319	0,035332408
317	40	5000	0,006	2,90E-05	99,99999379	0,041463159
318	40	6000	0,006	3,70E-05	99,9999944	0,046912188
319	40	6000	0,01	7,87E-05	99,999996	0,002697497
320	40	7000	0,004	3,33E-05	99,99999069	0,048866773
321	40	8000	0,002	3,47E-05	99,9999647	0,029892023
322	40	8000	0,008	7,21E-05	99,99999684	0,007085644
323	40	9000	0,006	4,67E-05	99,99999709	0,017197397
324	40	9000	0,008	8,01E-05	99,99999733	0,007560193
325	40	10000	0,004	5,58E-05	99,99999111	0,040126824
326	40	10000	0,006	5,74E-05	99,99999696	0,002466859
327	40	15000	0,006	8,86E-05	99,99999782	0,005384045
328	40	20000	0,006	1,05E-04	99,99999872	0,018902904
329	40	25000	0,002	7,20E-05	99,99998177	0,089627418
330	40	25000	0,004	7,19E-05	99,99999763	0,016335814
331	40	25000	0,006	1,33E-04	99,99999874	0,014567464
332	40	30000	0,002	8,17E-05	99,99998221	0,029852876
333	40	30000	0,004	8,23E-05	99,9999978	0,015929822
334	40	30000	0,006	1,57E-04	99,9999988	0,019873587
335	40	35000	0,006	1,77E-04	99,99999885	0,019445201
336	40	35000	0,01	2,14E-02	99,9999377	0,027916426
337	40	40000	0,002	1,02E-04	99,99998161	0,194597055
338	40	40000	0,004	9,62E-05	99,99999814	0,008994731
339	40	40000	0,006	1,95E-04	99,99999889	0,028588937
340	40	40000	0,008	3,73E-04	99,99999882	0,023528787
341	40	45000	0,008	4,10E-04	99,99999875	0,034886921
342	40	55000	0,01	2,50E-02	99,99993752	0,008512867
343	40	60000	0,002	1,14E-04	99,99998388	0,042182386
344	40	60000	0,006	2,45E-04	99,99999897	0,029972074
345	40	65000	0,004	1,35E-04	99,99999781	0,031699562
346	40	65000	0,01	2,63E-02	99,99993719	0,003870641
347	40	70000	0,002	1,41E-04	99,99998071	0,052370479
348	40	70000	0,008	2,93E-02	99,99993115	0,035154531
349	40	80000	0,002	1,04E-04	99,99998747	0,069841467
350	40	80000	0,006	2,83E-04	99,99999886	0,019884192
351	40	80000	0,01	2,81E-02	99,99993607	0,017859439
352	40	85000	0,006	2,91E-04	99,99999884	0,028224689
353	40	85000	0,008	3,10E-02	99,99993033	0,032362593
354	40	90000	0,008	3,15E-02	99,99993003	0,04281957
355	40	90000	0,01	2,91E-02	99,99993522	0,012348113
356	40	95000	0,002	1,31E-04	99,99998445	0,054034665
357	40	100000	0,002	1,18E-04	99,99998654	0,050877365
358	40	100000	0,006	3,12E-04	99,99999872	0,030210913
359	40	100000	0,008	3,24E-02	99,9999294	0,014423651
360	40	100000	0,01	3,00E-02	99,99993442	0,025009546
361	40	105000	0,002	9,99E-05	99,99998924	0,041098692
362	40	105000	0,006	3,11E-04	99,99999879	0,027182675
363	40	105000	0,01	3,03E-02	99,99993432	0,007724668
364	40	110000	0,002	1,29E-04	99,9999854	0,023526859
365	40	110000	0,004	1,54E-04	99,99999803	0,017693201
366	40	110000	0,006	3,23E-04	99,99999865	0,029442864
367	40	110000	0,008	3,32E-02	99,99992878	0,00987783
368	40	110000	0,01	3,06E-02	99,99993424	0,0354081
369	40	115000	0,002	1,54E-04	99,99998231	0,014145913
370	40	115000	0,01	3,07E-02	99,9999344	0,055797477
371	40	125000	0,008	3,42E-02	99,99992816	0,036826943
372	40	130000	0,004	1,63E-04	99,99999791	0,01886616
373	40	130000	0,01	3,16E-02	99,99993367	0,008602352

	Displacement (mm)	Resitence (Ohm)	Amplitude (m)	MSE	Cross Correlation	Mean Percentage Error
374	40	135000	0,002	9,09E-05	99,9999912	0,028375441
375	40	135000	0,004	1,56E-04	99,99999819	0,01744633
376	40	145000	0,004	1,56E-04	99,99999824	0,022205622
377	40	155000	0,004	1,80E-04	99,99999754	0,011027658
378	40	155000	0,006	3,54E-04	99,99999839	0,020617904
379	40	160000	0,004	1,75E-04	99,99999773	0,01332335
380	40	160000	0,01	3,29E-02	99,99993269	0,02981118
381	40	165000	0,008	3,61E-02	99,99992671	0,015970686
382	40	170000	0,002	8,66E-05	99,99999223	0,030505959
383	40	175000	0,004	1,57E-04	99,99999838	0,025275095
384	40	175000	0,006	3,71E-04	99,99999815	0,014620613
385	40	180000	0,01	3,36E-02	99,99993211	0,056519577
386	40	185000	0,006	3,84E-04	99,99999794	0,015044006
387	40	190000	0,004	1,67E-04	99,99999815	0,019016272
388	40	195000	0,004	1,81E-04	99,99999773	0,014063396
389	40	195000	0,008	3,72E-02	99,99992586	0,037392856
390	40	195000	0,01	3,41E-02	99,99993164	0,033909671
391	40	200000	0,002	1,61E-04	99,99998366	0,015630808
392	40	200000	0,006	4,74E-04	99,99999664	0,014456301
393	0	2000	0,002	1,59E-03	99,99999262	0,019621558
394	0	2000	0,004	1,04E-03	99,99999457	0,063041276
395	0	2000	0,006	1,42E-03	99,99999333	0,065031318
396	0	2000	0,008	1,74E-03	99,99999236	0,024449144
397	0	3000	0,004	4,29E-05	99,99999269	0,009354683
398	0	3000	0,006	1,43E-03	99,99999346	0,045786145
399	0	3000	0,01	1,66E-03	99,99999257	0,033155646
400	0	4000	0,004	1,73E-03	99,99999277	0,078792503
401	0	4000	0,01	4,33E-05	99,99999281	0,005661655
402	0	5000	0,004	1,06E-03	99,99999466	0,061104286
403	0	5000	0,008	5,06E-05	99,99999184	0,021303461
404	0	8000	0,008	1,22E-03	99,99999401	0,058259777
405	0	9000	0,002	1,54E-03	99,99999294	0,057563711
406	0	9000	0,004	1,65E-03	99,99999288	0,029597303
407	0	10000	0,008	1,15E-03	99,99999436	0,037213133
408	0	15000	0,006	1,50E-03	99,99999336	0,06682077
409	0	15000	0,01	1,89E-03	99,99999209	0,027624398
410	0	20000	0,002	1,15E-03	99,99999445	0,084128381
411	0	20000	0,008	1,64E-03	99,99999269	0,047479839
412	0	25000	0,002	5,55E-05	99,99999155	0,006428311
413	0	30000	0,002	1,21E-03	99,99999422	0,040361173
414	0	30000	0,006	5,85E-05	99,99999131	0,058438011
415	0	30000	0,01	1,84E-03	99,99999249	0,030389959
416	0	35000	0,006	1,31E-03	99,99999387	0,056645377
417	0	40000	0,004	1,55E-03	99,99999326	0,044283245
418	0	40000	0,008	1,74E-03	99,99999274	0,048991921
419	0	50000	0,006	1,84E-03	99,99999255	0,030001835
420	0	55000	0,006	1,38E-03	99,99999365	0,042924726
421	0	65000	0,002	1,74E-03	99,99999277	0,046126104
422	0	65000	0,006	5,48E-05	99,99999218	0,06085258
423	0	65000	0,008	1,29E-03	99,99999403	0,06920849
424	0	70000	0,006	1,71E-03	99,99999268	0,030014009
425	0	75000	0,002	5,34E-05	99,99999247	0,062971425
426	0	75000	0,004	1,83E-03	99,99999275	0,018072288
427	0	75000	0,008	5,14E-05	99,99999284	0,063185821
428	0	80000	0,006	1,58E-03	99,99999328	0,057275977
429	0	80000	0,008	1,72E-03	99,99999309	0,043353495
430	0	80000	0,01	2,00E-03	99,99999215	0,032779318
431	0	85000	0,002	1,34E-03	99,9999939	0,054047183
432	0	85000	0,006	1,57E-03	99,99999344	0,052093426
433	0	85000	0,01	1,91E-03	99,9999923	0,020141394
434	0	95000	0,002	5,22E-05	99,99999288	0,065239123
435	0	95000	0,006	1,31E-03	99,99999407	0,075068965
436	0	95000	0,008	1,57E-03	99,99999345	0,063112028
437	0	95000	0,01	1,78E-03	99,99999277	0,030470592
438	0	100000	0,006	5,68E-05	99,99999237	0,07433955
439	0	100000	0,01	1,29E-03	99,99999422	0,071646104

	Displacement (mm)	Resitence (Ohm)	Amplitude (m)	MSE	Cross Correlation	Mean Percentage Error
440	0	105000	0,01	1,78E-03	99,9999926	0,053341478
441	0	110000	0,002	5,49E-05	99,99999266	0,068730923
442	0	110000	0,008	1,51E-03	99,99999333	0,055847123
443	0	115000	0,002	1,71E-03	99,99999284	0,050010414
444	0	115000	0,004	1,75E-03	99,99999301	0,049556456
445	0	115000	0,008	1,53E-03	99,99999329	0,044707346
446	0	120000	0,002	1,72E-03	99,99999285	0,039760262
447	0	125000	0,004	1,75E-03	99,99999304	0,038725399
448	0	130000	0,008	1,83E-03	99,99999303	0,036069173
449	0	130000	0,01	5,44E-05	99,99999287	0,057623346
450	0	135000	0,008	1,53E-03	99,99999329	0,059048704
451	0	140000	0,002	1,71E-03	99,99999289	0,04336487
452	0	145000	0,004	1,79E-03	99,99999286	0,045511962
453	0	145000	0,006	1,85E-03	99,9999929	0,04245514
454	0	145000	0,008	5,49E-05	99,99999288	0,046040228
455	0	150000	0,006	1,95E-03	99,99999233	0,018406664
456	0	155000	0,002	1,89E-03	99,99999272	0,031957423
457	0	160000	0,006	5,53E-05	99,99999287	0,067217644
458	0	160000	0,008	1,31E-03	99,99999424	0,060406574
459	0	170000	0,01	1,57E-03	99,9999936	0,038299583
460	0	175000	0,01	1,96E-03	99,99999249	0,025302078
461	0	180000	0,004	5,37E-05	99,99999315	0,045157481
462	0	180000	0,006	1,32E-03	99,99999424	0,063979548
463	0	180000	0,01	1,95E-03	99,99999235	0,04922537
464	0	185000	0,002	1,89E-03	99,99999278	0,03297558
465	0	185000	0,006	1,48E-03	99,99999354	0,038111532
466	0	190000	0,004	1,57E-03	99,99999362	0,071682341
467	0	190000	0,01	1,96E-03	99,99999236	0,024962819
468	0	195000	0,002	1,97E-03	99,9999925	0,024487978
469	0	195000	0,004	1,60E-03	99,9999937	0,020884292
470	10	2000	0,004	1,99E-03	99,99999279	0,042775065
471	10	3000	0,002	1,88E-03	99,99999305	0,016381196
472	10	3000	0,008	5,31E-05	99,99999352	0,012547504
473	10	5000	0,004	1,74E-03	99,9999934	0,022711107
474	10	6000	0,002	1,86E-03	99,99999305	0,055114785
475	10	6000	0,004	1,81E-03	99,99999323	0,03122796
476	10	6000	0,01	5,47E-05	99,99999335	0,003475193
477	10	7000	0,004	1,87E-03	99,99999304	0,038541307
478	10	8000	0,004	1,79E-03	99,99999322	0,023442391
479	10	8000	0,008	1,81E-03	99,99999323	0,020091869
480	10	9000	0,01	5,64E-05	99,9999932	0,004246773
481	10	10000	0,006	1,76E-03	99,99999338	0,024752778
482	10	15000	0,002	1,75E-03	99,9999933	0,05112439
483	10	15000	0,006	1,70E-03	99,99999345	0,034163405
484	10	20000	0,01	2,11E-03	99,99999264	0,010426827
485	10	25000	0,004	6,00E-06	99,99994318	0,068243023
486	10	25000	0,008	1,10E-05	99,99997593	0,012571574
487	10	35000	0,01	4,06E-06	99,99999616	0,016107449
488	10	40000	0,004	4,20E-06	99,99999797	0,000985909
489	10	40000	0,006	8,17E-06	99,9999975	0,021373473
490	10	45000	0,008	7,85E-06	99,9999981	0,009542062
491	10	50000	0,002	9,05E-06	99,99999869	0,01879084
492	10	50000	0,004	1,14E-05	99,99996877	0,008622714
493	10	50000	0,008	1,97E-05	99,99998756	0,001696871
494	10	55000	0,01	8,38E-06	99,99999779	0,009615292
495	10	65000	0,002	1,39E-05	99,99999822	0,002369832
496	10	65000	0,008	2,07E-05	99,99996122	0,017489422
497	10	65000	0,01	1,16E-05	99,99999476	0,050132302
498	10	70000	0,002	1,46E-05	99,99999735	0,009045939
499	10	70000	0,004	1,41E-05	99,99999874	0,003921856
500	10	75000	0,004	2,55E-05	99,99999855	0,063542085
501	10	75000	0,008	1,58E-05	99,99997803	0,007061576
502	10	80000	0,008	1,19E-05	99,99999627	0,002847139
503	10	85000	0,004	2,02E-05	99,99999746	0,007178087
504	10	85000	0,008	2,74E-05	99,99999822	0,00030025
505	10	90000	0,01	1,57E-05	99,99998141	0,035623437

	Displacement (mm)	Resitence (Ohm)	Amplitude (m)	MSE	Cross Correlation	Mean Percentage Error
506	10	95000	0,002	1,62E-05	99,99999605	0,01832444
507	10	95000	0,006	2,21E-05	99,99999786	0,019949175
508	10	95000	0,008	3,30E-05	99,9999983	0,002489118
509	10	95000	0,01	2,27E-05	99,99999504	0,051877596
510	10	100000	0,004	2,45E-05	99,99999808	0,010295431
511	10	100000	0,008	2,84E-05	99,99999863	0,011441324
512	10	105000	0,002	2,08E-05	99,99999869	0,010087249
513	10	105000	0,006	2,83E-05	99,99999888	0,017142302
514	10	115000	0,002	5,81E-05	99,99999852	0,011146655
515	10	115000	0,006	2,18E-05	99,99998516	0,023610615
516	10	115000	0,008	3,40E-05	99,99999477	0,02153989
517	10	115000	0,01	5,94E-05	99,99999858	0,003371756
518	10	120000	0,002	2,67E-05	99,99998811	0,050849951
519	10	120000	0,004	3,35E-05	99,99999683	0,040499773
520	10	120000	0,006	3,99E-03	99,99997601	0,020777382
521	10	125000	0,002	5,33E-05	99,99999626	0,049188351
522	10	130000	0,01	9,05E-05	99,99999869	0,006109938
523	10	145000	0,008	5,52E-05	99,99998406	0,075734886
524	10	150000	0,002	5,04E-03	99,99997748	0,048741051
525	10	150000	0,006	6,55E-05	99,99998405	0,014900469
526	10	150000	0,008	7,81E-05	99,99999863	0,00940273
527	10	150000	0,01	5,86E-03	99,99997759	0,025111153
528	10	155000	0,01	7,02E-05	99,99998438	0,110151185
529	10	160000	0,006	7,72E-05	99,99999633	0,03749646
530	10	165000	0,008	9,10E-05	99,99999851	0,002124933
531	10	165000	0,01	9,66E-05	99,99999826	0,013974907
532	10	175000	0,002	6,44E-03	99,99997644	0,046666736
533	10	175000	0,006	6,39E-03	99,99997726	0,025681589
534	10	180000	0,006	6,84E-05	99,99999731	0,035461614
535	10	180000	0,008	6,81E-03	99,99997569	0,00082639
536	10	185000	0,002	6,59E-03	99,99997766	0,022846369
537	10	185000	0,008	1,26E-04	99,99999808	0,004403251
538	10	190000	0,006	6,89E-03	99,99997699	0,02801671
539	10	190000	0,01	6,96E-03	99,99997645	0,014636811
540	10	195000	0,002	8,98E-05	99,99998455	0,038549272
541	10	195000	0,008	7,35E-05	99,99999738	0,032688613
542	10	200000	0,008	7,17E-03	99,99997649	0,002243207
543	20	2000	0,002	1,10E-04	99,99999676	0,00873829
544	20	2000	0,006	7,15E-03	99,99997623	0,018788876
545	20	3000	0,004	6,79E-03	99,99997814	0,013098643
546	20	3000	0,01	1,16E-04	99,99999677	0,019613451
547	20	4000	0,008	7,13E-03	99,99997707	0,028620837
548	20	4000	0,01	7,21E-03	99,9999772	0,000576613
549	20	5000	0,006	1,05E-04	99,99999735	0,025703544
550	20	5000	0,008	7,42E-03	99,99997658	0,00057555
551	20	6000	0,008	7,28E-03	99,99997735	0,021166526
552	20	7000	0,008	8,92E-05	99,99998709	0,001709723
553	20	8000	0,004	1,01E-04	99,99999756	0,014750542
554	20	8000	0,006	7,54E-03	99,99997607	0,028375645
555	20	8000	0,008	7,95E-03	99,99997561	0,019704762
556	20	9000	0,004	1,09E-04	99,99998433	0,057951142
557	20	9000	0,006	1,30E-04	99,9999967	0,011072736
558	20	9000	0,008	7,77E-03	99,99997571	0,012969847
559	20	10000	0,008	8,12E-03	99,99997589	0,005080408
560	20	15000	0,002	9,50E-05	99,99998693	0,018939661
561	20	15000	0,004	1,20E-04	99,99999711	0,012099364
562	20	15000	0,006	7,92E-03	99,9999756	0,014851626
563	20	15000	0,008	7,45E-03	99,99997771	0,086621752
564	20	15000	0,01	1,10E-04	99,99998514	0,023947843
565	20	20000	0,01	8,46E-03	99,99997551	0,031362577
566	20	35000	0,002	9,70E-05	99,99998726	0,020097006
567	20	35000	0,004	8,00E-03	99,99997629	0,038234564
568	20	35000	0,008	1,06E-04	99,9999862	0,062567179
569	20	40000	0,006	1,14E-04	99,9999976	0,013718759
570	20	45000	0,002	8,91E-03	99,99997398	0,00340345
571	20	45000	0,004	1,18E-04	99,9999851	0,041145061

	Displacement (mm)	Resitence (Ohm)	Amplitude (m)	MSE	Cross Correlation	Mean Percentage Error
572	20	45000	0,01	1,13E-04	99,99999772	0,013978949
573	20	55000	0,004	8,53E-03	99,99997478	0,007894275
574	20	55000	0,008	9,07E-03	99,99997434	0,003979182
575	20	60000	0,002	8,07E-03	99,99997674	0,005113188
576	20	60000	0,008	1,10E-04	99,99998658	0,005636641
577	20	60000	0,01	1,38E-04	99,9999972	0,019101385
578	20	65000	0,01	9,60E-03	99,99997279	0,007021232
579	20	70000	0,002	8,85E-03	99,99997487	0,006620872
580	20	70000	0,004	1,30E-04	99,99999732	0,007114628
581	20	75000	0,004	8,80E-03	99,99997438	0,002556562
582	20	75000	0,008	7,98E-03	99,99997725	0,012171429
583	20	75000	0,01	1,27E-04	99,99999742	0,012550743
584	20	80000	0,002	9,45E-03	99,99997328	0,033745423
585	20	80000	0,004	1,11E-04	99,99998694	0,087557362
586	20	80000	0,008	9,91E-03	99,99997254	0,004083406
587	20	85000	0,002	1,03E-04	99,99998801	0,077027705
588	20	85000	0,004	9,37E-03	99,99997355	0,007087827
589	20	85000	0,006	1,06E-04	99,99998797	0,084512716
590	20	85000	0,008	1,54E-04	99,99999704	0,020416521
591	20	85000	0,01	1,01E-02	99,99997233	0,016777423
592	20	90000	0,002	1,07E-04	99,99998783	0,015502472
593	20	90000	0,004	1,56E-04	99,99999703	0,019242467
594	20	90000	0,01	9,54E-03	99,99997334	0,026712587
595	20	100000	0,006	8,31E-03	99,99997692	0,020155148
596	20	100000	0,01	9,45E-03	99,9999743	6,14066E-05
597	20	105000	0,004	8,84E-03	99,99997584	0,007094051
598	20	105000	0,006	1,19E-04	99,99998677	0,026045007
599	20	105000	0,008	9,45E-03	99,9999744	0,018249032
600	20	115000	0,004	1,04E-04	99,99998844	0,010828961
601	20	125000	0,002	9,48E-03	99,9999744	0,006267993
602	20	125000	0,004	1,01E-04	99,99998895	0,061224953
603	20	130000	0,002	1,38E-04	99,99999757	0,019018173
604	20	130000	0,006	1,00E-02	99,99997274	0,015514848
605	20	135000	0,004	8,94E-03	99,99997544	0,007582693
606	20	135000	0,008	8,78E-03	99,99997608	0,025231291
607	20	140000	0,008	9,17E-03	99,99997437	0,014402663
608	20	140000	0,01	9,99E-03	99,99997355	0,012335317
609	20	150000	0,002	8,83E-03	99,99997602	0,013080221
610	20	150000	0,008	1,18E-04	99,99998751	0,097665667
611	20	155000	0,008	9,22E-03	99,9999743	0,004005764
612	20	160000	0,01	9,60E-03	99,99997432	0,007332615
613	20	165000	0,004	9,84E-03	99,9999732	0,010220804
614	20	165000	0,006	9,03E-03	99,99997541	0,004554444
615	20	165000	0,008	1,03E-04	99,9999889	0,113969332
616	20	170000	0,002	1,02E-02	99,99997254	0,016334302
617	20	170000	0,004	9,37E-03	99,99997479	0,000827347
618	20	170000	0,006	1,22E-04	99,99998725	0,072595591
619	20	170000	0,008	1,03E-02	99,99997253	0,021352351
620	20	180000	0,004	9,75E-03	99,99997412	0,026937976
621	20	185000	0,004	1,08E-04	99,99998875	0,05621085
622	20	185000	0,006	1,68E-04	99,99999692	0,012443113
623	20	185000	0,008	1,31E-04	99,99998652	0,070963999
624	20	185000	0,01	1,62E-04	99,99999702	0,016451763
625	20	190000	0,006	9,42E-03	99,99997407	0,015973204
626	20	190000	0,01	9,81E-03	99,99997411	0,016022315
627	20	195000	0,004	1,51E-04	99,99999717	0,017303308
628	20	200000	0,002	8,92E-03	99,99997608	0,017023118
629	20	200000	0,01	7,06E-06	99,99992428	0,114262692
630	30	2000	0,002	1,81E-05	99,99999305	0,040272769
631	30	2000	0,006	3,31E-05	99,99999409	0,030011224
632	30	2000	0,008	1,87E-05	99,99999472	0,020647425
633	30	3000	0,004	4,78E-05	99,99999143	0,038579696
634	30	3000	0,01	3,46E-05	99,99999789	0,011714225
635	30	4000	0,002	2,22E-05	99,99995188	0,151039449
636	30	4000	0,004	3,65E-05	99,99998078	0,034939805
637	30	5000	0,008	5,40E-05	99,99991378	0,251388645

	Displacement (mm)	Resitence (Ohm)	Amplitude (m)	MSE	Cross Correlation	Mean Percentage Error
638	30	5000	0,01	4,62E-05	99,9999818	0,075646946
639	30	6000	0,01	3,31E-05	99,99999623	0,009738325
640	30	7000	0,002	4,93E-05	99,99999634	0,001004478
641	30	7000	0,008	3,73E-05	99,99995211	0,214385067
642	30	8000	0,006	3,39E-05	99,99999695	0,013765836
643	30	9000	0,004	8,44E-05	99,99999731	0,012824684
644	30	9000	0,01	3,54E-05	99,99996386	0,030445734
645	30	10000	0,002	4,10E-05	99,99999075	0,037788384
646	30	10000	0,004	4,07E-05	99,99999752	0,00143916
647	30	20000	0,002	8,34E-05	99,99999871	0,02330974
648	30	20000	0,004	5,51E-05	99,99995074	0,093234618
649	30	25000	0,008	6,40E-05	99,99998645	0,080845243
650	30	25000	0,01	4,01E-05	99,99999796	0,004542629
651	30	30000	0,004	6,65E-05	99,99999822	0,004412779
652	30	30000	0,006	5,50E-05	99,99995733	0,150805066
653	30	30000	0,008	7,06E-05	99,99999526	0,011349567
654	30	30000	0,01	9,11E-05	99,9999973	0,00573913
655	30	35000	0,01	3,95E-05	99,99999732	0,022743801
656	30	40000	0,004	7,81E-05	99,999998	0,007123364
657	30	40000	0,006	3,61E-05	99,9999893	0,018864921
658	30	45000	0,002	4,94E-05	99,99999809	0,001712128
659	30	50000	0,002	2,39E-04	99,99999926	0,027791336
660	30	55000	0,002	6,30E-05	99,99999777	0,014780773
661	30	55000	0,004	1,11E-04	99,99999891	0,013090847
662	30	55000	0,006	2,99E-04	99,9999992	0,040495092
663	30	60000	0,002	8,24E-05	99,99998116	0,013866552
664	30	60000	0,004	7,71E-05	99,99999745	0,009252256
665	30	60000	0,006	2,63E-04	99,99999874	0,026661892
666	30	65000	0,01	2,04E-02	99,99993675	0,011448495
667	30	70000	0,008	8,59E-05	99,99999763	0,016043387
668	30	75000	0,004	1,59E-04	99,99999869	0,01579751
669	30	75000	0,008	2,99E-04	99,99999876	0,022145719
670	30	75000	0,01	1,51E-04	99,99999926	0,028651142
671	30	80000	0,004	2,60E-04	99,99999939	0,029824225
672	30	85000	0,002	2,29E-02	99,99993682	0,02543837
673	30	85000	0,006	1,21E-04	99,99997831	0,100349657
674	30	90000	0,008	3,65E-04	99,99999868	0,031643968
675	30	90000	0,01	2,36E-02	99,99993736	0,022736239
676	30	95000	0,008	1,49E-04	99,99997475	0,027320714
677	30	95000	0,01	9,62E-05	99,99999818	0,012084632
678	30	100000	0,004	1,62E-04	99,99999943	0,021555761
679	30	105000	0,002	2,50E-02	99,99993589	0,017055904
680	30	105000	0,004	2,14E-04	99,99999876	0,01110711
681	30	110000	0,008	2,65E-02	99,99993303	0,004114874
682	30	110000	0,01	2,50E-02	99,9999376	0,012167928
683	30	115000	0,01	1,24E-04	99,99998126	0,062542845
684	30	125000	0,006	1,78E-04	99,99999939	0,023913543
685	30	130000	0,002	2,69E-02	99,99993451	0,016242574
686	30	135000	0,002	9,95E-05	99,99998611	0,071072727
687	30	135000	0,006	2,86E-02	99,99993104	0,015698747
688	30	140000	0,006	2,64E-02	99,99993672	0,004038474
689	30	140000	0,008	1,84E-04	99,99997371	0,067394482
690	30	140000	0,01	2,25E-04	99,99999896	0,024057625
691	30	145000	0,006	2,71E-02	99,99993631	0,041318323
692	30	145000	0,008	1,97E-04	99,99999935	0,019582721
693	30	155000	0,002	2,84E-02	99,99993446	0,004818795
694	30	155000	0,004	1,05E-04	99,99998678	0,078181937
695	30	160000	0,004	1,43E-04	99,99999758	0,000883943
696	30	160000	0,008	1,02E-04	99,99998749	0,031935793
697	30	165000	0,002	1,74E-04	99,9999968	0,010361043
698	30	165000	0,01	2,21E-04	99,99999921	0,024847924
699	30	170000	0,004	1,64E-04	99,99997902	0,031627242
700	30	180000	0,004	1,88E-04	99,99999651	0,00640377
701	30	180000	0,01	2,12E-04	99,99999928	0,024931535
702	30	185000	0,002	3,06E-02	99,99993102	0,041957571
703	30	185000	0,01	1,26E-04	99,99998474	0,057362725

	Displacement (mm)	Resitence (Ohm)	Amplitude (m)	MSE	Cross Correlation	Mean Percentage Error
704	30	190000	0,002	2,37E-04	99,99999911	0,028479198
705	30	190000	0,004	3,24E-02	99,99992831	0,003562056
706	30	195000	0,004	3,11E-02	99,99993163	0,016256302
707	30	200000	0,002	1,28E-04	99,99998675	0,046385904
708	40	2000	0,002	3,36E-02	99,9999279	0,019677981
709	40	2000	0,004	3,04E-02	99,99993392	0,021125976
710	40	3000	0,008	1,09E-04	99,99998948	0,035894176
711	40	4000	0,002	3,76E-04	99,9999991	0,035787456
712	40	4000	0,004	3,47E-02	99,99992652	0,002289414
713	40	5000	0,002	1,43E-04	99,99998521	0,021200855
714	40	5000	0,004	2,22E-04	99,99999754	0,022172807
715	40	5000	0,008	3,32E-02	99,99992908	0,00850455
716	40	6000	0,008	3,22E-02	99,99993194	0,036192678
717	40	7000	0,004	1,90E-04	99,99997928	0,020147363
718	40	8000	0,008	2,37E-04	99,99999723	0,015566148
719	40	8000	0,01	4,35E-04	99,99999867	0,029102376
720	40	9000	0,008	3,17E-02	99,99993304	0,060254054
721	40	10000	0,006	1,56E-04	99,99998399	0,036732677
722	40	20000	0,004	2,54E-04	99,99999666	0,016021017
723	40	25000	0,01	3,77E-04	99,99999907	0,03068107
724	40	30000	0,002	3,14E-02	99,9999337	0,078204961
725	40	30000	0,008	2,55E-04	99,99999668	0,024275522
726	40	35000	0,01	3,95E-04	99,999999	0,033952089
727	40	40000	0,004	3,35E-02	99,99992933	0,038976527
728	40	40000	0,01	2,36E-04	99,99999722	0,021683341
729	40	45000	0,008	3,76E-04	99,99999914	0,034464348
730	40	50000	0,002	3,50E-02	99,9999274	0,018781461
731	40	50000	0,006	1,36E-04	99,9999869	0,035548296
732	40	50000	0,008	2,58E-04	99,99999664	0,019241487
733	40	50000	0,01	3,69E-02	99,99992508	0,062129329
734	40	55000	0,002	3,29E-02	99,99993218	0,005743294
735	40	55000	0,006	2,34E-04	99,9999974	0,018476945
736	40	55000	0,008	3,87E-04	99,99999904	0,031993441
737	40	60000	0,002	3,49E-02	99,99992802	0,046198192
738	40	60000	0,008	3,20E-02	99,99993363	0,026694324
739	40	65000	0,01	1,84E-04	99,99998096	0,011184027
740	40	70000	0,004	2,10E-04	99,99999802	0,025864045
741	40	75000	0,006	4,58E-04	99,99999833	0,023296167
742	40	75000	0,008	3,45E-02	99,99992868	0,035433383
743	40	80000	0,01	3,41E-02	99,99993085	0,010955468
744	40	85000	0,004	2,35E-04	99,99997455	0,034744589
745	40	90000	0,01	1,94E-04	99,99999841	0,027847379
746	40	95000	0,004	4,27E-04	99,99999862	0,027379706
747	40	95000	0,006	3,53E-02	99,99992766	0,028457977
748	40	95000	0,008	3,23E-02	99,99993336	0,017669486
749	40	95000	0,01	1,93E-04	99,99997988	0,034330993
750	40	100000	0,006	2,63E-04	99,99999638	0,014964075
751	40	100000	0,008	3,54E-02	99,99992924	0,053118943
752	40	105000	0,002	1,45E-04	99,99998604	0,029677548
753	40	105000	0,004	2,59E-04	99,99999654	0,01586326
754	40	105000	0,008	3,99E-04	99,99999886	0,033981462
755	40	110000	0,002	1,20E-04	99,99998916	0,028086562
756	40	110000	0,004	2,23E-04	99,99999763	0,025383083
757	40	110000	0,006	4,85E-04	99,99999788	0,034278792
758	40	110000	0,008	3,29E-02	99,99993293	0,056680576
759	40	115000	0,01	1,05E-04	99,99999113	0,028752791
760	40	120000	0,004	4,47E-04	99,9999983	0,021604796
761	40	120000	0,006	3,68E-02	99,99992624	0,036057855
762	40	125000	0,006	3,31E-02	99,99993273	0,024739786
763	40	125000	0,01	1,29E-04	99,99998808	0,021846497
764	40	135000	0,006	1,93E-04	99,9999985	0,029493342
765	40	140000	0,004	4,90E-04	99,99999775	0,017942238
766	40	140000	0,008	3,87E-02	99,99992383	0,054405183
767	40	145000	0,002	3,38E-02	99,99993179	0,020164364
768	40	145000	0,008	1,09E-04	99,9999908	0,01398766
769	40	150000	0,002	2,91E-04	99,99999602	0,01636062

	Displacement (mm)	Resitence (Ohm)	Amplitude (m)	MSE	Cross Correlation	Mean Percentage Error
770	40	165000	0,01	3,88E-02	99,99992369	0,029795791
771	40	170000	0,002	3,54E-02	99,99992976	0,053551507
772	40	170000	0,004	1,76E-04	99,99998265	0,027303456
773	40	170000	0,006	2,23E-04	99,99999778	0,01961779
774	40	175000	0,006	5,06E-04	99,99999754	0,018511839
775	40	175000	0,008	3,91E-02	99,99992344	0,007211865
776	40	180000	0,002	3,56E-02	99,99992961	0,012476954
777	40	180000	0,004	4,51E-04	99,99999811	0,025066477
778	40	185000	0,004	3,61E-02	99,99992732	0,037607677
779	40	185000	0,01	1,82E-04	99,99998238	0,002791267
780	40	190000	0,002	5,81E-04	99,9999967	0,027347319
781	40	190000	0,01	3,77E-02	99,99992542	0,040060234
782	40	195000	0,006	2,31E-04	99,99997705	0,019646869
783	40	195000	0,008	2,26E-04	99,99999775	0,027428604

Table A.1: Resultados com dados simulados desconhecidos pela rede

Appendix B

Program script

B.1 Main.m

```
close all, clear all, clc

run('DataAsc.m')

run('DataDes.m')

run('ANNTreino.m')

run('Resultados.m')

run('DataExp.m')

run('ResultadosExp.m')
```

B.2 DataAsc.m

```
%%
%Prepara dados

addpath ..\
ListaA=dir('../f_*_X_*_R_*_A_*.mat');
Listd=[];

%Lista Todas as Amplitudes possíveis para uma dada abertura
for i = 1:numel(ListaA)
    Arquivo=ListaA(i).name ;
    Under=strfind(Arquivo,'_');
    Dot=strfind(Arquivo,'.');

    d=str2num(cell2mat(extractBetween(Arquivo, Under(7)+1, Dot(end)-1))); %Abertura
    R=str2num(cell2mat(extractBetween(Arquivo, Under(5)+1, Under(6)-1))); %Resistencia
```

```
    f=str2num(cell2mat(extractBetween(Arquivo, Under(1)+1, Under(2)-1))); %Frequência
    Amp=str2num(cell2mat(extractBetween(Arquivo, Under(3)+1, Under(4)-1)));%Amplitude

    Listd=[Listd; d R Amp f];

end

Listd=sortrows(Listd,[1 2 3 4]);

%adição=================================================

%Seleciona linhas que serão usadas só para teste
Unid=unique(Listd(:,1));
UniR=unique(Listd(:,2));
UniA=unique(Listd(:,3));

totalAmo=numel(Unid)*numel(UniA)*numel(UniR); %numero de combinações totais de amplitude e
testeAmo=round(totalAmo/3); %número de amostras que serão para os testes finais. 1/3 do tot
LinTest=randperm(totalAmo,testeAmo); %linhas da matriz com a combinação escolhidas randomic
LinTest=sort(LinTest');

%Criando matriz de combinação
[m,n,l] = ndgrid(Unid, UniR,UniA);
Combinada = [m(:),n(:), l(:)];
Combinada=sortrows(Combinada,[1 2 3]);
CombSep=Combinada(LinTest,:);

Separa=false; %diz se os dados serão separados ou não
% u_mulTest={};
% y_mulTest={};
conta=1;
%=========================================================

Lastf=0; %Ultima frequencia carregada

U=[];
Y=[];
u_mul={};
y_mul={};

for i=1:numel(Listd(:,1))

    d=Listd(i,1);
    R=Listd(i,2);
    Amp=Listd(i,3);
    f=Listd(i,4);
```

```
NomeStr=strcat('../f_', num2str(f) ,'_X_', num2str(Amp) , '_R_', num2str(R) ,'_A_', num2

%Trata dados
data= load(NomeStr);
TabelaSaida= struct2array(data);
t=TabelaSaida(:,1)'; %tempo
x=TabelaSaida(:,2)'; %deslocamento
Vel=TabelaSaida(:,3)'; %velocidade
Ic=TabelaSaida(:,4)';%corrente
Vc=Ic*R; %calculo da tensão

%Entradas
fin=Amp*cos(2*pi*f*t); %função da posição para entrada na ANN

if Lastf<f
   if numel(U)==0
      U=fin;
      Y=Vc;
   else
     U=[U fin(2:end)];
     Y=[Y Vc(2:end)];
   end
else


   %Acrescenta outras entradas ao U, nomeadamente deslocamento e resistência
   U=[U; Lastd*ones(1,numel(U)); (LastR)*ones(1,numel(U)); ones(1,numel(U))];

   %cria o cell array para entradas e saídas
   u_cel=num2cell(U,1);
   y_cel=num2cell(Y,1);

   if Separa
       Uteste(:,:,conta)=U;
       Yteste(:,:,conta)=Y;
       conta=conta+1;
   else

       if isempty(u_mul)
           u_mul=u_cel;
           y_mul=y_cel;
       else
         u_mul=catsamples(u_mul,u_cel,'pad'); %concatena entradas
         y_mul=catsamples(y_mul,y_cel,'pad'); %concatena saídas
       end
   end
```

```
      U=fin;
      Y=Vc;
      %=========================

    if nnz(ismember(CombSep,[d R Amp], 'rows'))
       Separa=true;

    else
       Separa=false;
    end

    %=========================

   end

   Lastf=f;
   LastR=R;
   Lastd=d;
end

 save('TestDataV9.mat','Uteste','Yteste', '-v7.3')
 save('DataTreino.mat', 'u_mul', 'y_mul','-v7.3')
 save('DataV9.mat','-v7.3')
 clear ListaA Listd TabelaSaida Uteste YTeste u_mul y_mul u_cel y_cel
```

B.3 DataDes.m

```
%%
%Prepara dados
% load('DataTreino.mat');
% load('DataV9_Desc.mat', 'CombSep');

ListaA=dir('../Descendente/f_*_X_*_R_*_A_*.mat');
Listd=[];


%Lista Todas as Amplitudes possíveis para uma dada abertura
for i = 1:numel(ListaA)
    Arquivo=ListaA(i).name ;
    Under=strfind(Arquivo,'_');
    Dot=strfind(Arquivo,'.');

    d=str2num(cell2mat(extractBetween(Arquivo, Under(7)+1, Dot(end)-1))); %Abertura
    R=str2num(cell2mat(extractBetween(Arquivo, Under(5)+1, Under(6)-1))); %Resistencia
    f=str2num(cell2mat(extractBetween(Arquivo, Under(1)+1, Under(2)-1))); %Frequência
    Amp=str2num(cell2mat(extractBetween(Arquivo, Under(3)+1, Under(4)-1)));%Amplitude
```

```
    Listd=[Listd; d R Amp f];

end

Listd=sortrows(Listd,[1 2 3 4]);

%adição=================================================

%Seleciona linhas que serão usadas só para teste
Unid=unique(Listd(:,1));
UniR=unique(Listd(:,2));
UniA=unique(Listd(:,3));

totalAmo=numel(Unid)*numel(UniA)*numel(UniR); %numero de combinações totais de amplitude e
testeAmo=round(totalAmo/3); %número de amostras que serão para os testes finais. 1/3 do tot
LinTest=randperm(totalAmo,testeAmo); %linhas da matriz com a combinação escolhidas randomic
LinTest=sort(LinTest');

%Criando matriz de combinação
[m,n,l] = ndgrid(Unid, UniR,UniA);
Combinada = [m(:),n(:), l(:)];
Combinada=sortrows(Combinada,[1 2 3]);
CombSep=Combinada(LinTest,:);

Separa=false; %diz se os dados serão separados ou não
% u_mulDescTest={};
% y_mulDescTest={};
conta=1;
%=========================================================

Lastf=0; %Ultima frequencia carregada

U=[];
Y=[];
u_mulDesc={};
y_mulDesc={};

for i=1:numel(Listd(:,1))

    d=Listd(i,1);
    R=Listd(i,2);
    Amp=Listd(i,3);
    f=Listd(i,4);


   NomeStr=strcat('../f_', num2str(f) ,'_X_', num2str(Amp) , '_R_', num2str(R) ,'_A_', num2
```

```
%Trata dados
data= load(NomeStr);
TabelaSaida= struct2array(data);
t=TabelaSaida(:,1)'; %tempo
x=TabelaSaida(:,2)'; %deslocamento
Vel=TabelaSaida(:,3)'; %velocidade
Ic=TabelaSaida(:,4)';%corrente
Vc=Ic*R; %calculo da tensão

%Entradas
fin=Amp*cos(2*pi*f*t); %função da posição para entrada na ANN

if Lastf<f
   if numel(U)==0
      U=fin;
      Y=Vc;
   else
     U=[U fin(2:end)];
     Y=[Y Vc(2:end)];
   end
else


   %Acrescenta outras entradas ao U, nomeadamente deslocamento e resistência
   U=[U; Lastd*ones(1,numel(U)); (LastR)*ones(1,numel(U)); -ones(1,numel(U))];

   %cria o cell array para entradas e saídas
   u_cel=num2cell(U,1);
   y_cel=num2cell(Y,1);

   if Separa
       UtesteDes(:,:,conta)=U;
       YtesteDesc(:,:,conta)=Y;
       conta=conta+1;
   else

       if isempty(u_mulDesc)
           u_mulDesc=u_cel;
           y_mulDesc=y_cel;
       else
         u_mulDesc=catsamples(u_mulDesc,u_cel,'pad'); %concatena entradas
         y_mulDesc=catsamples(y_mulDesc,y_cel,'pad'); %concatena saídas
       end
   end
   U=fin;
   Y=Vc;
```

```
      %=========================

    if nnz(ismember(CombSep,[d R Amp], 'rows'))
       Separa=true;

    else
       Separa=false;
    end

    %=========================

   end

   Lastf=f;
   LastR=R;
   Lastd=d;
end

 save('TestDataV9_Desc.mat','UtesteDes','YtesteDesc', '-v7.3')
 save('DataTreino_Desc.mat', 'u_mulDesc', 'y_mulDesc','-v7.3')
 save('DataV9_Desc.mat','-v7.3')
 clear ListaA Listd TabelaSaida UtesteDes YtesteDesc u_mulDesc y_mulDesc
```

B.4 ANNTreino.m

```
 %%
%ANN Super teste
%   u_mul - input time series.
%   y_mul - feedback time series.

%load ficheiro
load('DataTreino.mat');
load('DataTreino_Desc.mat');


%u_mul e y_mul juntar com u_mulDesc e y_mulDesc
% X = u_mul;
% T = y_mul;

X = catsamples(u_mul,u_mulDesc,'pad');
T = catsamples(y_mul,y_mulDesc,'pad');

% Choose a Training Function
% 'trainlm' is usually fastest.
% 'trainbr' takes longer but may be better for challenging problems.
% 'trainscg' uses less memory. Suitable in low memory situations.
```

```
% FuncTreino=["trainlm" "trainbr"]; %duas funções a serem treinadas
FuncTreino="trainlm";

%Guarda melhores resultados
% BestPerf=10;
% BestDelay=0;
% BestNeuron=0;
% BestFun='Nenhuma';

fun=FuncTreino;
% for fun=FuncTreino

trainFcn = fun;  % Funções de backpropagation.

neurons = 13;
delay=6;

% for neurons=10:1:16
%     for delay=2:1:10

% Create a Nonlinear Autoregressive Network with External Input
        inputDelays = 1:delay;
        feedbackDelays = 1:delay;
        hiddenLayerSize = neurons;
        net = narxnet(inputDelays,feedbackDelays,hiddenLayerSize,'open',trainFcn);


        % Choose Input and Feedback Pre/Post-Processing Functions
        % Settings for feedback input are automatically applied to feedback output
        % For a list of all processing functions type: help nnprocess
        % Customize input parameters at: net.inputs{i}.processParam
        % Customize output parameters at: net.outputs{i}.processParam
        net.inputs{1}.processFcns = {'removeconstantrows','mapminmax'};
        net.inputs{2}.processFcns = {'removeconstantrows','mapminmax'};

        % Prepare the Data for Training and Simulation
        % The function PREPARETS prepares timeseries data for a particular network,
        % shifting time by the minimum amount to fill input states and layer
        % states. Using PREPARETS allows you to keep your original time series data
        % unchanged, while easily customizing it for networks with differing
        % numbers of delays, with open loop or closed loop feedback modes.
        [x,xi,ai,t] = preparets(net,X,{},T);

        % Setup Division of Data for Training, Validation, Testing
        % For a list of all data division functions type: help nndivision
        net.divideFcn = 'divideblock';  % Divide data randomly
```

```
        net.divideMode = 'time';  % Divide up every sample
        net.divideParam.trainRatio = 70/100;
        net.divideParam.valRatio = 15/100;
        net.divideParam.testRatio = 15/100;

        % Choose a Performance Function
        % For a list of all performance functions type: help nnperformance
        net.performFcn = 'mse';  % Mean Squared Error

%         net.trainParam.showWindow = false; %hide train tool

        tic

        % Train the Network
        [net,tr] = train(net,x,t,xi,ai);

        TempoTreino=toc;
%
%         % Test the Network
        y = net(x,xi,ai);
        e = gsubtract(t,y);
        performance = perform(net,t,y);
%
%         % Recalculate Training, Validation and Test Performance
%         trainTargets = gmultiply(t,tr.trainMask);
%         valTargets = gmultiply(t,tr.valMask);
%         testTargets = gmultiply(t,tr.testMask);
%         trainPerformance = perform(net,trainTargets,y);
%         valPerformance = perform(net,valTargets,y);
%         testPerformance = perform(net,testTargets,y);

save('DataRede.mat','-v7.3')
save('RedeNeuro.mat', 'net', '-v7.3')

clear
```

B.5 Resultados.m

```
%%
%Teste com dados separados
SomaErr=0;
TabelaTeste=[];

% for T=1:varTest
load(('TestDataV9.mat'))
load(('TestDataV9_Desc.mat'))
```

```
load('RedeNeuro.mat')
load('DataV9_Desc.mat', 'CombSep')

CombSepD=CombSep;

load('DataV9.mat', 'CombSep')

Uteste=cat(3,Uteste,UtesteDes);
Yteste=cat(3,Yteste,YtesteDesc);
CombSep=cat(1,CombSep,CombSepD);

clear CombSepD UtesteDes YtesteDes

for i=1:length(Uteste(1,1,:))

    u_cel=num2cell(Uteste(:,:,i),1);
    y_cel=num2cell(Yteste(:,:,i),1);

    [x,xi,ai,t] = preparets(net,u_cel,{},y_cel);

    y = net(x,xi,ai);
    e = gsubtract(t,y);
    MSE = perform(net, t, y); %MSE da rede

    SomaErr=SomaErr+mean(cell2mat(e));

    r=xcorr(cell2mat(y), cell2mat(t), 'coeff');
    correlation=max(r)*100;

    %calculo do erro medio percentual
    MatrizE=cell2mat(e);
    MatrizT=cell2mat(t);

    %numeros muito proximos de zero serão desconsiderados na matriz T
    %Para isso, criou-se a MatrizReguladora, que será 1 para numeros acima
    %de 0.01V e 0 para valores menores.

    MatrizReguladora=abs(MatrizT)>0.01;

    ErrPerc=100*abs(mean((MatrizE./MatrizT).*MatrizReguladora));

    TabelaTeste=[TabelaTeste; CombSep(i,:) MSE correlation ErrPerc ];

end

ErrMed=SomaErr/length(Uteste(1,1,:));
ErrPercMed=ErrPerc/length(Uteste(1,1,:));
```

```
% end

save ('Net_F_x_X_x_R_x_A_x_Final.mat', '-v7.3')
save ('TabelaTeste.mat','TabelaTeste', '-v7.3')
```

B.6 DataExp.m

```
close all, clear all, clc

run('DataAsc.m')

run('DataDes.m')

run('ANNTreino.m')

run('Resultados.m')

run('DataExp.m')

run('ResultadosExp.m')
```

B.7 ResultadosExp.m

```
load('DataExpRede.mat')
load('RedeNeuro.mat')

[x,xi,ai,t] = preparets(net,u_mul,{},y_mul);

y = net(x,xi,ai);
e = gsubtract(t,y);
MSE = perform(net, t, y); %MSE da rede

%correlação cruzada
r=xcorr(cell2mat(y), cell2mat(t), 'coeff');
correlation=max(r)*100;

%calculo do erro medio percentual
MatrizE=cell2mat(e);
MatrizT=cell2mat(t);

%numeros muito proximos de zero serão desconsiderados na matriz T
%Para isso, criou-se a MatrizReguladora, que será 1 para numeros acima
%de 0.01V e 0 para valores menores.

MatrizReguladora=abs(MatrizT)>0.01;
```

```
ErrPerc=100*abs(mean((MatrizE./MatrizT).*MatrizReguladora));


% end

save ('ResultadoExp.mat', '-v7.3')
```

B.8 filtro.m

```
function Filtrada = filtro(In,limV)
    y=In';
    T = 0.001;           % Sampling period
    Fs = 1/T;            % Sampling frequency
    L = size(y,1);       % Length of signal
    t = (0:L-1)*T;

    ttfY = fft(y); %Fast Fourrier Transform

    %Calcular o espectro de dois lados.
    %Em seguida, calcular o espectro de uma face P1 com base em P2 e o comprimento de sinal
    P2 = ttfY/L;
    P1 = P2(1:floor(L/2+1));
    P1(2:end-1) = 2*P1(2:end-1);


    f = Fs*(0:(L/2))/L;
    mask=abs(P1)>limV; %calcula máscara
    Ajuste=P1.*mask;
    Ajuste(2:end-1)=(1/2)*Ajuste(2:end-1);
    conjfilp=conj(flip(Ajuste(1:end)));
    inv=[Ajuste(1:end-1); conjfilp(1:end-1)] ;   % volta a por todo em complexo

    inv2=L*inv;

    Filtrada=ifft(inv2); %transformada inversa

    %Ajusta o tamanho do sinal novo com o original caso seja diferente
    if size(Filtrada,1)~=size(y,1)
        Filtrada=[Filtrada; 0];
    end
end
```